The Hong Kong Polytechnic University

Department of Electrical Engineering

GAS DISCHARGE IN HOLLOW-CORE FIBERS AND ITS APPLICATION IN WAVEGUIDE GAS LASERS

SHI XIN

A thesis submitted in partial fulfillment of the requirements for the degree of Doctor of Philosophy

Nov 2008

CERTIFICATE OF ORIGINALITY

I hereby declare that this thesis is my own work and that, to the best of my knowledge and belief, it reproduces no material previously published or written, nor material that has been accepted for the award of any other degree or diploma, except where due acknowledgement has been made in the text.

_____

Xin SHI

ACKNOWLEDGEMENTS

I would like to express my sincere gratitude to my chief supervisor, Professor Wei Jin, for his continuous encouragement and guidance of my work. I am also very grateful to my co-supervisor, Prof. M. Süleyman Demokan, for his useful suggestions. I would like to thank my co-worker, Professor Xinbing Wang, for his valuable guidance and discussions. I have been truly lucky to be guided by three friendly people with great insight.

I would like to acknowledge the support and technical help of Professor H. Y. Tam, Dr. H. L. Ho, Dr. J. Ju, Dr. Y. L. Hoo, and Ms. X. L. Zhang.

Finally, I want to express my deepest gratitude to my parents, and my brother for their endless love and support.

ABSTRACT

Compact and flexible solid-state lasers are challenging the dominant market of gas lasers (especially the CO_2 lasers) in the recent years. Solid-state lasers seem to be the direction of the future. The features of compactness and portability are the dream of researchers in the field of gas lasers. When the gas lasers, especially the vessel containing the gain medium, reduce to small size, they form a new branch of gas lasers—waveguide gas lasers. The waveguide CO_2 gas lasers were developed rapidly since 1970s and are widely used in commercial products nowadays.

However the sizes of previous waveguide gas lasers are still huge compared with their rival—solid-state lasers. Conventional hollow waveguide theory indicates that the waveguide loss of a simple hollow waveguide is considerable if the aperture of the waveguide is small. The advances in hollow-core photonic bandgap (PBG) fiber gave us the inspiration to develop novel fiber gas lasers based on such new hollow-core fibers. These novel waveguide structures break the limitation predicted by the simple hollow waveguide theory and provide us with the opportunity for building compact, flexible, and miniature fiber gas lasers which are expected to find applications in many fields.

However there are still many unknowns in the construction of hollow-core fiber gas lasers. For example: whether the population inversion (prerequisite for lasing) will happen in such a small size tube, and which type of excitation will be the most efficient to produce the population inversion? Many other details need be addressed before a successful experimental demonstration can be made. Although the research on

waveguide gas lasers has made significant progress over the past three decades, the research on discharge in micro-size (i.e., size of inner diameter down to 200μm or less) capillaries and lasers based on such capillaries are still not yet reported to our knowledge.

The low waveguide losses in hollow-core fibers indicate that they are good waveguides as well as discharge tubes. The calculations which follow the theory of laser resonators suggest that the feedback configuration of flat mirrors placed at the ends of hollow-core fiber is the best choice for hollow-core fibers. Hollow-core PBG fibers can be coiled down to very small size with negligible loss and are good candidates for making long cavity length but still compact fiber gas lasers.

Calculations of population inversion indicate that there exists gain for gas-filled hollow-core fibers with inner diameter bigger than 11 μm. Our calculations also suggest that considerable gas pressure is needed for the very small tubes to achieve population inversion. These provide the theoretical support for constructing a novel fiber gas laser from the viewpoint of gas discharge physics.

The vacuum system for constructing fiber gas lasers is studied in detail. Gas flow in hollow-core fibers is different from that in conventional laser tube because of their very small bore sizes. When considering the outgassing rate of inner surface of the hollow-core fibers, the calculations indicate that outgassing might pose a problem in achieving high degree of vacuum and hinder the lasing of the fiber gas laser.

Based on the theoretical analysis and experimental results, we also discuss the technical problems encountered in the construction of fiber gas lasers, such as vacuum requirement, optical alignment problem, and fiber cleaving.

We carried out a series of experiments to explore the gas discharge in small size gas-filled hollow-core fibers and succeeded in obtaining gas discharge in 250, 150, and 50 μm inner-diameter (i.d.) hollow-core fibers by using longitudinal direct current excitation. Stable glow discharges of at least several minutes were observed for these hollow-core fibers. A flash glow was also observed for a hollow-core fiber with an i.d. of ~20 μm. Breakdown of helium and argon gases in a 26.2cm-length 250μm-i.d. hollow-core fiber was achieved with a voltage of less than 30kV. Considering the facts that a waveguide gas laser with 430μm-i.d and 20cm-length has been constructed eariler and that a smaller bore-size and longer length of gain tube would provide larger gain, it should then be possible to construct hollow-core fiber gas lasers with an inner diameter of 250μm or less.

The successful demonstration of miniature fiber gas lasers would open doors for many new applications such as rotation sensing and flow measurement.

CONTENTS

Abstract i

Contents iv

Chapter 1 Introduction 1

1.1 Introduction to gas lasers and waveguide gas lasers 1

1.2 Motivation 2

1.3 Thesis outline 3

References 5

Chapter 2 Background 6

2.1 Gas lasers 6

2.1.1 Conventional gas lasers 6

2.1.2 Waveguide gas lasers 11

2.2 He-Ne lasers 14

2.2.1 Conventional He-Ne lasers 14

2.2.2 Waveguide He-Ne lasers 16

2.3 Fiber ring laser gyros based on fiber gas lasers 19

2.4 Summary 24

References 24

Chapter 3 Laser resonators based on hollow-core fibers 29

3.1 Waveguide losses of hollow-core fibers 29

3.1.1 Simple hollow waveguide 30

3.1.2 Complex hollow waveguide 35

3.2 Macro-bending losses in hollow-core fibers 45

3.2.1 Bending loss in simple hollow waveguide 46

3.2.2 Bending loss in PBG waveguide 48

3.3 Coupling efficiency in hollow waveguide laser resonator 54

3.3.1 Types of waveguide laser resonator 54

3.3.2 Three low loss configurations in the Fabry-Perot resonator 56
3.3.3 Calculations for small bore size hollow-core fibers 60
3.3.4 Other potential feedback designs for hollow-core fibers 62
3.4 Summary 66
References 66
Chapter 4 Theories of waveguide He-Ne laser with small bore size 73
4.1 Modeling of transverse RF excited waveguide He-Ne laser 73
4.2 Modeling of longitudinal DC excited waveguide He-Ne laser with tube diameter ≥ 200 μm 76
4.3 Modeling results for longitudinal DC excited waveguide He-Ne laser with tube diameter <200μm 82
4.4 Summary 85
References 86
Chapter 5 Vacuum system and gas flow in hollow-core fibers 88
5.1 Vacuum system 88
5.2 Gas flow in hollow-core fibers 91
5.3 Summary 96
References 96
Chapter 6 Gas discharge in hollow-core fibers 98
6.1 Excitation methods for waveguide gas lasers 98
6.2 DC discharge regimes 101
6.3 Gas breakdown in hollow-core fibers 105
6.3.1 Gas breakdown theories 105
6.3.2 Experimental setup and phenomenon 106
6.3.3 Experimental results 108
6.4 *I-V* characteristics of gas discharge in hollow-core fibers 113
6.5 The effect of fiber bend on gas discharge 116
6.6 Spectrums of glow discharge 117
6.7 Summary 118

References 119

Chapter 7 Problems in designing fiber gas lasers 121

7.1 The problems due to the requirement of high vacuum 121

7.1.1 The high vacuum system 121

7.1.2 The gas chambers 123

7.2 The problems due to the alignment of mirrors 125

7.2.1 Mirrors close to the ends of hollow-core fiber 125

7.2.2 Alignment of mirrors 129

7.3 The problem due to cleaving of hollow-core fibers 130

7.4 Summary 132

References 132

Chapter 8 Research summary and future work 135

8.1 Research summary 135

8.2 Future work 138

Appendix: Publications 140

CHAPTER 1

INTRODUCTION

1.1 Introduction to gas lasers and waveguide gas lasers

Since the demonstration of the first helium-neon laser in 1960, gas lasers have experienced rapid development from 1960s to 1980s. Various gas lasers such as CO_2 lasers, hydrogen and deuterium fluoride chemical lasers, excimer and exciplex lasers, and metal vapor lasers were demonstrated by researchers.

When the tube or vessel containing the gain medium reduces to small sizes, the tube will also serve as a simple waveguide to confine the light. This type of lasers are called waveguide gas lasers, Smith [1] reported the first waveguide He-Ne laser working at 0.633μm with a glass-capillary-tube of 20cm-length and 430μm-inner diameter (i.d.) in 1971. The peak gain of the fundamental mode (EH_{11}) was 2.7dB/m, and the laser output has an approximately Gaussian output-beam profile and an output power of 1mW. Since then, few experiments related to waveguide He-Ne lasers have been reported. Gonchukov et al. constructed a waveguide He-Ne laser at 3.39 μm with a tube of 510μm-i.d. in 1975 [2] and another one at 632.8nm with a tube of 490μm-i.d. in 1976 [3]. Dovbeshko demonstrated a waveguide He-Ne laser working at 632.8nm with a tube of 1mm-i.d. in 1996 [4].

The early waveguide gas lasers were constructed from either simple hollow circular dielectric (or metal) waveguides, or planar (or rectangle) waveguides. Marcatili and Schmeltzer analyzed these simple waveguides [5] and showed that

waveguide loss increases considerably when the bore size of the hollow waveguide reduces to below 200 μm. It seems that the waveguide laser with a tube of 430μm-i.d. constructed by Smith is still the smallest He-Ne laser that has ever been reported in the open literature.

1.2 Motivation

Recent advances in low-loss hollow-core fibers and novel hollow-core photonic bandgap (PBG) fibers open up new possibilities such as high power laser pulse delivery and shaping, ultra-sensitive and distributed gas and liquid detection and nonlinear optics for gases. These hollow-core fibers enable us to replace the capillary waveguide in previous waveguide gas lasers by new hollow-core fibers and this will bring out a new type of waveguide gas lasers—fiber gas lasers. The success of this new type of fiber gas lasers would bring new opportunities and possibilities to the field of gas lasers and lead to many new devices which could find wide spread application in measurement and sensing. The fiber gas lasers can potentially be made to be compact and portable and can be integrated into the fiber optic system.

Constructing novel waveguide He-Ne lasers by using small bore size hollow-core fibers however also bring new problems that need to be studied carefully before an efficient fiber gas laser can be constructed. The hollow-core fibers have inner diameters from 5 to 250 μm and outer diameters 125 to 344 μm, and are much smaller in size compared with conventional capillary waveguide in bulk glass. The problems arising from the very small size capillaries include:

(1) Whether population inversion can be achieved by appropriate excitation methods.

(2) Whether waveguide loss is sufficiently small in comparison with the gain of the gas tube.

(3) Whether suitable feedback mirror configurations exist to form an appropriate laser cavity.

These problems all need to be studied carefully and comprehensively to find the most appropriate cavity structure and discharge configuration in order to realize a waveguide gas laser.

1.3 Thesis outline

The thesis is organized as follows:

Chapter 2 We review the development and applications of gas lasers in the past decades in section 2.1, with a focus on the waveguide gas laser in section 2.1.2. We review some characteristics of conventional He-Ne lasers in section 2.2.1. Several waveguide He-Ne lasers constructed by previous researchers are summarized in section 2.2.2. In section 2.3 we introduce the He-Ne ring laser gyros (RLGs) and review past efforts to find suitable substitutes for high performance He-Ne RLGs. We present the advantages of novel fiber ring laser gyros based on the new fiber gas lasers.

Chapter 3 We introduce the existing, simplified hollow waveguide theory and make calculation for tubes with inner-diameter smaller than 400μm. The waveguide loss of simple hollow waveguide is discussed in section 3.1.1. Complicated hollow waveguides and their guiding mechanisms are introduced in section 3.1.2. The macro-bending losses in simple hollow waveguide and PBG waveguide are discussed in section 3.2. We review various resonators of waveguide lasers in section 3.3.1. From the theories of

laser resonator as discussed in section 3.3.2, we introduce three low loss configurations. We calculate the coupling losses for small bore size hollow-core fibers and find suitable feedback configuration for these hollow-core fibers in section 3.3.3.

Chapter 4 We discuss population inversion and other requirements for lasing in this chapter. The previous modeling of transverse RF excited waveguide He-Ne laser is introduced in section 4.1. The modeling of longitudinal DC excited waveguide He-Ne laser with tube diameter larger than 200 μm is discussed in section 4.2. We use this model to extend the calculation to tubes of smaller inner-diameter and present the results in section 4.3.

Chapter 5 We describe our new vacuum system in section 5.1. The gas flow in hollow-core fibers is investigated in detail from the point of view of flow theory in section 5.2.

Chapter 6 We introduce excitation methods of waveguide lasers in section 6.1. The discharge regimes in the whole process of gas discharge are described in section 6.2. We investigate the breakdown characteristics and current-voltage (I-V) characteristics in section 6.3 and 6.4 respectively. The bending effect on gas discharge in hollow-core fibers is presented in section 6.5. Spectrum of glow discharge is given in section 6.6.

Chapter 7 We discuss the problems due to the requirement of vacuum in section 7.1. The problems due to the alignment of mirrors are presented in section 7.2. Another problem of cleaving large outer-diameter hollow-core fibers is also discussed in section 7.3.

Chapter 8 In this last chapter, we summarize our past efforts to building a fiber gas laser in section 8.1 and discuss the future work which needs to be carried out to achieve

lasing in hollow-core fibers in section 8.2.

References

1. P. W. Smith, “A waveguide gas laser,” *Appl. Phys. Lett.*, vol. 19, pp. 132-134, 1971.
2. S. A. Gonchukov, S. T. Kornilov, and E. D. Protsenko, “Oscillation modes of a gas laser with waveguide resonator,” *Sov. J. Quantum Electron.*, vol. 6, pp. 996-997, 1976.
3. S. A. Gonchukov, S. T. Kornilov, V. N. Petrovskii and E. D. Protsenko, “Helium-Neon waveguide laser,” *Sov. J. Quantum Electron.*, vol. 5, pp. 232-233, 1975.
4. A. A. Dovbeshko, “Small-size waveguide He-Ne laser with HF (SHF) pumping for optoelectronic systems for speed measurements,” *Proc. SPIE - The International Society for Optical Engineering*, vol. 2729, pp. 48-56, 1996.
5. E. A. J. Marcatili and R. A. Schmeltzer, “Hollow metallic and dielectric waveguides for long distance optical transmission and lasers,” *Bell Syst. Tech. J.*, vol. 43, pp. 1783-1809, 1964.

CHAPTER 2

BACKGROUND

Gaseous (low-density) gain media are used in approximately half of the existing commercial lasers. This fraction will probably decrease in the future owing to the compactness and potential increased reliability of solid-state lasers, but many applications of gaseous lasers will no doubt remain for years to come. Certainly for very short-wavelength lasers, gaseous or plasma media will always be the dominant media. This chapter reviews the research and development of gas lasers, especially He-Ne waveguide gas lasers; and discusses the possibility of constructing novel fiber gas lasers with the newly developed hollow-core fibers.

2.1 Gas lasers

2.1.1 Conventional gas lasers

Albert Einstein predicted the effect of stimulated emission in 1917. Charles Towns, Nikolai Basov, and Aleksander Prokhorov shared a Nobel Prize for their theoretical works in 1964. The man, who first achieved a coherent radiation from his ruby laser, was Theodore Maiman; however, he was not a Nobel Prize Laureate. Javan elaborated the first helium-neon (He-Ne) laser in 1960 [1]. The He-Ne laser operating at 1.15 μm initiated a new branch in optics—gas lasers. Soon, the next milestone was reached in 1964 by Patel [2], who invented a laser operating on carbon dioxide (CO_2) molecules. After a few modifications such as the addition of nitrogen (N_2) and He, the laser gave

an output of 100 watts. Nowadays, applications of lasers in different branches of science and technology have become a reality and the gas lasers which we are interested have fulfill leading roles in scientific research, industrial technology, and many other branches of human activity.

Since the 1960s, gas laser technology has demonstrated a very rapid rate of development. Flourishing investigations on gases, high vacuum technology, discharges, and plasma were the factors that accelerated the development of gas lasers at that time. Additionally, well-developed spectroscopy brought significant information about energy structures of different gas media—the base to discover new laser transitions.

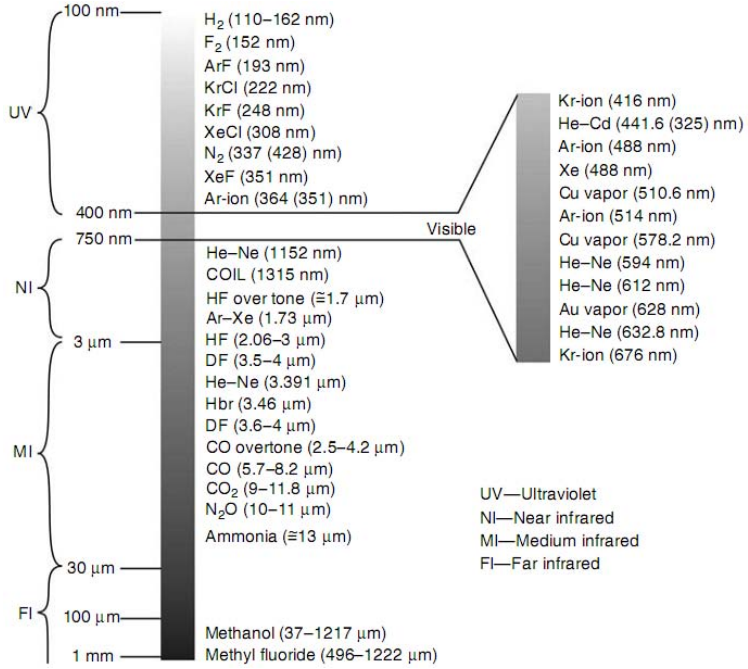

Figure 2.1 The spectral map of popular gas laser radiation [3].

Gas lasers have several advantages. Gas laser output covers all optical spectra from far infrared (FIR) radiation to x-ray. Some representative examples are shown in Fig. 2.1. The relatively low density of gas medium demonstrates narrow and well-defined spectral emission lines, which makes them stable sources of optical radiation (in output power and frequency). Long lifetime has been achieved for gas laser devices because

of well-developed high-vacuum technologies. For instance, many who work in the laboratory or industry can use a He-Ne laser even a few decades old without any noticeable degradation. In many lasers, recycling of the gas sufficiently increases their lifetime. A huge advantage of gases is their ability to mix in different ratios and at different pressures to form highly homogeneous media. Only gas media have the possibility of flowing fast through the laser device. In that way, refreshing and heat removal can be easily achieved. Gas lasers can be easily scaled in length, area, and volume without a significant increase in the cost of the device. The well-developed technique of gas discharges allows exciting gas media in reasonable, easily formable, laser cavities. According to its nature, gas adopts shapes limited by a laser cavity. The other advantage is the possibility of using isotopes to shift the spectrum of laser radiation.

Table 2.1 Global industrial laser revenues-$Million [4]

Laser	2004	2005	%	2006	%
CO_2	597	634	6	673	6
Solid-state	480	476	-8	429	-10
Fiber laser	55	91	65	139	52
Other	39	40	2	46	15
Total	1171	1241	6	1287	4

Today, CO_2 lasers are applied in industries for cutting, welding, drilling; in medicine for surgery; in environment for detecting pollution and analyzing compositions of the atmosphere; in communications; and in military applications. However Gas lasers are facing the competition from fiber lasers and diode lasers as

indicated in Table 2.1. A new report reveals that sales of fiber lasers are set to double by 2011. The fiber laser market is worth $240 million in the year of 2007, a growth of 39 per cent since 2006, and the report predicts an increase of at least 26 per cent per year for the next four years [5].

Industry experts have been predicting the death of gas lasers in favor of fiber and diode lasers for the past 15 years. However, the precision, control, low cost, robustness and flexibility of CO_2, nitrogen, ion and helium-neon lasers are opening up new applications all the time.

CO_2 lasers are a mature technology. There haven't been any quantum leaps recently, as the technology has been around since the 1980s. However, development is far from dead. The customization of resonator designs for different power levels has optimized performance, with narrow gap resonators providing greater laser beam intensity and improved beam quality for higher-power lasers, and free space resonators further improving the efficiency and cost-effectiveness of low-power lasers. In addition, ceramics, which have excellent thermal conductivity, have been used to aid cooling of heat generated by the plasma, which had previously been a big disadvantage of CO_2 lasers.

The range of powers available in industrial gas lasers, from less than 1W to a possible 20kW, is another factor that sets them apart. This too has improved recently, allowing a greater range of applications. CO_2 lasers were typically in the 1kW range fifteen years ago. However, there has been a gradual increase, and now powers of up to 6kW are common. This, together with better design, has opened up both welding and cutting applications. High power is achieved by increased pumping of the gain medium,

which can cause thermal and mechanical stress, so the lasers need to be much larger to provide stability. The higher processing speeds could lead to a greater call for automated loading systems.

In addition to a greater range of powers, CO_2 laser beams also have higher quality than solid-state beams. This means they can be focused to very small spot sizes, giving the high power density necessary for these applications. These factors allow the high-precision cutting of thin glass used for cell phones, plasma display panel (PDP) and liquid crystal display (LCD) displays using lower-power CO_2 lasers from Coherent company [6]. This application uses a thermal process: a laser beam heats up the surface, after which a liquid stream provides a ‘thermal shock’ that directly breaks the glass. The quality of the break is so good that it doesn’t need an additional grinding process, unlike mechanical methods that would introduce micro-scratches.

Ion lasers, with Argon and Krypton as their gain medium, produce a stable, controllable output of up to 12 different wavelengths. However, their disadvantages mean they are now often overlooked for many applications. Ion lasers are very large and have an efficiency of one hundredth of a per cent, but their tunableness and extremely high beam quality open up a number of applications. The biggest market is the semiconductor industry. Ion lasers are used to engrave optical photomasks that are used as a template when creating printed circuit boards. They are also employed in the inspection of semiconductor wafers. Ion lasers have a large market in the entertainment industry, where they are used for light shows due to their high visibility and high output power. However, this may not be for long because of the invading by solid-state lasers.

For another kind of gas lasers, He-Ne lasers, the range of wavelengths proves to be the biggest advantage. Like diode lasers, He-Ne lasers work primarily in the red part of the spectrum, but unlike diode lasers, they can also produce a range of green, yellow and orange laser light. The emission can be tuned using a prism in the laser cavity that is tilted using a motor to transmit different wavelengths. These lasers work at much lower powers, typically 35mW or less. He-Ne lasers are even cheaper than CO_2 lasers. The narrower line-width and thermal stability of the beams make them ideal for use in holograms and interferometry. The beam is also naturally circular with low divergence, unlike the elliptical beam of diode lasers that must be corrected with complex optics. In the past they were used widely in barcode scanners, but laser diodes are now used for this application because they are cheaper and smaller. He-Ne lasers are also used for fingerprint identification, as the grease on fingers fluoresces under certain wavelengths of light. Other possible applications include cartography, printing, DNA sequencing and biotechnology engineering.

2.1.2 Waveguide gas lasers

A waveguide laser can be distinguished from a conventional laser by the characteristic that, over some portion of the propagation path, the circulating radiation is guided and does not obey the laws of free space propagation. As a consequence, the conventional resonator theories [7], which are derived under the assumption of free space propagation between two reflecting surfaces, do not adequately describe the spatial mode distributions, frequency spectra, losses or stability characteristics of waveguide lasers. Using the rather loose definition given above, the term waveguide laser can be applied to a large number of devices which utilize gaseous, liquid, or solid active

media.

Waveguide gas lasers, operating at wavelengths in the visible through submillimeter regions of the spectrum, have been reported. Experimental studies of laser gases excited in conventional lasers by electron impacts, such as He-Ne [8, 9] and CO_2 [10-12], indicate that both gain and optimum fill pressure vary approximately inversely with tube diameter. Because of the increased line broadening and larger saturation intensities associated with higher operating pressures, waveguide gas lasers are ideally suited to serve as compact, tunable spectroscopic sources; wideband laser local oscillators in heterodyne communications, radiometry, and radar systems; mode-locked short pulse generators; or broadband power amplifiers. High pressure operation also allows single longitudinal mode operation and full utilization of the molecular line width in laser gases which are normally inhomogeneously broadened, such as helium-neon mixtures.

Marcatili and Schmeltzer's theoretical calculation shows that a small-bore capillary can support low-loss transmission for the lowest order mode [13]. Smith reported the first waveguide He-Ne laser working at 0.633μm made from 20cm length of 430μm-diameter-bore glass-capillary-tubing [14]. In 1972, Smith proposed and demonstrated a transversely excited (TE) waveguide laser [15], which has the potential advantage of providing efficient excitation of the laser medium at high gas-filling pressures. Although the first demonstration of waveguide gas laser was the type of He-Ne, there was no further development in the field of waveguide He-Ne laser in the past several decades.

Practically the waveguide resonator is defined by a simple criterion—the Fresnel

number N_F should be lower than unity:

$$N_F = \frac{a^2}{\lambda L} < 1 \tag{2.1}$$

where a is half of the resonator aperture, λ is the free-space wavelength, and L is the resonator length.

For example, for a typical CO_2 waveguide with the square transverse dimensions $2a \times 2a = 2 \times 2\text{mm}^2$, L=400mm, and λ=10.6μm, the Fresnel number is ~0.2. When the Fresnel number exceeds unity, the resonator can be treated as an open resonator. In practice, for a CO_2 laser with the same length L and transverse dimension $2a$=5 mm, the resonator becomes an open one (N_F=1.5). In that case, a Gaussian resonator should be applied.

The advantage of using waveguide resonators for molecular CO_2 lasers lies in the fact that it allows to decrease transverse dimensions of the beam inside the waveguide. Small transverse dimensions allow increasing diffusive cooling efficiency (where the 010 level is depopulated by collisions with helium atoms, which transport waste heat to the walls). There is another advantage: due to better cooling condition, the pressure of the mixture can be increased considerably, according to the practical formula

$$pd \approx 25 \text{ (Torr cm)} \quad \text{for square waveguide structures} \tag{2.2}$$

$$pd \approx 19 \text{ (Torr cm)} \quad \text{for planar waveguide structures} \tag{2.3}$$

where p is the pressure and d is the transverse dimension of the square waveguide or slab (for planar structure).

For d=2 mm, the total pressure of mixture more than 100 Torr can be applied. Higher pressure means higher density of gain medium and higher output power. Hence,

waveguide lasers require much shorter length to obtain the same output power than the low-pressure DC-excited CO_2 lasers.

2.2 He-Ne lasers

2.2.1 Conventional He-Ne lasers

The He-Ne laser was one of the first lasers ever developed and is still one of the most widely used lasers. The lasers are trouble-free and have extremely long operating lifetime. They operate in a low-pressure mixture of helium and neon gases, and the laser transitions occur within the neutral atomic species. The most common wavelength is the 632.8-nm transition in the red portion of the spectrum, Additional wavelengths become available: in the green at 543.5 nm, the yellow at 594 nm, the orange at 612 nm, and the infrared at 1.15, 1.523 and 3.39 μm. There are numerous other infrared wavelengths that lase but generally not found significant commercial applications. One particularly strong transition at 3.39 μm competes with the 632.8-nm transition, and they have a common upper laser level. Therefore it must be quenched by creating higher loss in the laser cavity at that wavelength to allow the 632.8-nm transition to lase. These lasers generally produce powers in the range of 0.5 to 50 mW in the red, with much lower powers on the other transitions. The lasers operate continuous wave and have a very stable low-nosie output. The gain bandwidth follows the Doppler-broadened emission linewidth a FWHM (full width half maximum) of 1.5 GHz. A laser cavity length of 0.3 m would thus allow several longitudinal modes to lase simultaneously within the laser cavity. The complete laser assembly is typically 0.15-0.5 m in length, with lateral dimensions of the order of several tens of

millimeters.

The gain in a number of neutral gas lasers, at optimum discharge conditions of gas pressure and discharge current varies approximately as the reciprocal of the diameter of the discharge tube [16-20]. The lasers in which this gain relationship is observed include the 1.1523-, 3.39-, and 0.6328-μm He-Ne lasers.

The maximum unsaturated gain G_m in a He-Ne discharge optimized for gain at 632.8nm is described by the relation [8]

$$G_m = 3\times10^{-2}\, l/D \quad \text{percent} \tag{2.4}$$

where l is the discharge length in cm and D is the internal diameter of the tube in cm. This expression has been found to predict the measured gain to within 10 percent accuracy for a number of laser tubes with different fills that include 5:1 and 7:1 ratios of He^4: Ne, and a 7:1 ratio of He^3:Ne. The relation only applies when competition with the high-gain $3s_2$-$3p_4$, 3.39μm transition is eliminated. When competition with the 3.39μm transition is not eliminated, a more complicated relationship

$$G_m \cong \left[1+0.5\left(\frac{D_0}{D}\right)^{1.4}\right]^{l/l_0} \tag{2.5}$$

has been found to apply where D_0=1mm and l_0=100cm, and D and l, are in mm and cm respectively [9].

Optimum discharge conditions for obtaining maximum gain and output power on the Ne-I 632.8 nm, $3s_2$-$2p_4$ transition in a He-Ne mixture when oscillation at 3.39μm is suppressed are: 1) He:Ne pressure ratio = 5:1; 2) pressure and tube-diameter product pD=3 to 5 Torr-mm, where p is the total pressure [8, 21].

The small gain of most He-Ne laser transitions requires particularly high-quality,

low-loss optics and a Gaussian configuration of optical resonators. Very high selectivity and low-loss mirrors have to be used in a laser resonator to choose the required wavelength of radiation. Most small He-Ne tubes support a gain of about 0.12 to 0.15 m^{-1}, so a tube 30 cm in length has a gain of only about 4 to 5%. Small gains (a few percentage per pass) of most transitions also determine high reflectivity of the outcoupling mirror (usually below or around 1%).

2.2.2 Waveguide He-Ne lasers

Although the first waveguide laser was demonstrated on the mixture of He-Ne [14], there are few researchers that have ever constructed practical waveguide He-Ne lasers since then. Smith used a 430μm diameter tube as the waveguide and discharge container. The follower Dovbeshko [22, 24] used a little bigger tube as the cavity. All the structural parameters of waveguide He-Ne lasers that can be found in the literatures are listed in Table 2.2.

Table 2.2 Structural parameters

Wavelength	632.8nm	632.8nm	632.8nm	3.39μm
Length	20cm	15.2cm	7cm	15cm
Diameter	430μm	490μm	1mm	510μm
Gas ratio (He : Ne)	10:1	10:1	15.2:1	5.5:1
Pressure	7 Torr	6.3 Torr	3.4 Torr	7 Torr
Excitation	DC plus RF (longitudinal)	DC plus RF	RF (longitudinal)	DC (1mA) plus microwave (15W)
Reflection of mirrors	99%	99.8%	97%, 9.65%	88-90%
Maximum output intensity	1mW		1.125mW	0.5mW
Gain	2.7 dB/m			170 dB/m
Author	Smith [14]	Gonchukov [22]	Dovbeshko [23]	Gonchukov [24]

It seems strange that few experiments have been performed related to waveguide He-Ne lasers since 1971. Most attentions are put on the transverse excited waveguide CO_2 laser and that configuration is widely used in commercial CO_2 lasers now.

One of the important reasons is that CO_2 lasers can provide much higher output power than helium-neon lasers, and this is also true for the waveguide type. The much higher output power makes them attractive in the industrial applications. No new applications have been reported for smaller bore size waveguide He-Ne lasers in the past decades.

As mentioned previously, the gain varies approximately as the reciprocal of the diameter of the discharge tube. However, simple hollow waveguide theory of Marcatili and Schmeltzer indicates that the waveguide loss increases with the decreasing of the bore size of the discharge tube [13]. Therefore, there exists an optimum bore diameter for maximum gain in a glass capillary He-Ne laser operating at 632.8 nm. Seelig surveyed the experimental literature on the He-Ne lasers and derived an equation for small signal gain at 632.8 nm given by [25]

$$g_0 = \frac{1}{I}\frac{dI}{dL} \approx 7.2\times10^{-3} mpj \left[\frac{(1-m)^2}{mpR + (1-0.2p)\left(9.5pjR^2 + \dfrac{6.4\times10^{-3}}{pR}\right)} - 2 \right] \tag{2.6}$$

where R is the tube radius, j is the current density, p is the total pressure, and $m=p_{Ne}/p$ is the fractional pressure of neon.

Considering the waveguide loss of EH_{11} mode by using the formula of Marcatili and Schmeltzer [13], Seelig suggested that bore diameter of 0.2 mm is the optimum value for obtaining maximum gain. Hence, it seems that there was no need to develop

waveguide He-Ne lasers by using smaller bore size tubes. By the way, fabrication of smaller capillary waveguide in bulk glass with good uniformity over a reasonably long length also seems difficult.

However, recently progress on the hollow-core fibers with a layer of higher-index anti-resonant coating and the novel hollow-core photonic bandgap (PBG) fibers with a 2-dimensional holey photonic crystal cladding allows the demonstration of a much lower waveguide loss of (from 0.02 dB/m to 1 dB/m) for hollow-core size of from 5 to 250 μm [26, 27]. The losses of the hollow-core PBG fibers do not increase significantly even when they are subject to bending with a diameter of a few centimeters or less. In the mean time, there are efficient feedback configurations for the hollow-core fiber to form a laser cavity. These configurations include having high reflection mirrors at the ends of the hollow-core fiber [28, 29], splicing solid-core fibers with in-fiber Bragg gratings or fiber loop mirrors to the two ends of the hollow-core fiber and splicing the two arms of a fiber directional coupler to the hollow-core fiber to form a ring cavity. These indicate that it should be possible to construct a novel miniature fiber gas (i.e., He-Ne) lasers with a relatively small gain required from hollow-core gas tube. These fiber He-Ne gas lasers are expected to have the same excellent monochromaticity as their bulk counter-parts but have the advantage of full compatibility with the optical fiber systems. These fiber He-Ne lasers would found applications in precision measurement and instrumentation [30] such as passive ring resonator gyros, fiber ring laser gyros, large path-length difference fiber interferometers, fiber ring flow meters and methane gas detectors based on the 3.39 μm He-Ne line locked to a methane absorption line.

2.3 Fiber ring laser gyros based on fiber gas lasers

Unlike CO_2 lasers, conventional He-Ne lasers developed slowly in the past decades. The He-Ne laser may be the only option for many pointing, alignment, and scanning applications in many fields. Not long ago, many supermarket bar-code scanners and even some high-end handheld scanners used He-Ne lasers, as did the original (early 1980s) CD and laser disk players. Today, most applications have migrated toward more compact semiconductor laser diode. However, in some applications where beam quality, beam collimation, and coherence length are important, He-Ne lasers are still used extensively. He-Ne laser is indeed the de facto standard laboratory laser, with uses ranging from alignment of optics to testing of optical component. For holography, the He-Ne laser is still the laser of choice because of its good coherence length compared to other types of lasers. The same is true for many precision measurement applications and the ability to use unique cavity configuration (e.g., a ring) allows the He-Ne laser to be used as the basis for instruments such as laser gyroscopes for aircraft.

The optical gyroscopes are, of course, all based on the Sagnac effect which was first described and demonstrated by Sagnac in 1913 [31]. But it was Rosenthal in 1962 [32] who first proposed the use of lasers to implement the Sagnac effect and this gave birth to the very successful He-Ne ring laser gyro (RLG), as first demonstrated by Macek and Davis in 1963 [33]. And in 1976 [34], Vali and Shorthill initiated the excitement of using a multi-turn fiber coil to significantly enhance the sensitivity of the basic Sagnac interferometer, which created the fiber optic gyro (FOG) that is now becoming a strong rival of the RLG. The third approach of implementing the Sagnac effect is by the use of a passive resonator instead of an active one, as proposed and

demonstrated by Ezekiel and Balsamo in 1977 [35].

The success of the He-Ne laser RLG did not come very easily or quickly [36]. To survive at all, it needed to satisfy three major criteria: simultaneous counter propagating lasers sharing the same gain and cavity; opportunity for perfect reciprocity; and a means of eliminating lock-in at low rotation rates that is caused by back scattering. The elimination of gain competition in the He-Ne amplifier to enable simultaneous lasing along counter-propagating directions has been achieved by the use of two isotopes of Neon. These isotopes are unique in that they have different transition frequencies at 632.8nm but this difference is still within the Doppler width of each transition so as to achieve a composite of two partially overlapping gain curves. Perfect reciprocity is achieved by using the exact same cavity for both CW and CCW lasers and the lock-in problem is eliminated by either mechanical dither, or by using four frequency-operations instead of two.

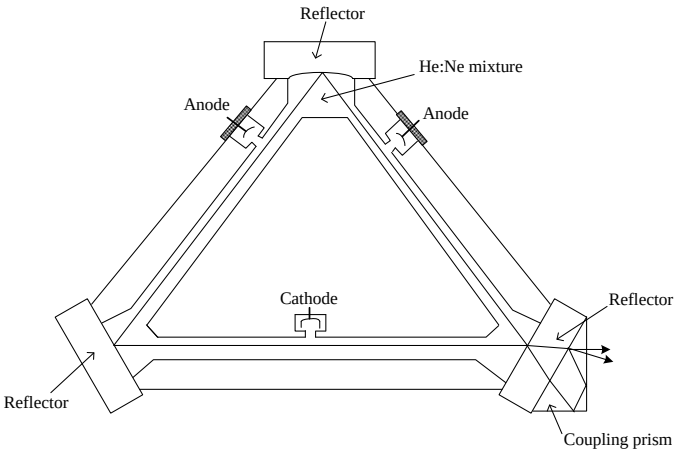

Figure 2.2 He-Ne RLG.

The objections to the He-Ne RLG include the use of a gas discharge, high voltages, a very expensive cavity carved out from a low expansion coefficient block of material, very low-loss cavity mirrors which are shown in Fig. 2.2 and the need for mechanical

dither as in many of the RLGs in operation.

In the presence of rotation, the optical paths and hence the frequencies of the counter-propagating lasing beam will be different and the frequency difference is given by [37]:

$$\Delta f = f_{cw} - f_{ccw} = -\frac{4A}{\lambda P}\Omega \tag{2.7}$$

where λ is the laser wavelength, f_{cw} and f_{ccw} are respectively the frequencies of the clockwise and counter-clockwise lasing beams. A is the area and P is the perimeter of the optical path, and Ω is the rotation rate. RLGs, compared to their mechanical counterparts, have the advantages of no moving parts and hence relatively insensitive to a number of error sources such as shock and vibration and have shorter repairing time. In addition, RLGs have large dynamic range (from below 0.01°/hr to over 1000°/hr) and digital (frequency) output. However, the cost is high because of the high quality mirror required and the special manufacturing technology that is not commonly used for other applications. It took a while to develop but the He-Ne RLG works well! To date, there has not been another accurate laser RLG other than the He-Ne RLG.

Over the past several decades, there has been much research done to find a solidstate replacement for the He-Ne system by using, for example, an optically pumped solid-state amplifier. The use of semiconductor amplifiers for ring laser gyros is very attractive and has also been investigated. Again, as in the case of optically pumped solid state RLGs, gain competition is the key problem to overcome [38].

Another successful type of optical gyroscope is the interferometric fiber optic gyroscope (IFOG). This type of gyros is based on a multi-turns fiber optic two-beam

interferometer (Fig. 2.3). The two beams travel through the same fiber coil but along opposite directions. The phase difference between the two beams is related to rotation rate by [39]:

$$\Delta\phi = \frac{8\pi AN}{\lambda c}\Omega = \frac{2\pi LD}{\lambda c}\Omega \tag{2.8}$$

where D is the diameter of the fiber coil, c is the velocity of light, N is the number of turns of the fiber coil, and L is the total length of the fiber coil ($L=N\pi D$).

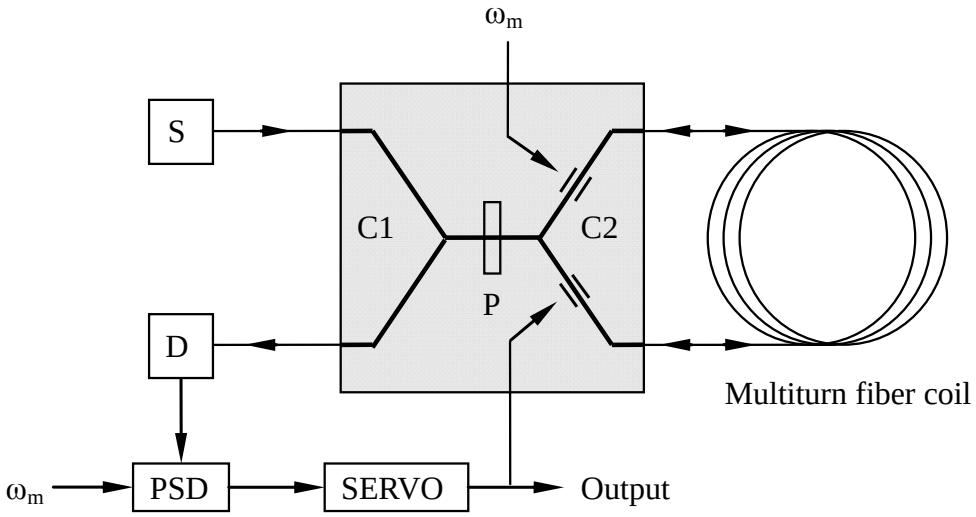

Figure 2.3 Interferometric fiber optic gyroscope (IFOG).

To achieve reasonable detection resolution, long single mode optical fibers of hundreds of meters to kilometers are required. An IFOG typically uses a broadband, low coherence source. This, coupled with the use of a good quality polarizer, a polarization maintaining fiber, special fiber-coil-winding and magnetic shield techniques, substantially reduces the noises and errors due to back reflection/scattering, the Kerr effect, the polarization effect, the time-dependent thermal effect, and external magnetic field effects. The advantage of IFOG includes no moving parts and hence resistance to shock and acceleration; being able to use the components developed in fiber optic communication industry and hence lower cost; performance can be tailored

by varying the length of the fiber used but still being packed in a small rugged form [40].

Although IFOGs have been successfully applied for a number of applications, research is still being conducted to further improve the performance of gyros in terms of short-term noise, long-term drift, and scale factor stability; and on reducing the complexity and cost to enable lower-cost inertial-navigation gyros to be manufactured [41].

Attempts have been made to create a ring laser gyro in a fiber format. It is not possible to create a fiber ring laser gyro (FRLG) by simply placing a conventional solid-state optical amplifier within a fiber ring-resonator because of the inherent competition for gain between the counter-propagating lasers [42]. The stimulated Brillouin effect in fibers made it possible to realize directional optical amplification in the fiber loop and hence enable simultaneous lasing along the two counter-propagating directions. Such a stimulated Brillouin FRLG has been investigated [42] but not to the degree of IFOG.

The recent advent of low-loss hollow-core fibers makes it possible to realize a FRLG with a gas-phase optical-waveguide (fiber) amplifier. Low-loss hollow-core fibers at various wavelengths from 0.633μm to 1.55μm and longer are available and continue to improve in performance. Hollow-core PBG fibers have been filled with hydrogen gas to study Raman scattering and filled with acetylene gas for wavelength reference and for gas detection [43, 44]. The filling of such a hollow-core fiber by, for example, a He:Ne mixture would allow a hollow-core FRLG to be built, which can be used as a rotation sensor, similar to bulk RLGs. As bulk RLGs have been investigated

for quite a long time, the solutions to overcome various undesirable error effects, such as the “lock-in” phenomenon, may be directly borrowed for use in He-Ne FRLGs, and hence minimize the effort in identifying the counter-measures to overcome these extraneous effects.

2.4 Summary

We reviewed the research and development of gas lasers, especially waveguide He-Ne lasers, and identified that it is possible to develop novel compact fiber He-Ne gas laser with the newly developed hollow-core fibers. These fiber He-Ne lasers would have important applications in interferometer fiber sensors and gyroscopes. In the following chapter, we will report our theoretical and experimental work toward the development of such fiber gas lasers, and discuss various possibilities and technical constraints.

References

1. A. Javan, W. R. Bennett, Jr., and D. R. herriot, “Population inversion and continuous optical maser oscillation in a gas discharge containing a He-Ne mixture,” *Phys. Rev. Lett.*, vol. 6, pp. 106-110, 1961.
2. C. K. N. Patel, “Continuous-Wave Laser Action on Vibrational-Rotational Transitions of CO_2,” *Phys. Rev.*, vol. 136, pp. A1187-A1193, 1964.
3. M. Endo and R. F. Walter, *Gas lasers*, CRC press, 2006.
4. http://www.industrial-lasers.com/display_article/246483/39/none/none/Feat/Fiber-l

asers-tip-the-scale.

5. http://su.pennnet.com/press_display.cfm?ARTICLE_ID=311397.
6. http://www.coherentinc.com/Applications/index.cfm?fuseaction=Forms.AppLevel2&AppLevel2ID=125.
7. H. Kogelnik, T. Li, "Laser beams and resonators," *Applied Optics.*, vol. 5, pp. 1550-1567, 1966.
8. P. W. Smith, "On the optimum geometry of a 6328Å laser oscillator," *IEEE J. Quant. Electron*, vol. 2, pp. 77-79, 1966.
9. G. Herziger, W. Holzapfel, W. Seelig, "Berechnung und experimenteller vergleich des verstarkungsfaktors fur den laserubergang 6328Å in einer he-ne-gasentladung," *Z. Physik*, vol.200, pp. 103-105, 1967.
10. P. K. Cheo, "Effects of gas flow on gain of 10.6 micron CO_2 laser amplifiers," *IEEE J. Quant. Electron*, vol. 3, pp. 151-155, 1967
11. T. F. Deutsch, "Gain and fluorescence characteristics of flowing CO_2 laser systems," *IEEE J. Quant. Electron*, vol. 3, pp. 683-689, 1967.
12. E. T. Antropov, I. A. Silin-Bekchurin, N. N. Sobolev, and V. V. Sokovikov, "Gain measurement in the CO_2 laser discharge," *IEEE J. Quant. Electron*, vol. 4, pp. 790-796, 1968.
13. E. A. J. Marcatili and R. A. Schmeltzer, "Hollow metallic and dielectric waveguides for long distance optical transmission and lasers," *Bell Syst. Tech. J.*, vol. 43, pp. 1783-1809, 1964.
14. P. W. Smith, "A waveguide gas laser," *Appl. Phys. Lett.*, vol.19, pp.132-134, 1971.
15. P. W. Smith, P. J. Maloney, and O. R. Wood, "waveguide TEA laser," *Appl. Phys.*

Lett., vol. 23, pp. 524-526, 1973.

16. W. R. Bennett, “Gaseous Optical Masers,” *Applied Optics*, vol. 1, pp. 24-61, 1962.
17. C. K. N. Patel, W. R. Bennett, R. A. Mcfarland, et al., “Infrared spectroscopy using stimulated emission techniques,” *Phys. Rev. Lett.*, vol. 9, pp. 102-107, 1962.
18. R. A. Mcfarlane, C. K. N. Patel, W. R. Bennett, et al., “New helium-neon optical maser transitions,” *Proc. Inst. Radio Engrs.*, vol. 50, pp. 2111-2114, 1962.
19. P. O. Clarke, “Investigation of the operating characteristics of the 3.5 μ xenon laser,” *IEEE J. Quant. Electron*, vol. 1, pp. 109-113, 1965.
20. W. R. Bennett, R. A. Mcfarland, W. L. Faust, et al., “Dissociative excitation transfer and optical maser oscillation in Ne-02 and Ar-O_2 rf discharges,” *Phys. Rev. Lett.*, vol. 8, pp. 470-473, 1962.
21. E. I. Gordon, A. D. White, “Similarity laws for the effects of pressure and discharge diameter on gain of He-Ne lasers,” *Applied Physics Letters*, vol. 3, pp. 199-201, 1963.
22. S. A. Gonchukov, S. T. Kornilov, and E. D. Protsenko, “Oscillation modes of a gas laser with waveguide resonator,” *Sov. J. Quantum Electron.*, vol. 6, pp. 996-997, 1976.
23. A. A. Dovbeshko, “Small-size waveguide He-Ne laser with HF (SHF) pumping for optoelectronic systems for speed measurements,” *Proc. SPIE - The International Society for Optical Engineering*, v. 2729, pp. 48-56, 1996.
24. S. A. Gonchukov, S. T. Kornilov, V. N. Petrovskii and E. D. Protsenko, “Helium-Neon waveguide laser,” *Sov. J. Quantum Electron.*, vol. 5, pp. 232-233, 1975.

25. V. W. H. Seelig, “Verstärkung von He-Ne-Lasern mit sehr dfünnen Entladungsrohren,” *J. Appl. Math. Phys. (ZAMP)*, vol. 25, pp. 728-736, 1974.

26. J. Macomber and G. Nelson, “Light-guiding fused-Silica capillary tubing,” *The Application Notebook* (LCGC North Am., 2002), p. 48.

27. C. M. Smith, N. Venkataraman, M. T. Gallagher, D. Müller, J. A. West, N. F. Borrelli, D. C. Allan, and K. W. Koch, “Low-loss hollow-core silica/air photonic bandgap fibre,” *Nature*, vol. 424, pp. 657-659, 2003.

28. R. L. Abiams, “Coupling losses in hollow waveguide laser resonators,” *IEEE J. Quantum Electron.*, vol. 8, pp. 838-843, 1972.

29. J. J. Degnan and D. R. Hall, “Finite-aperture waveguide-laser resonators,” *IEEE J. Quantum Electron.*, vol. 9, pp, 901-910, 1973.

30. S. L. Zhang, *Principle of orthogonal polarized lasers*, Tsinghua University Press, Bejing, 2005.

31. G. Sagnac, “L’ether lumineux demontre par l’effet du vent relatif d’ether dans un interferometer en rotation uniforme”, *C. R. Acad Sci.*, vol. 95, pp. 708-710, 1913.

32. A. H. Rosenthal, “Regenerative circulatory multiple-beam interferometry for the study of light propagation effects,” *J. Opt. Soc. Am.*, vol. 52, pp. 1143-1147, 1962.

33. W. M. Macek and D. T. M. Davis, Jr., “Rotation rate sensing with traveling wave ring laser”, *Appl. Phys. Lett.*, vol. 2, pp. 67-68, 1963.

34. V. Vali and R. W. Shorthill, “Fiber ring interferometer,” *Appl. Opt.*, vol. 15, pp. 1099-1100, 1976.

35. S. Ezekiel and S. R. Balsamo, “Passive ring resonator laser gyroscope,” *Appl. Phys. Lett.*, vol. 30, pp. 478-480, 1977.

36. J. E. killpatrick, “The Laser Gyro,” *IEEE Spectrum*, vol. 67, pp. 44-55, 1967.

37. W. W. Chow, et al., “The ring laser gyro,” *Rev. Mod. Phys.*, vol. 57, pp. 61-104, 1985.

38. M. Sorel, G. Giuliani, A. Scirè, R. Miglierina, S. Donati, and P. J. R. Laybourn, “Operating regimes of GaAs-AlGaAs semiconductor ring lasers: experiment and model, ” *J. of Quantum Elect.*, vol. 39, pp. 1187-1195, 2003.

39. W. K. Burns, *Optical fiber rotation sensing*, Academic Press, 1994.

40. H. K. Kim et al., “Fiber-optic gyroscope using an air-core photonic bandgap fiber,” *Proc. SPIE*, vol. 5855, pp. 198-201, OFS’17, Belgium, May 2005.

41. R. A. Bergh, H. C. Lefevre and H. J. Shaw, “An overview of fiber-optic gyroscopes,” *J. Lightwave Technol.*, vol. 2, pp. 91-107, 1984.

42. F. Zarinetchi, S. P. Smith and S. Ezekiel, “Stimulated Brillouin fiber-optic laser gyroscope,” *Opt. Lett.*, vol. 16, pp. 229-231, 1991.

43. F. Benabid, et al., “Compact, stable and efficient all-fibre gas cells using hollow-core photonic crystal fibres,” *Nature*, vol. 434, pp. 488-491, 2005.

44. Y. L. Hoo, W. Jin, et al., “Gas diffusion measurement using hollow-core photonic bandgap fiber,” *Sensors and Actuators B-Chemical*, vol. 165, pp.183-186, 2005.

CHAPTER 3

LASER RESONATORS BASED ON HOLLOW-CORE FIBERS

Low-loss cavity is an important step toward the success of the proposed waveguide (fiber) gas lasers. The major internal cavity losses may be divided into two components: the waveguide losses experienced by the fundamental mode, and the coupling losses for this mode. This chapter calculates losses associated with various types of hollow-core fibers and studies the coupling between fiber mode and the cavity. We will discuss the problems arising from using hollow-core fibers as laser tube and prove the feasibility of our purpose from the view of laser resonator.

3.1 Waveguide losses of hollow-core fibers

The light beam in a conventional He-Ne laser propagates in form of free space modes if the diameter of the laser tube is bigger than 1 mm. If the diameter of the tube reduces to 500 μm or smaller, the inner wall of the tube can serve as simple waveguide to confine the light. Then the propagating mechanism of these small tubes is different from that of larger tubes.

It seems that the waveguide gas laser with the tube of 430μm-i.d. constructed by Smith [1] is still the smallest one that has ever been constructed. Over the past several decades, no experimental investigations have been performed on waveguide gas laser that uses smaller waveguide tubes. The important reason may be that smaller bore size tube suffers greater waveguide loss in according to conventional hollow waveguide theory [2]. There may be other reasons, for example, the waveguides used in previous

waveguide gas lasers are capillary waveguide in bulk glass as shown in Fig. 3.1a and it is difficult to make smaller size waveguide tube with good uniformity and long length.

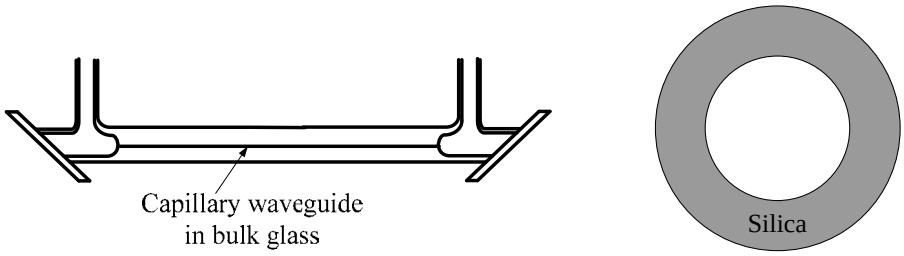

(a) (b)

Figure 3.1 (a) a capillary waveguide in bulk glass; (b) an ordinary capillary.

3.1.1 Simple hollow waveguide

The two structures shown in Fig. 3.1 are both the simple hollow waveguides. The hollow dielectric waveguides have varieties of configurations. The waveguide cross-section may be of arbitrary shape, and the most common structures are the cylindrical, rectangular, and planar guides. The planar or hollow-slab guide can be viewed as a special case of the rectangular guide where one transverse dimension is much larger than the other. Most hollow-core fibers are the cylindrical guides. Therefore here we mainly discuss the cylindrical type.

The modes of hollow cylindrical dielectric waveguides having diameters much larger than a wavelength were first derived by Marcatili and Schmeltzer [2]. In addition to the assumption that guide diameters are larger compared to a wavelength, the theory is also restricted to low-order, low-loss modes whose propagation constants γ are nearly equal to the plane-wave value. Fairly complex approximations for the field components containing terms up to and including order λ / a have been derived [3] where λ is the wavelength and a is the radius of the guide. To this order of

approximation, the *z*-components of electric and magnetic field for the hybrid EH_{nm} modes do not vanish. However, if one considers guides sufficiently large so that terms of order λ / a may be ignored, the fields approach the simple TEM-like solutions given below.

Circular Electric Modes TE_{0m} ($m \geq 1$)

$$E_\phi = J_1(\frac{u_{0m} r}{a}) e^{i(\gamma z - wt)}, H_r = -\sqrt{\frac{\varepsilon_0}{\mu_0}} E_\phi, H_z = 0(\lambda / a) \tag{3.1}$$

Circular Magnetic Modes TM_{0m} ($m \geq 1$)

$$E_r = J_1(\frac{u_{0m} r}{a}) e^{i(\gamma z - wt)}, H_\phi = -\sqrt{\frac{\varepsilon_0}{\mu_0}} E_r, E_z = 0(\lambda / a) \tag{3.2}$$

Hybrid Modes EH_{nm} ($n \neq 0, m \geq 1$)

$$\begin{aligned} &E_\phi = J_{n-1}(\frac{u_{nm} r}{a}) \cos(n\phi) e^{i(\gamma z - wt)}, E_r = J_{n-1}(\frac{u_{nm} r}{a}) \sin(n\phi) e^{i(\gamma z - wt)} \\ &H_\phi = \sqrt{\frac{\varepsilon_0}{\mu_0}} E_r, H_r = -\sqrt{\frac{\varepsilon_0}{\mu_0}} E_\phi, E_z = 0(\lambda / a), H_z = 0(\lambda / a) \end{aligned} \tag{3.3}$$

where u_{nm} is the m th root of the equation $J_{n-1}(u) = 0$ and the notation $0(\lambda / a)$ implies that particular field component is reduced by an approximate factor of λ / a .

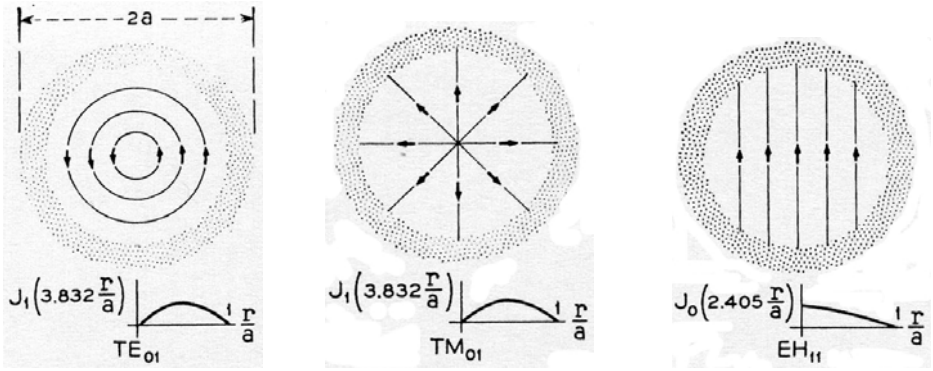

Figure 3.2 Electrical field lines of modes in hollow dielectric waveguides:TE_{01}, TM_{01} and EH_{11}[2].

The electrical field lines of TE_{01}, TM_{01} and EH_{11} are shown in the Fig. 3.2. TE_{01}, TM_{01} are circular modes and EH_{11} is a linear polarized mode. It shall be mentioned

here that the above notation of EH_{11} corresponds to the notation of HE_{11} and the notation of LP_{01} presently in existence.

The higher-order approximations describe fields which do not quite vanish at the guide boundary, but decay exponentially within a thin segment of the waveguide wall. The propagation constants γ in Eq. (3.1) through Eq. (3.3) are given by [4]

$$\gamma = k\left[1-\frac{1}{2}(\frac{u_{nm}}{ka})^2(1-\frac{i2v_n}{ka})\right] \tag{3.4}$$

$k = 2\pi/\lambda$ is the propagation constant for an infinite plane wave in the core material.

$$v_n = \frac{1}{\sqrt{v^2-1}} \quad \text{for } TE_{0m} \text{ modes (n=0)}$$

$$v_n = \frac{v^2}{\sqrt{v^2-1}} \quad \text{for } TM_{0m} \text{ modes (n=0)} \tag{3.5}$$

$$v_n = \frac{v^2+1}{2\sqrt{v^2-1}} \text{ for } EH_{nm} \text{ modes } (n \neq 0)$$

Where $v = \sqrt{\varepsilon_1/\varepsilon_0}$, v is the refractive index of the waveguide, ε_1 and ε_0 are the complex electric permittivity of the external and internal media. The real part of the propagation constant γ is therefore

$$\beta_{nm} = \mathrm{Re}\{\gamma\} = \frac{2\pi}{\lambda_{nm}} = k\left[1-\frac{1}{2}\left(\frac{u_{nm}}{ka}\right)^2\left(1+\frac{2}{ka}\mathrm{Im}\{v_n\}\right)\right] \tag{3.6}$$

Where λ_{nm} is the guide wavelength of the radiation in the mode described by the n and m. The attenuation of the modes in the guide is given by the imaginary component, that is

$$\alpha_{nm} = \mathrm{Im}\{\gamma\} = \left(\frac{u_{nm}}{k}\right)^2\frac{1}{a^3}\mathrm{Re}\{v_n\} \tag{3.7}$$

The mode with lowest attenuation is TE_{01} if $v > 2.02$ and EH_{11} if $v < 2.02$. The

losses for high order modes are much larger, therefore the resonator mode is almost a pure EH_{11} waveguide mode if $v < 2.02$.

For EH_{11} mode when λ=632.8 nm, it can be expressed as

$$\alpha = \frac{u_{11}^2}{4\pi^2}\frac{c^2}{a^3}\frac{1}{f_{23}^2}\frac{\frac{1}{2}(n_1^2+1)}{\sqrt{n_1^2-1}},\ f_{23} = 4.74\times10^{14}/s,\ \ u_{11} = 2.4048 \tag{3.8}$$

Here $\frac{P_{out}}{P_{in}} = R_1R_2e^{(G-\alpha)\times 2L} > 1$ is necessary in the initial state of lasing, it will reach a balance when the laser is working at stable state and then $R_1R_2e^{(G-\alpha)\times 2L} = 1$. The loss parameters of ordinary fibers use dB/m as the unit. The relationship between the unit dB/m and /m can be expressed as:

$$\alpha(dB/m) = -\frac{10}{L}\log(\frac{P_{out}}{P_{in}})$$

$$P_{out} = P_{in}\exp(-2\alpha L)$$

$$\alpha(dB/m) = -\frac{10}{L}\log_{10}[\exp(-2\alpha L)] = -\frac{10}{L}\times(-2\alpha L)\times\log_{10}e = 20\times\alpha\times\log_{10}e = 8.686\times\alpha \tag{3.9}$$

Table 3.1 Waveguide loss of EH_{11} mode at the wavelength of 632.8 nm

Bore diameter D (μm)	5.1	50	150	250	430
α_{11} (/m)	5216	5.5358	0.205	0.0443	0.0087

The refractive index of silica at 632.8 nm is 1.456. We calculate the loss of EH_{11} mode for the simple hollow waveguide (Fig. 3.1a or 3.1b) with diameter from 5 to 430 μm. The results are shown in Table 3.1. The case of D=430 μm corresponds to the glass tube used by Smith [1] as shown in Fig. 3.1a and the tube is a simple hollow waveguide that grazing incidence happening in the interface between glass and air. The sum of waveguide loss and coupling loss between waveguide tube and the mirrors

estimated by Smith is smaller than 1% (0.0251/m) which coincides with calculated result from the simple hollow waveguide theory.

It is very clear that waveguide loss of the fundamental mode (EH_{11} mode for glass tube) increases with the reducing of the bore size of the tube. Since the gain varies approximately as the reciprocal of the diameter of the discharge tube, Seelig suggested that bore diameter of 200 μm is the optimum value for obtaining maximum gain [5]. It can be seen that the loss is increased to an unacceptable level when the diameter is reduced to below 150 μm, and construction of gas lasers with such small tubes is impractical.

Since glass tubes were widely used as laser tubes in the past, the lowest-loss EH_{11} (sometimes also expressed as HE_{11}) mode and the coupling between this mode and feedback mirrors were investigated thoroughly. In the metallic hollow waveguide, the circular electrical modes (TE_{0m}) have the lowest loss, while the circular magnetic modes (TM_{0m}) and hybrid modes (EH_{nm}) are rapidly attenuated. In the 1970s, just before the advent of low loss optical fibers, the TE_{01} mode in metallic waveguides was ever considered for high bandwidth communication since it is the lowest loss mode of transmission for oversized circular waveguides. Nowadays optical fibers have clearly shown their superiority over metallic waveguides for this application.

The metallic hollow waveguide exhibits well transmission performance in the infrared wavelength compared with dielectric hollow waveguides. However, a new type of hollow waveguide by depositing one layer of Ag and one layer of AgI on the internal surface of the silica tube can achieve well transmission in the infrared range while having good performance of macro-bending [6].

3.1.2 Complex hollow waveguide

Specially designed complex hollow-core waveguides can achieve much smaller loss than the simple hollow waveguide. Recently newly developed hollow-core photonic bandgap (PBG) fiber and hollow-core Bragg fiber demonstrated this point.

Hollow-core PBG fiber is a branch of so called photonic crystal fiber (PCF). PCF is an optical fiber comprising a photonic crystal cladding and a core which breaks the periodicity [7, 8]. The cladding structure is usually formed by air holes arrayed in a triangular lattice in silica glass. In PCFs, two waveguiding mechanisms are used: modified total internal reflection (MTIR) and PBG effect. PBG is a novel waveguiding mechanism, which enables totally new functions such as transmission in a hollow core with extremely low loss and nonlinearly [7] (Fig. 3.3a). On the other hand, various new functions such as large chromatic dispersion and small mode area are realized even in PCFs based on MTIR (Fig. 3.3b). Since the periodicity in the structure is not essential for those new functions in MTIR-based PCFs, fibers which have air holes and guide light by MTIR are often called holey fibers (HF) rather than PCF.

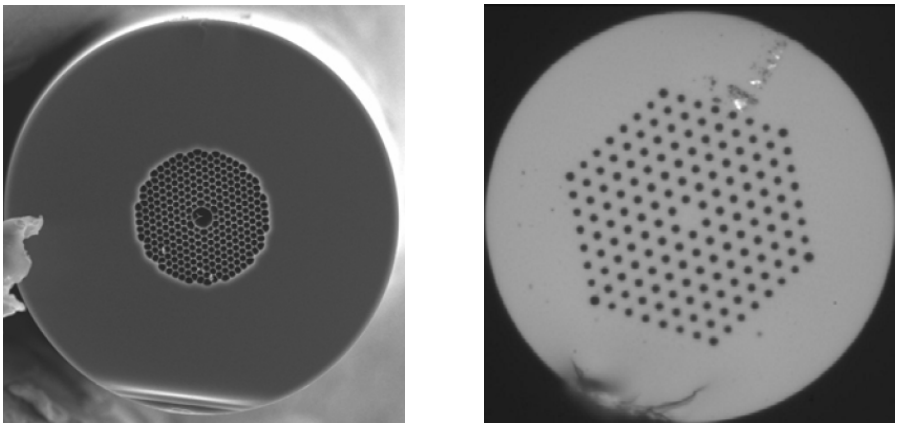

(a) (b)

Figure 3.3 (a) PCF based on PBG guidance, (b) HF based on MTIR guidance [9].

Based on PBG mechanism light can be strictly guided, without leakage, in a hollow air core [7]. Light in certain wavelength bands is trapped in the air by a full two-dimension photonic band gap of the cladding, and it can be guided in a single mode. The intrinsic need for a two-dimension PBG requires that the fiber cladding contain a nearly perfect periodic array of air holes with a high air-filling fraction and a small pitch (the distance between adjacent holes in the lattice). The fiber core was formed by including a larger air hole in the center of the perform, and the fiber cladding consists of a triangular array of air holes in silica [8]. By placing the air holes in a honeycomb lattice, one can introduce the core simply by adding an extra central air hole. This extra air hole causes a defect in the honeycomb photonic crystal at which light can be confined, and thus guided, provided that the surrounding photonic crystal cladding exhibits a PBG effect at the operating frequency.

The type of HC-633-1 from Crystal Fiber Company [9] is a commercial hollow-core PBG fiber which has a transmission window around 633 nm and the cross-section view of this fiber is shown in Fig. 3.3a. The typical attenuation spectrum from the datasheet is given in Fig. 3.4. In the wavelength range from 580 to 670 nm, the attenuation is smaller than 0.6dB/m. At the point of 633 nm, the value of attenuation is 0.49 dB/m (0.056/m) and it is much smaller than the value of 5216/m which is the attenuation of the simple hollow waveguide with the same bore diameter of 5.1 μm. From the near field intensity and corresponding intensity distribution shown in Fig. 3.5, it is clear that most of the light is well confined in the central big hole, which means the light will be amplified if there is gain medium in the central hole.

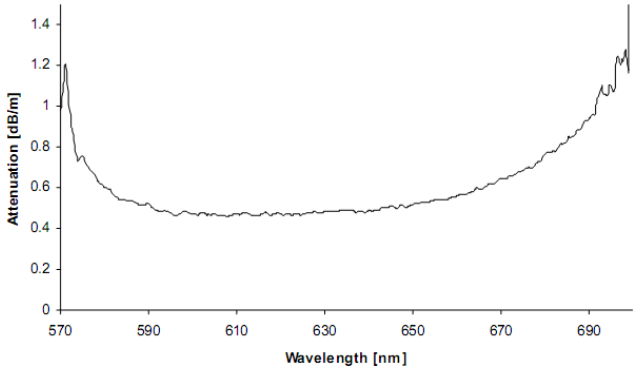

Figure 3.4 Typical attenuation spectrum [9].

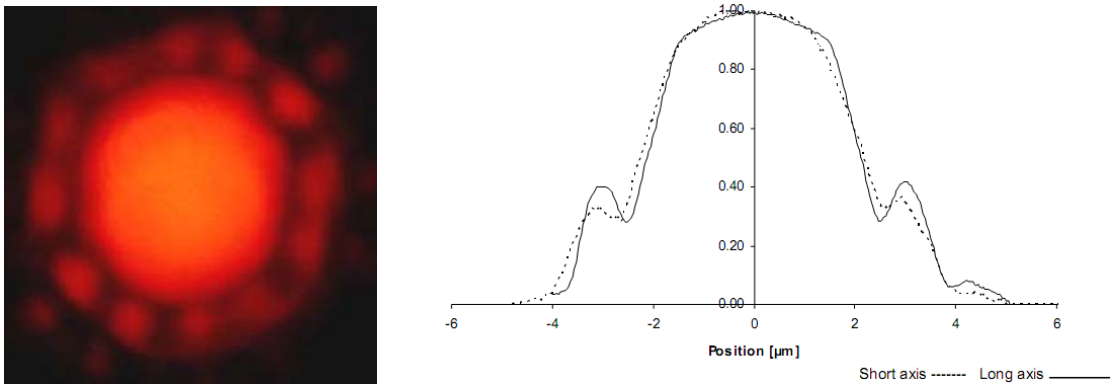

Figure 3.5 Near field intensity and corresponding intensity distribution of HC-633-1 [9].

The type of hollow-core PBG fiber shown in Fig. 3.3a has a structure with two-dimensional (2D) periodicity. In the following we will study the hollow-core Bragg fiber which has a one-dimensional (1D) periodic structure.

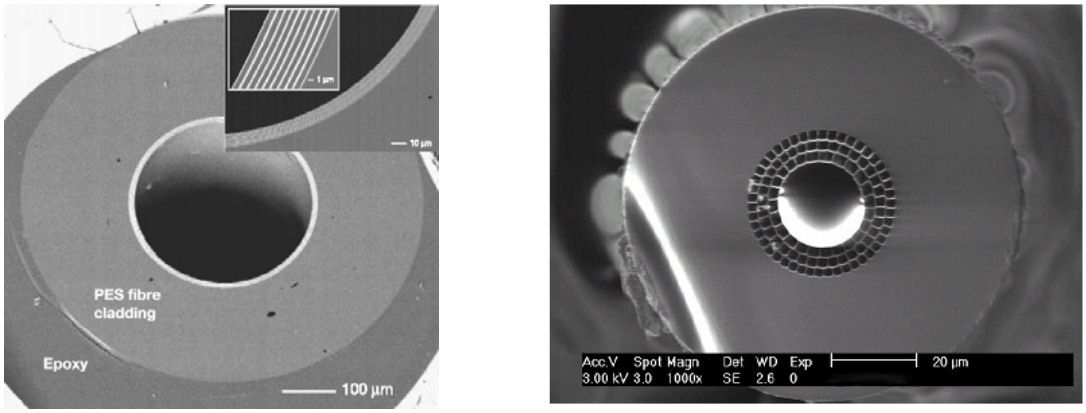

(a) (b)

Figure 3.6 Hollow-core Bragg fiber with (a) periodic PES-AS_2SE_3 cladding [10], (b) periodic air-silica cladding [11] respectively.

Hollow-core Bragg fiber can be divided into two types as shown in Fig. 3.6 [10, 11]. It is very clear that the structure in Fig. 3.6a is 1D periodic. The air-silica Bragg fiber shown in Fig. 3.6b seems a little different from that in Fig. 3.6a because of the tiny support bridge between the air-ring. However, since the support bridge thickness (~45nm) is much smaller than the optical wavelength of interest, we can, to a good approximation, neglect their presence and regard the region between the high index silica layers as composed entirely of air. Then its structure can be also viewed as 1D periodicity.

In the insert figure of Fig. 3.6a, the hollow core appears black, the poly(ether sulphone) (PES) layers and cladding appear grey, and the As_2Se_3 layers appears bright white. The diameter of the hollow core is ~275 μm; the PES layers (grey) have a thickness of 900 nm, and the As_2Se_3 layers (bright) are 270 nm thick (except for the first and last As_2Se_3 layers, which are 135 nm). Fig. 3.7 shows the transmission spectrums of such hollow-core Bragg fibers. In the Fig. 3.7a, the spectrums in blue and in red correspond to different refractive index contrast in the periodic structure. By varying the refractive index contrast, thickness of the layers and the diameter of the hollow-core, the fundamental photonic bandgap could be at 3.1 μm, at 3.55 μm or at 10.6 μm as indicated in the Fig. 3.7. The measured transmission loss at 10.6 μm was found to be less than 1.0 dB/m for the hollow-core Bragg fiber which has a hollow core with the diameter of 700 μm [10].

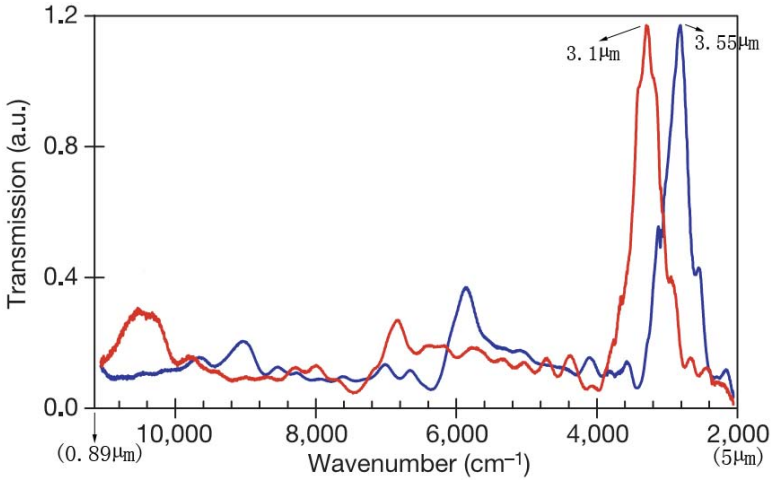

(a)

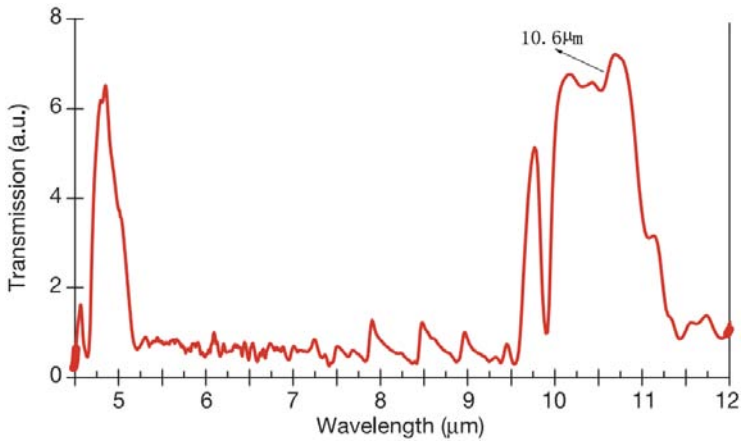

(b)

Figure 3.7 Transmission spectrums of hollow-core Bragg fibers which have fundamental photonic bandgaps at 3.1μm, 3.55μm (a) and ~10.6μm (b) respectively [10].

Ibanescu et al. presented the electric-field time-average energy density for the five modes in a transverse cross section of the waveguide as shown in Fig. 3.8 [12]. The color scheme is such that the energy density goes from zero (black) to maximum (yellow). The thin blue contours represent the contours between the different layers of the hollow-core Bragg fiber.

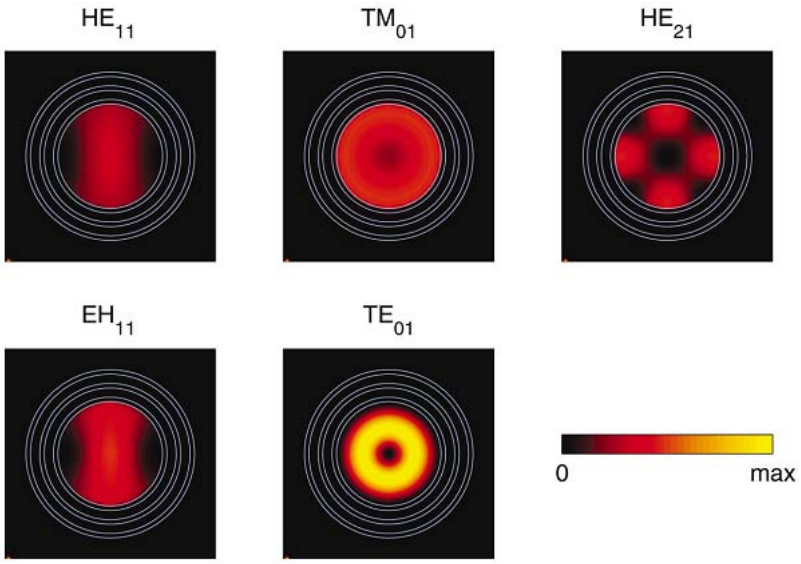

Figure 3.8 Transverse energy density of five modes [12].

Unlike the previous hollow-core Bragg fiber having cladding structures with a large index contrast, G. Vienne et al. reported another type of hollow-core Bragg fiber which has a air-silica structure as shown in Fig. 3.6b [11]. In this type of fiber, both the fiber core and the low index cladding layers are composed of air and others are composed of silica. The microstructure is 35 μm in diameter, with a 20 μm air core in its center. The silica rings are separated by 2.3 μm thick air rings comprising support bridges estimated to be only around 45 nm thick. They fabricated a series of fibers with different outer diameters (OD), and the transmission spectrums are shown in the Fig 3.9. This Bragg fiber supports low loss modes (less than 1 dB/m) in the wavelength range of 0.82 μm to 2.86 μm. The transmission window shifts to short wavelength when the OD of the fiber reduces.

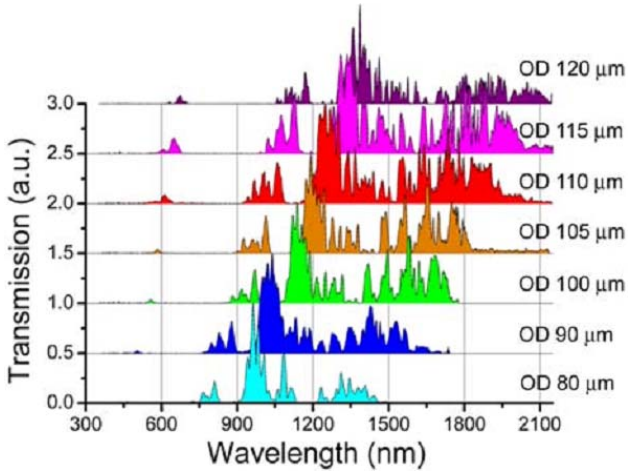

Figure 3.9 Transmission spectrums of hollow-core air-silica Bragg fibers with different ODs [13].

From the cutback measurement of a 50-m-long fiber, they found that the loss of the OD120 sample is approximately 1.5dB/m at a wavelength of 1.4μm, where the transmission spectrum reaches its peak. With only three rings of silica layers, the loss of this air-silica hollow-core Bragg fiber compares favorably with the previous introduced hollow-core Bragg fiber reported, which has nine Bragg cladding pairs and has a transmission loss approximately 1dB/m at the wavelength of 10.6μm. The numerical results from Foroni et al. indicate that the confinement loss (CL) values significantly decrease by more than one order of magnitude if increasing the number of layer from 3 to 4 for the OD90 fiber [14].

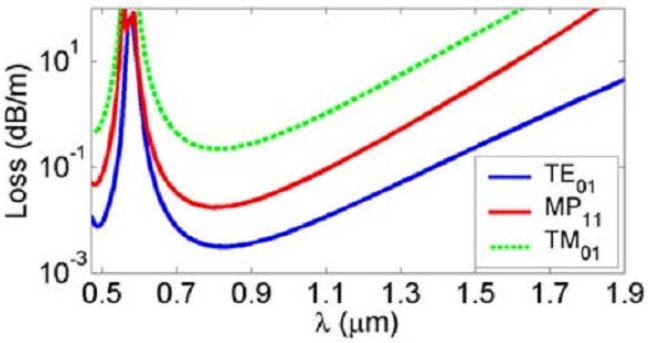

Figure 3.10 Confinement losses of the TE_{01}, TM_{01}, and HE_{11} modes in the OD90 sample calculated in [13].

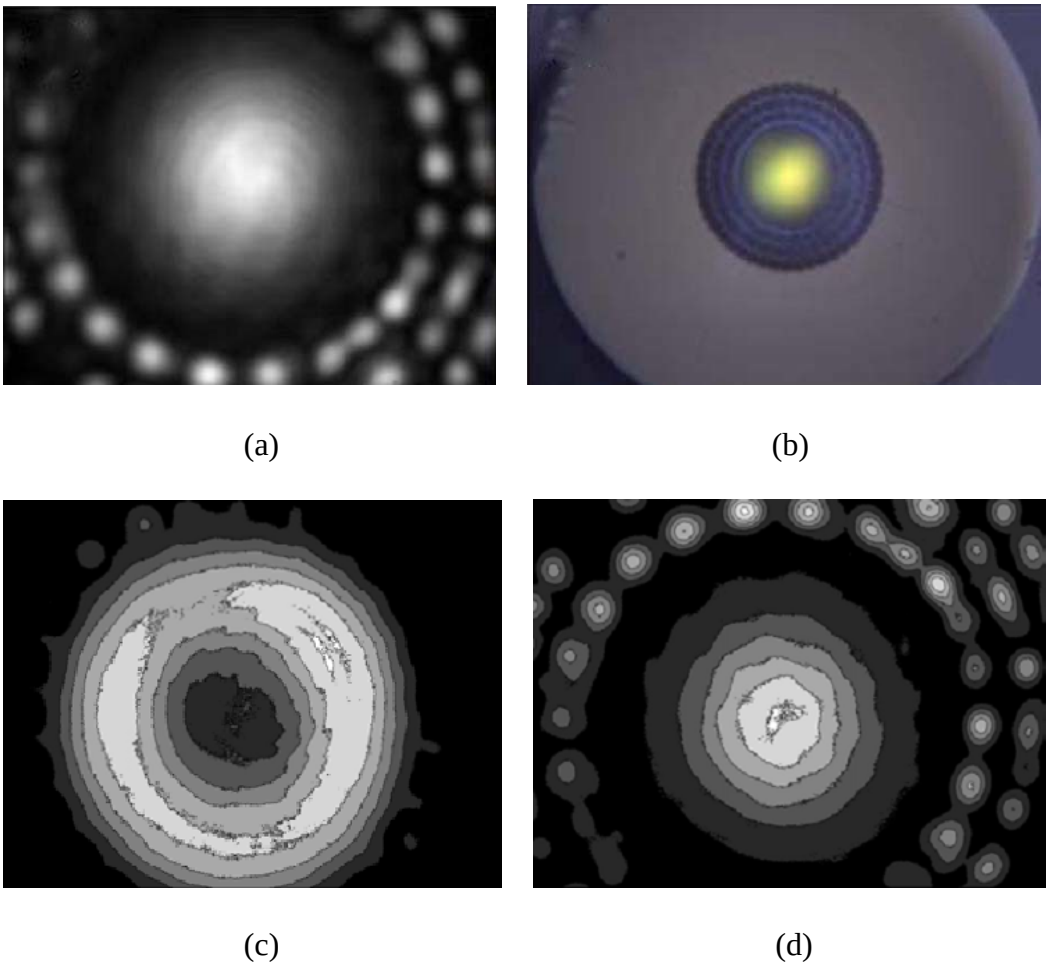

(a) (b)

(c) (d)

Figure 3.11 (a) The experimental mode profile in the OD90 sample at a wavelength of 1060 nm, (b) The image of the output facet of the OD105 sample with white light input [13]; Measured near field pattern (c) TE_{01} mode, (d) HE_{11} mode [11].

The confinement loss of TE_{01}, TM_{01}, and HE_{11} modes in the OD90 sample calculated by Vienne et al. [13] is presented in the Fig. 3.10. The MP_{11} used in the figure is mixed polarization mode and it equal to HE_{11} that is usually used in the literature. As indicated in Fig. 3.10, TE_{01} mode is the mode with lowest leakage loss in Bragg fibers. The leakage loss of the TE_{01} mode can be as small as less than 0.01dB/m around 0.8μm. This mode was ever attracted extremely interesting for telecommunications not only for the small loss, but also for no polarization degeneracy, and is therefore not subject to polarization mode dispersion (PMD) [15]. Observed

mode profile and the near field pattern of TE_{01} and HE_{11} modes are shown in the Fig. 3.11.

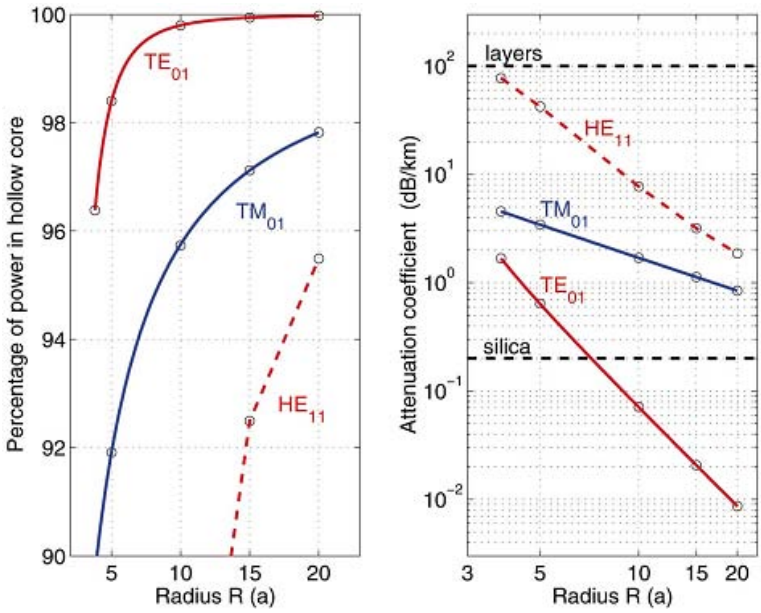

(a) (b)

Figure 3.12 (a) Percentage of power in the hollow core of Bragg fiber is plotted for three modes as a function of core radius; (b) The attenuation coefficient of the three modes is plotted as a function of core radius [12].

The two types of hollow-core Bragg fibers shown in Fig. 3.6 have similar structure that the low index layers are replaced by air layers in Fig. 3.6b. The confinement of electromagnetic energy in the hollow core of the Bragg fiber which has a similar structure as shown in Fig. 3.6a is plotted for three modes as a function of core radius [12]. Actual data is shown as open circles. The attenuation coefficient of the three modes is plotted as a function of radius. The attenuation coefficient in silica fibers (0.2dB/km) and a much larger attenuation coefficient (100dB/km) of the materials in the multilayer mirror are labeled in Fig. 3.12b. The core radius *R* in the Fig. 3.12 is in the unit of *a* which is the total thickness of a pair of layers. When the core radius *R* is

sufficiently big, the attenuation of TE_{01} mode will be very small and almost 100% of power of TE_{01} mode will well confined in the hollow-core of the Bragg fiber. It is same as the air-silica Bragg fiber that TE_{01} mode is the lowest-loss mode. There is also a little different from the air-silica Bragg fiber that the second lowest-loss mode is not the HE_{11} mode as shown in Fig. 3.10, but the TM_{01} mode.

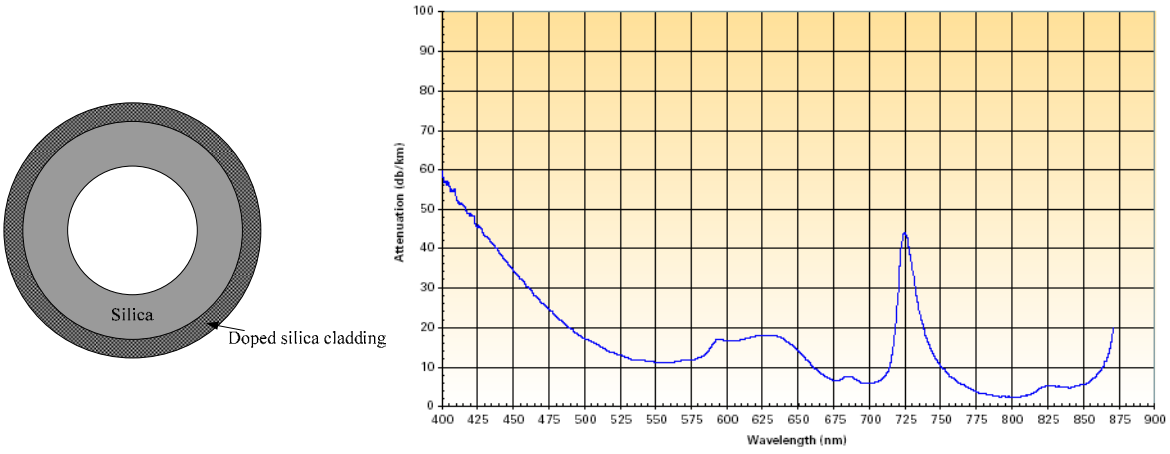

Figure 3.13 The schematic structure and attenuation of the light guiding capillaries [6].

Due to the exponential radial decay induced by the band gap of the hollow-core Bragg fiber, most of the electromagnetic energy will exist in the hollow core and some of it will mainly focus in the first few layers. More pairs of layers will lead to better confining performance and lower leaky loss. We will introduce another type of hollow-core fiber which has only one pair of layer. The schematic structure and attenuation of this fiber are shown in Fig. 3.13. The structure is so simple and similar to that of ordinary capillary and it is also called light guiding capillary. It has a low-loss transmission in the visible wavelength range. There are three sizes of bore diameter (D=50, 150 and 250 μm) in the commercial products [6]. The attenuation in Fig. 3.13 was from standard cut-back attenuation on 253m segment of light guiding capillary with D=150μm. The technician from Polymicro Company pointed out that

the attenuation curves of light guiding capillary with *D*=50, 250μm are close to that as shown in Fig. 3.13.

From Fig. 3.13, the attenuation of light guiding capillary with *D*=150μm is 0.0021/m (18.2dB/km) at 633nm and this value is suggested to be that of light guiding capillaries with *D*=50, 250μm. Compared with the values (5.5358, 0.205 and 0.0443/m) from Table 3.1, the waveguide loss is greatly reduced only by adding a layer of doped silica cladding. We speculate that the low-loss modes in this hollow-core fiber will also be TE_{01}, TM_{01} and HE_{11} modes like that of hollow-core Bragg fibers. Although it has low attenuation, the electromagnetic energy will extend more into the silica and doped silica layers when the bore diameter reduces due to its weak ability of confinement.

By varying the structure surrounding the central hollow core, the hollow-core PBG fiber, the hollow-core Bragg fiber and the light guiding capillary all obtain much lower waveguide loss than that of capillary waveguides in bulk glass which have the same bore diameters. The advances in these hollow-core fibers gave us the inspiration to develop novel fiber gas lasers based on such new hollow-core fibers. These novel waveguide structures break the limitation predicted by the simple hollow waveguide theory and provide us with the opportunity for building compact, flexible, and miniature fiber gas lasers which are expected to find applications in many fields.

3.2 Macro-bending losses in hollow-core fibers

One of the perceived advantages of fiber gas lasers is that the hollow-core fiber may be bent to small coils which allows longer cavity length to produce reasonably lasing without significantly increase of its physical size. This section discusses the

macro-bending losses in hollow-core fibers. Since there are two types of hollow-core fibers which have completely different guiding mechanisms as illustrated previously, their bend loss characteristics are expected to be different and we will discuss them respectively.

3.2.1 Bending loss in simple hollow waveguide

Marcatili and Schmeltzer [2] presented a theory to evaluate bending losses in hollow circular waveguides. To a curved hollow waveguide as shown in Fig. 3.14, the bending loss depending on bending radius *R* is derived as following form

$$\alpha_{nm}(R)=\alpha_{nm}(\infty)\left\{1+\frac{4}{3}\left(\frac{2\pi a}{u_{nm}\lambda}\right)^4\left(\frac{a}{R}\right)^2\cdot\left[1-\frac{n(n-2)}{u_{nm}{}^2}+\frac{3}{4}\delta_n(\pm1)\frac{\mathrm{Re}\sqrt{\nu^2-1}}{\mathrm{Re}\dfrac{\nu^2+1}{\sqrt{\nu^2-1}}}\cos 2\theta_0\right]\right\} \quad (3.10)$$

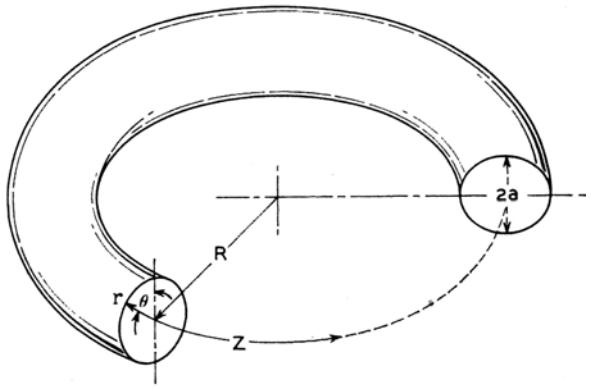

Figure 3.14 The curved hollow dielectric waveguide and the associated toroidal coordinate system (r, θ, Z).

where $\alpha_{nm}(\infty)$ is the attenuation constant for modes in the straight guide ($R=\infty$), u_{nm} is the m th root of the equation $J_{n-1}(u)=0$; $v=\sqrt{\varepsilon_1/\varepsilon_0}$, v is the refractive index of the waveguide, ε_1 and ε_0 are the complex electric permittivity of the external and internal media; θ_0 is the angle between the electric field direction and the plane of curvature.

Further from Eq. (3.10), the radius of curvature which doubles the straight guide attenuation is

$$R_0 = \frac{2}{\sqrt{3}}\left(\frac{2\pi}{u_{nm}}\right)^2 \frac{a^3}{\lambda^2}\left[1 - \frac{n(n-2)}{u_{nm}^{\ 2}} + \frac{3}{4}\delta_n(\pm 1)\frac{\mathrm{Re}\sqrt{\nu^2-1}}{\mathrm{Re}\dfrac{\nu^2+1}{\sqrt{\nu^2-1}}}\cos 2\theta_0\right]^{\frac{1}{2}} \qquad (3.11)$$

For a straight hollow glass waveguide with v=1.456, and inner diameter D=2a, λ=0.6328μm, the bending loss for EH_{11} mode doubles its straight attenuation loss when R_0≈46m for D=250μm; for D=50μm, R_0≈0.37m; and for D=5.1μm, R_0≈0.4mm.

Miyagi [16] pointed out that the theory of Marcatili and Schmeltzer [2] didn't consider field deformations depending on R^{-2} (R; bending radius) which substantially affect the bending losses in their formulation, i.e., the power losses can be evaluated by the ratio of the radiated power from a waveguide per unit length and the total power carried by the mode of the waveguide. The experiment studying on bending losses of the TE_{01} mode in metallic waveguides at infrared [17] also indicated that the theory of Marcatili and Schmeltzer should be modified so as to include the higher losses due to the mode coupling effect. Miyagi [18] presented a new method to evaluate the propagation constants in the general class of circular bent waveguides characterized by a surface impedance and admittance. Their bending loss formulas are completely different from the theory of Marcatili and Schmeltzer and believed to be more accurately.

The normalized attenuation constant α/α_∞ in curved dielectric or metallic hollow waveguide can be expressed as following:

$$\frac{\alpha}{\alpha_\infty}=1-\frac{1}{6}\left(\frac{2\pi a}{u_{0m}\lambda}\right)^4\left(\frac{a}{R}\right)^2\left\{1-3\frac{\mathrm{Re}\left[\frac{\nu^2}{(\nu^2-1)^{1/2}}\right]}{\mathrm{Re}\left[\frac{1}{(\nu^2-1)^{1/2}}\right]}\right\} \qquad \mathrm{TE}_{0m}\ \text{mode} \qquad (3.12)$$

$$\frac{\alpha}{\alpha_\infty}=1-\frac{1}{6}\left(\frac{2\pi a}{u_{0m}\lambda}\right)^4\left(\frac{a}{R}\right)^2\left\{1-3\frac{\mathrm{Re}\left[\frac{1}{(\nu^2-1)^{1/2}}\right]}{\mathrm{Re}\left[\frac{\nu^2}{(\nu^2-1)^{1/2}}\right]}\right\} \qquad \mathrm{TM}_{0m}\ \text{mode} \qquad (3.13)$$

$$\frac{\alpha}{\alpha_\infty}=1+\frac{1}{3}\left(\frac{2\pi a}{u_{nm}\lambda}\right)^4\left(\frac{a}{R}\right)^2\left\{1-\frac{4n(n-2)}{{u_{nm}}^2}+\frac{3}{8}\delta_n(\pm1)\frac{\mathrm{Re}[(\nu^2-1)^{1/2}]}{\mathrm{Re}\left[\frac{\nu^2+1}{(\nu^2-1)^{1/2}}\right]}({u_{nm}}^2-2)\cos 2\theta_0\right\}$$

EH_{nm} mode (3.14)

For a straight hollow glass waveguide with ν=1.456, and inner diameter D=2a, λ=0.6328μm, the bending loss for EH_{11} mode doubles its straight attenuation loss when R_0≈28.5m for D=250μm. For D=50μm, R_0≈0.23m; and for D=5.1μm, R_0≈0.24mm.

Although the bending radius R_0 decreases with the decreasing of inner diameter of the hollow circular waveguide, the waveguide loss increases rapidly as indicated in Table 3.1 for simple waveguide as shown in Fig. 3.1. It seems that bending loss would not be a big problem for small size hollow-core fibers with inner diameter smaller than 50μm if the straight waveguide loss could be reduced by proper waveguide design.

3.2.2 Bending loss in PBG waveguide

Several researchers [19-22] calculated bending losses in solid-core PCFs, and their results indicate that solid-core PCFs can be bent to several centimeters while keeping very low bending loss. Olszewski et al. [23] predicted that bending loss in large mode area photonic crystal fibers oscillates with wavelength as shown in Fig. 3.15. Martynkien et al. [24] carried out loss measurements for different fiber bend radii and

for different angular orientations and their results confirm the oscillatory behavior of bending loss vs. wavelength predicted by Olszewski et al.

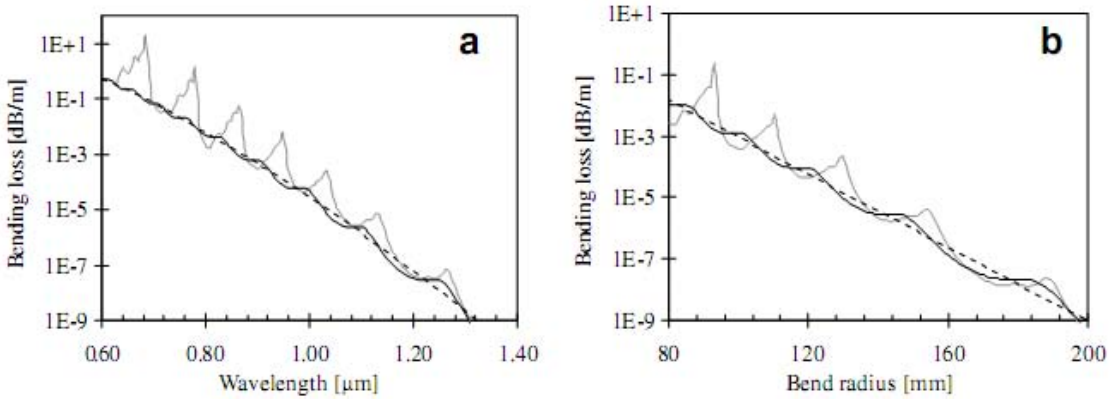

Figure 3.15 (a) Comparison of spectral dependence of bending loss calculated using the FEM (solid gray line) and the simplified analytical formula with and without oscillation term (respectively solid black and dashed black line). The calculations were performed for the fiber with the following structural parameters: Λ =10μm, d/Λ = 0.4, Nr = 10, and bending radius R = 100 mm; (b) The dependence of the bending loss on bending radius calculated for the same fiber at λ= 0.8μm [23].

Hansen et al. [25] investigated macro-bending losses in two types of hollow-core PBG fiber with cores formed by re-moving both 7 and 19 unit cells. The fibers have core diameters of approximately 10 μm and 15 μm, and they support single mode and multimode transmission respectively. The cladding structure of the single-mode fiber is comprised of ten rings of holes while the multimode fiber has eight rings of holes surrounding the core.

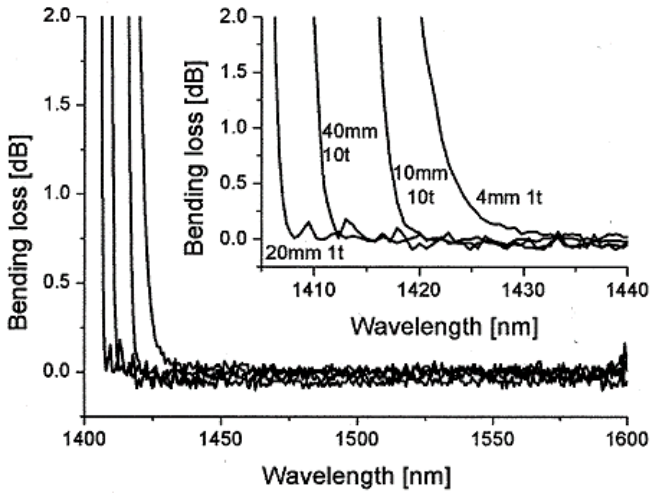

Figure 3.16 Loss measurements for the single-mode hollow-core PBG fiber with core diameter of 10 μm [25].

To measure the macro-bending loss, firstly a straight-fiber reference measurement was performed. While the coupling conditions were maintained, the fibers were then subject to different degrees of bending. Bends of 40 mm (10 turns), 20 mm (1 turn), 10 mm (10 turns), and 4 mm (1 turn) were studied. A splice to a standard single mode fiber pigtail was used to maintain stable coupling conditions to the single mode fiber. Their results are shown in Fig. 3.16 and 3.17. Except for the short wavelength edge, the measured bending loss is 0dB±0.1dB as shown in Fig. 3.16. Only at the short wavelength transmission band edge, the bending seems to induce loss. The accuracy of the measurements depends on the position in the bandgap.

Fig. 3.17 shows the transmission spectra measured for the multimode hollow-core PBG fiber. The same qualitative behavior as for the single-mode hollow-core PBG fiber is seen. At a local maximum, the transmission spectra are in excellent agreement, within 0.2 dB, while rapid fluctuations are seen at the local minima. As the transmission minima are caused by coupling between the core mode and surface modes,

a process that is highly sensitive to environmental changes to the fiber, such fluctuations are expected.

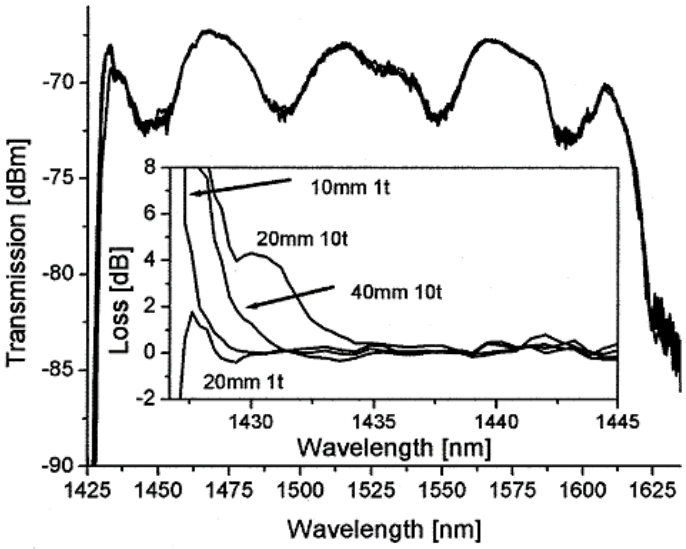

Figure 3.17 Loss measurements for the multi-mode hollow-core PBG fiber with core diameter of 15μm [25].

Both hollow-core photonic bandgap (PBG) fibers and solid-core photonic crystal fibers (PCFs) can be bent to circles with diameter about several centimeters while keeping very small loss. Comparing with the simple hollow waveguide, the macro bending loss in hollow-core PBG fibers is much smaller due to their special guiding mechanism and stronger confinement ability.

The Macro-bending loss of the hollow-core Bragg fiber with periodic PES-AS_2SE_3 layers is shown in Fig. 3.18. Fig. 3.18a was measured by using a Fourier Transform Infrared (FTIR) spectrometer. The fibers were bent at an angle of 90 degrees around metal cylinders of varying radii. A straight length of fiber after the bend was held constant at ~15 cm. In the measurement of Fig. 3.18b, the fiber was ~2.5 meters long with a core diameter of 700 microns and was bent 15 cm from the output. Loss values are obtained by comparing the total transmitted power through the bent fiber to the

same fiber when held straight [26]. The total bending loss is below 1dB for the bend with the largest radius and this loss increases by a few tenths of a dB with decreasing bend radius.

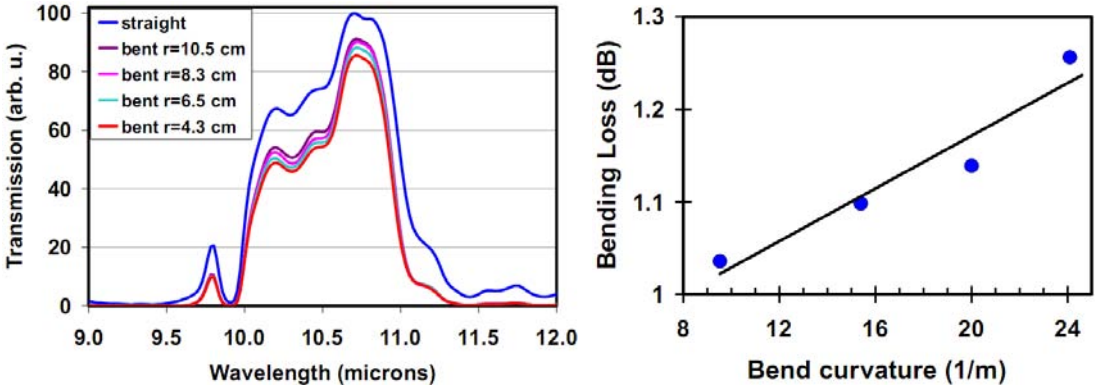

(a) (b)

Figure 3.18 (a) Transmitted intensity vs. wavelength for a ~50 cm long hollow fiber measured using an FTIR spectrometer; (b) Measured bend loss vs. bend curvature for CO_2 laser transmission through 90 degree fiber bends [26].

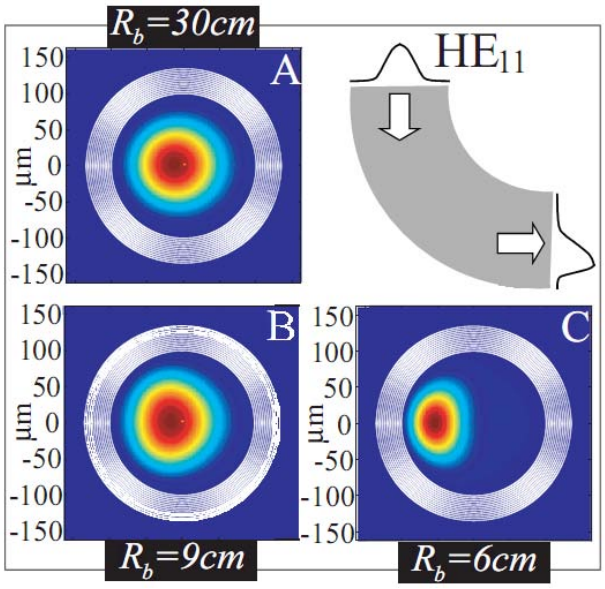

Figure 3.19 Plots of intensity distribution of hollow-core Bragg fiber at the bend output, under HE_{11} launching conditions for various values of bending radius [27].

Intensity distribution at the bend output, under HE_{11} launching conditions for

various values of bending radius, is shown in Fig. 3.19. With the reducing of bending radius, Intensity distribution of HE_{11} will shift to the opposite direction of bending [27]. This shifting leads to the coupling between HE_{11} mode and high-order modes with higher loss. When the bending radius becomes small, the coupling becomes bigger and lead to larger bending loss.

Since the inter-mode coupling coefficient depends on the difference in the propagation constant between modes. Reducing the core size will reduce the number of propagating modes and thus may also reduce the bending losses. This conclusion is similar to that obtained for the simple hollow waveguide discussed in previous section. However, decreasing the core size should also increase total propagation losses due to material interaction, increased radiation.

It must be mentioned that the two types of hollow-core Bragg fibers have still no commercial products. There are no hollow-core Bragg fibers optimized to match the laser wavelengths of He-Ne mixture at which achieving very small attenuation. The existing hollow-core fibers that can be used as laser tube of fiber He-Ne gas lasers are the hollow-core PBG fiber (HC-633-1) and the light guiding capillaries introduced previously. Since HC-633-1 have bore diameter of 5.1 μm, it is hard to achieve stable discharge in such small bore size and bring other technical problems that will be discuss in the following chapter. Although light guiding capillaries have bigger bore diameters of 50, 150 and 250 μm, their weak ability of confinement make them unsuitable to construct fiber gas lasers that have coiled cavity. Our experiments will base on HC-633-1 and light guiding capillaries. The effort to find better hollow-core fibers which have sufficient large bore diameter and small waveguide loss at the laser

wavelengths will also need to be made.

3.3 Coupling efficiency in hollow waveguide laser resonator

The waveguide losses have been discussed in the previous section. In this section we will discuss the coupling losses between the waveguide mode and the cavity. Coupling loss represents the fraction of the radiation which is not converted into the fundamental waveguide mode after reflection from a cavity mirror [28]. It is natural to divide these losses into two parts: the aperture part, representing the fraction of the radiation escaping outside the waveguide aperture, and the non-aperture part, which is the radiation that reaches the waveguide, but is not converted into the fundamental waveguide mode, acting as a perturbation of this mode, and is transformed into higher order waveguide modes.

3.3.1 Types of waveguide laser resonator

There are different types of feedback used in waveguide gas lasers. Laser feedback may be implemented in several ways. The most common approach is to insert the waveguide into a Fabry-Perot resonator using internal (Fig. 3.20a) or external (Fig. 3.20b) mirrors. Alternatively, one may use distributed feedback (Fig. 3.20c), distributed Bragg reflection (Fig. 3.20d) or a ring configuration (Fig. 3.20e). Following Wang [29], we define a distributed feedback (DFB) laser as one in which the backward Bragg scattering is confined to the active medium and a distributed Bragg reflector (DBR) laser as one in which the Bragg scattering is limited to regions beyond the active medium, as shown in Fig. 3.20c and 3.20d respectively. In both cases, the backward Bragg scattering is caused by periodic variations in the properties of the

waveguide. Such a variation can be implemented through the use of corrugated guides or gratings etched into one or more surfaces of the guide. These techniques, usually used in conjunction with planar guides, are of interest because of their compatibility with the planar processing technology of integrated optics. The periodic structures also play a role in defining the operating frequency of the laser and are sometimes used to couple radiation from the guide.

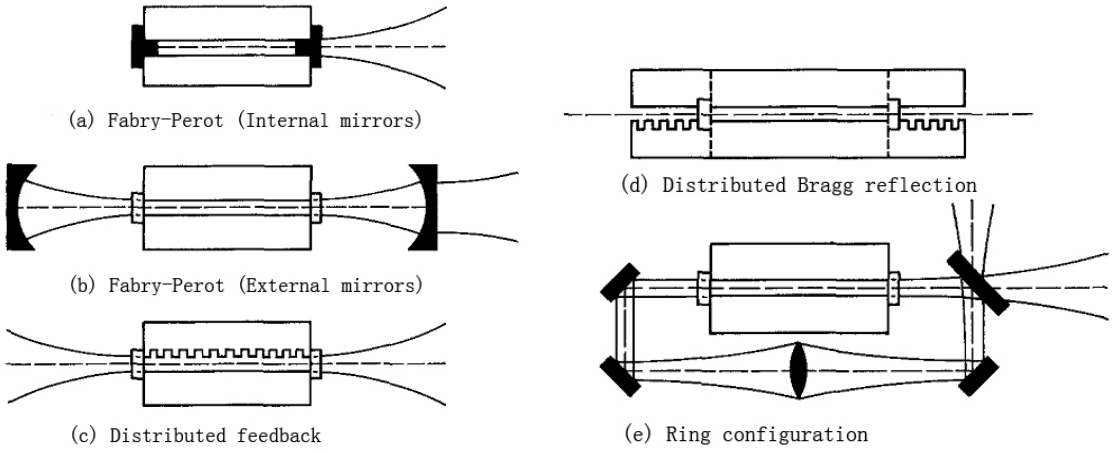

Figure 3.20 Various types of waveguide laser resonator [29].

In these different feedback configurations shown in the Fig. 3.20, the feedback as shown in 3.20a and 3.20b are most commonly used in the waveguide gas lasers that had been reported in the literatures. The feedback in Fig. 3.20a can be viewed as the special case of that in Fig. 3.20b that the distances between the laser tube and two mirrors are zero. The variant type that one side has an internal mirror and the other side has an external mirror is also used in waveguide gas lasers. The feedback in Fig. 3.20c and 3.20d are popularly used in semiconductor lasers and solid-state fiber lasers, while the feedback in Fig. 3.20e is used in both gas lasers (e.g. ring laser gyro-RLG) and fiber lasers. It seems that all the configurations except that one in Fig. 3.20c may be used for fiber gas lasers, and we will discuss each of the configurations in the

following section.

3.3.2 Three low loss configurations in the Fabry-Perot resonator

We will discuss the feedback configurations shown in Fig. 3.20a and 3.20b in this section. Fig. 3.21 shows the schematic of one mirror and one end of the laser tube. When $R = \infty$ and $z = 0$, it will be the case shown in Fig. 3.20a.

In the section 3.1 we discussed the waveguide loss in hollow-core fibers. From the discussion different types of hollow-core fiber have different lowest-loss modes due to the design of the waveguide. Normally the lowest-loss mode in the hollow-core fibers is one of the three low-order modes: HE_{11}, TE_{01} and TM_{01} mode, and we will discuss the problem of coupling by considering the single HE_{11} mode as an example.

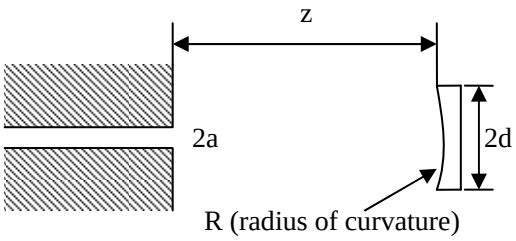

Figure 3.21 Geometry for calculation of coupling loss.

The HE_{11} mode is circularly symmetric, linearly polarized, and contains over 98% of its energy in a central lobe. Since a resonator mode dominated by the HE_{11} waveguide mode is desirable for most applications, it is of interest to determine those mirror configurations which efficiently couple the HE_{11} mode back into the guide. Abrams [30], and also Degnan and Hall [31] have computed the fraction of energy returned to the guide in the HE_{11} mode after the same mode is launched into free space and returned to the guide by an external spherical reflector. Abrams define the confocal parameter of the “approximating Gaussian” as

$$b = \pi w_0^2 / \lambda_0 \tag{3.15}$$

where λ_0 is the free-space wavelength, and w_0=0.643562a is the radius of the Gaussian beam waist which maximizes the overlap integral of a Gaussian with the HE_{11} mode distribution in a circular guide of radius a.

The confocal parameter introduced by Abrams [30] is useful in explaining the qualitative features of the coupling feature. From conventional resonator theory [32], the phase front curvature a distance z from the Gaussian beam waist is given by

$$R = b(\frac{z}{b} + \frac{b}{z}) \tag{3.16}$$

Degnan and Hall have considered finite mirror apertures in the modeling that Abrams has omitted in his calculation, and they set other basic parameters in the calculation:

$$\alpha = k_0 a^2 / R \quad \beta = z / R \quad \gamma = d / a \tag{3.17}$$

Where $k_0 = 2\pi / \lambda$ and d is the radius of the mirror (assumed equal to ∞ in the Abrams' calculations). The α used in Eq. (3.17) is different from that used as loss coefficient in previous section.

Eventually Abrams [30] and Degnan [31] both obtained similar conclusions for three low loss configurations (< 2%):

I) Flat mirrors close to the guide entrance ($R/b = \infty$, $z/b < 0.1$, or $\alpha = 0$, $\beta \approx 0$)

II) Large radius of curvature mirrors whose centers of curvature lie approximately at the guide entrance ($z \approx R \geq 8b$, or $\alpha \leq 0.6$, $\beta \approx 1$)

III) Shorter radius of curvature mirrors a distance one-half the radius of curvature from the guide ($R/b = 2$, $z/b = 1$ or $\alpha = 2.415$, $\beta = 0.5$)

For case I, 100% coupling efficiency will be achieved for all waveguide modes by placing the flat directly against the guide. Moving the flat a small distance *z* from the guide entrance introduces an HE_{11} coupling loss given by

$$\rho = 57(\frac{z}{b})^{3/2} \ [\%] \qquad (\frac{z}{b} \le 0.4) \tag{3.18}$$

Case II is also relatively easy to understand. At a sufficiently large distance from the waveguide aperture, the launched waveguide mode evolves into its far-field distribution with spherical wave fronts centered approximately at the guide entrance. If a spherical mirror having a curvature matching the phase front is placed at that position, the electric field distribution emerging from the guide is imaged back onto itself with near-perfect fidelity. Clearly, the above argument is insensitive to the shape of the field distribution at the guide implying that Case II is a low-loss configuration for all waveguide modes in the limit of large apertures. As in Case I, therefore, the spatial distributions of the resonator modes in the guide are very nearly identical to those of the individual waveguide modes. Unlike Case I, however, additional transverse mode discrimination can be provided by limiting the aperture of the external mirror.

Case III, the mirror is sufficiently near-field relative to the guide so that the curvature of the impinging wave front differs significantly with waveguide mode number. Thus, unlike the HE_{11} mode, higher-order waveguide modes are not coupled with high efficiency back into the guide. Higher-order modes diverge more rapidly than the fundamental HE_{11} mode. Specifically, it has been shown that, while the HE_{11} mode suffers a coupling loss of only 1.4%, the HE_{12} mode loss is about 78%. Thus, Case III is interesting because it provides excellent transverse mode discrimination even with large mirror apertures.

Kubarev [33] found a small 'technical' error in Ref. [30] when calculating the phases of the Gaussian modes. This error alerts the optimal cavity configurations and increases the minimal losses. Although in other cases the differences are small, this is not a priori evident without solving the problem rigorously. Kubarev [33] recalculated the coupling loss for HE_{11} mode, and obtained a little different result from the Abrams [30]. The cavities of three types have mirrors with the optimal curvature and the mirrors are located at distance in the following three ranges:

$$z/b \le 0.12, \quad z/b \ge 8.3, \quad 0.77 \le z/b \le 1.27 \tag{3.19}$$

The selected criterion satisfies simultaneously two conditions for the optimal mirror: the coupling losses should be $\le 2\%$, and the non-aperture part of the coupling losses should be $\le 1\%$.

The first and second ranges of distances have been used for a long time in practice. The first range corresponds to the "classical" waveguide lasers with plane mirrors near the waveguide ends [34-39]. Experiments show that when the distances between a mirror and the waveguide are small, the coupling losses are very low: they are much less than the other internal losses in the cavity.

The second optimal range of distances began to be used from the moment of appearance of infra-red (IR) and visible-radiation waveguide lasers. These lasers have a capillary waveguide and spherical mirrors located at large distances from the waveguide ends. Although in the first such lasers the distance was not optimal (z/b=3.2 in Ref. [40] and z/b=2.6 in Ref. [41]), already in the work reported in Ref. [42] the mirrors were located at a distance z/b=5.5. It was demonstrated experimentally [43] that the output power of a laser increases on reduction in the internal cavity losses

when the parameter z/b is increased from 7.6 to 19.7. The range of large distances z/b corresponds to the far-field zone where all the Gaussian modes have approximately the same phases and, therefore, a mirror with $R \approx z$ inverts the amplitude and the phase of the field at the waveguide end.

In many cases—such as free-electron lasers (FELs), sub-millimeter and IR lasers with intracavity components—the distance between a mirror and the waveguide end must not be too small and at the same time not too large. In such cases it is desirable to use the third optimal range of distances ($0.77 \le z/b \le 1.27$).

3.3.3 Calculations for small bore size hollow-core fibers

From the conclusions of Abrams [38], Degnan [31] and Kubarev [33], we can calculate the cavity parameters for the different dimensions of hollow-core fibers that will be used in our experiments.

Table 3.2 Cavity parameters for 632.8nm (He-Ne) with different bore diameters

$2a$	Case I (loss=1.3%)		Case II (loss=1.3%)			Case III (loss=1.3%)		
(μm)	R(cm)	z(cm)	R(cm)	z(cm) $z \approx R$	d(mm)	R(cm)	z(cm)	d_{opt}(mm)
5.1	∞	1.07×10^{-4}	0.01 2.5 25	0.01 2.5 24.95	0.05 11.6 115.7	2.67 $\times10^{-3}$	1.34 $\times10^{-3}$	6.1 $\times10^{-3}$
50	∞	0.01	1.03 2.5 25	1.03 2.5 24.95	0.5 1.21 12.1	0.257	0.1285	0.06
100	∞	0.04	4.14 25	4.13 24.95	1 6	1.028	0.514	0.12
150	∞	0.09	9.31 25	9.29 24.95	1.5 4	2.313	1.16	0.18
250	∞	0.25	25.86 50	25.8 49.9	2.5 4.8	6.42	3.21	0.3
430	∞	0.75	76.5 100	76.34 99.8	4.2 5.5	19.01	9.51	0.52

The typical hollow-core PCF (HC-633-01) of Crystal-fiber Company which can

support a single mode and low loss transmission for 632.8nm wavelength has a 5.1μm-diameter core. The light guiding capillaries of Polymicro Company have a series of inner-diameters: 50μm, 150μm and 250μm. The calculated cavity parameters are shown in Table 3.2.

The bore diameters, radii of curvature of the mirrors, the distance and the diameter of the mirrors listed in the Table 3.2 correspond to the coupling loss of 1.3%. For case I, the loss reduces with the decreasing the distance *z*. In case II, if *R*=25cm is chosen for 2*a*=50μm, the loss will be smaller than 1.3% if the radius of mirror is bigger than 12.1mm. For case III, the *R* can only vary in a small range around the value listed in Table 3.2 for different bore diameters. The *d* listed in Table 3.2 for case III are optimal values. The loss of ~1.3% is the lowest value that can be achieved in Case III.

As shown in Table 3.2, the radius of curvature of the mirror decreases when the bore diameter of the waveguide becomes smaller for case III. For the hollow-core PCF with 5.1μm-diameter core the *R* need to be 26.7 μm for case III which is impractical for spherical reflection mirrors. It is easier to make mirrors with larger radius of curvature than making small ones. When the bore diameters are small than 150 μm, the *R* becomes very small, which means that it is difficult to find suitable mirrors for case III.

In case II, we can use mirrors with large *R*, however, the needed size (*d*) of the mirror will become large. For example, when 2*a*=5.1μm, if *R*=25cm is selected, only $d \geq 115.7$mm can achieve a loss lower than 1.3%. For small bore size hollow-core fibers ($2a<50\mu m$), the increasing of *R* will lead to the need of large size of mirror. However, larger value of *R* corresponds to a longer distance of *z*. Supposed *R*=25cm, *z* will be

24.95cm. It is no big deal for conventional gas lasers, for example, He-Ne lasers use a Brewster window to seal the end of laser tube and place the mirror a distance of 24.95cm away. But it will be a big problem for hollow-core fibers since fixing a Brewster window on the end of hollow-core fibers is not as easy as conventional He-Ne lasers. We also can remove this window, but it will need a large size of chamber to include the distance of 24.95cm.

Hence, case I (flat mirror near the end of the waveguide) seems the best choice of the design for hollow-core fibers. If the case I is selected as the cavity configuration, the maximum allowed distance between the flat mirror and the end of the waveguide decreases with the reduction of the tube diameter, provided that the coupling loss smaller than 1.3% is requested. When the D=5.1μm, the flat mirror is almost needed to touch the end of the hollow-core fiber. For the case I used in hollow-core fibers with D<250 μm, the small distance between the flat mirror and the end of tube will bring new problems if conventional DC excitation or combination of DC and RF excitation is adopted, for example, the discharge current will easily damage the surface of the mirror caused by thermal effect. Evacuating the gases in the hollow tubes will become difficult because of the small clearance. The latter chapter will discuss these problems in detail.

3.3.4 Other potential feedback designs for hollow-core fibers

We have discussed the Fabry-Perot configuration for hollow-core fibers in the previous section and we will present other potential designs for hollow-core fibers in this section.

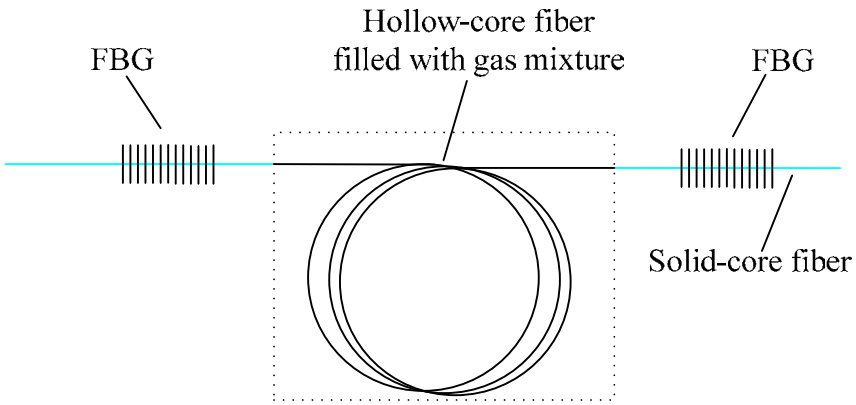

Figure 3.22 Feedback configuration based on FBG.

For our concerning that use the hollow-core fiber as the laser tube, it seems that the type shown in Fig. 3.20d is the most suitable one in the all types. The technique of fiber Bragg grating (FBG) has ripened over the past two decade. The high reflectivity (>99%) has been obtained for many wavelengths [44, 45]. Similar to the structure shown in Fig. 3.20d, it is natural to achieve a feedback configuration as shown in Fig. 3.22.

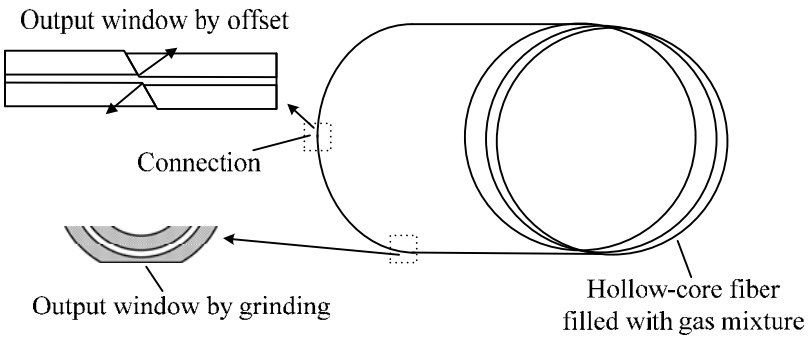

Figure 3.23 Self-ring with output window by grinding.

Laser tubes based on hollow-core fibers can more easily form a ring cavity than that shown in Fig. 3.20e. If other things are not considered, connecting the two ends of a hollow-core fiber will form a ring cavity as shown in Fig. 3.23. Two ways of achieving the output window are shown in Fig. 3.23. We can either grind a small part of the hollow-core fiber to form a output window, or cut the end of fiber at an angle

and make the two ends misaligned to form a output window.

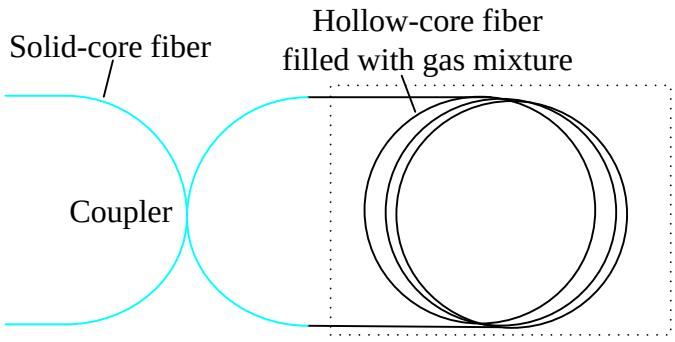

Figure 3.24 Ring feedback based on fiber coupler respectively.

Fig 3.24 presents another type of design of feedback configuration. This structure uses a fiber coupler to form a ring cavity. We can easily acquire a output from the fiber and connect this device with other components conveniently. If the coupler could be the form of hollow-core fibers, it can be more easily used.

There is a technical problem for feedback configurations shown in Fig. 3.22 and Fig. 3.24. The connection loss between the hollow-core fiber and the normal solid-core fiber can not be neglected when building He-Ne gas laser which has a small gain.

The most popular method of connection is the splicing. For the case of splicing between hollow-core PBG fiber and single-mode fiber, splice losses in the range 1-2.3dB were demonstrated in recent publications [46-51]. It is estimated that a perfect splicing procedure yield a loss of 0.6-0.8 dB. Of this, 0.15 dB arises from the refractive index mismatch between the fiber cores, and is therefore fundamental. The rest is due to modal field mismatch, which is estimated by the butt-joint approximation to be 0.4-0.6 dB [46]. There exists the action of surface tension along the many glass-air interfaces within the holey structure during the splicing, the viscosity of which offers much less resistance to deformation than the solid glass in the outer cladding of the

fiber. The end view in Fig. 3.25 clearly indicates this effect. Even the minimum splicing loss 0.6 dB equals to 12.9% loss, this loss is much bigger than the tolerance loss in He-Ne gas lasers.

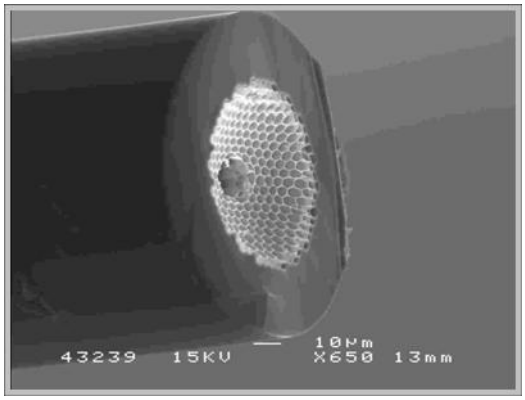

Figure 3.25 End view of a hollow-core PBG fiber cleaved at the junction of splice [46].

For the case of connection between the normal hollow-core fiber (structure without air-silica layers) and the solid-core fiber, the loss may be smaller than previous case. But 4% of Fresnel reflection can not be eliminated and this minimum loss shall be considered. The summation of this loss and reflection loss in fiber Bragg grating makes it difficult to make a fiber gas laser.

However if the sufficient longer fiber gas laser can be implement in the future, enough gain will make the types shown in Fig. 3.22 and 3.24 the best choices because output laser from the normal fiber makes it convenient in many applications. Although the type shown in Fig. 3.22 and 3.24 is potentially the most suitable one in the all types, it still can not be adopted as our first choice at present.

It seems all the configurations except that one in Fig. 3.20c may be used for fiber gas lasers. There was no report about forming a mirror inside the hollow-core fiber at past. However the recent report [52] about the long period grating in hollow-core PBG fibers provides the possibility of this configuration although a lot of investigations

shall be carried to achieve a good reflectivity at the desired wavelength.

3.4 Summary

In this chapter, we investigated the waveguide loss and macro-bending loss for different types of hollow-core fibers. Normally the lowest-loss mode in the hollow-core fibers is one of the three low-order modes: HE_{11}, TE_{01} and TM_{01} mode, and we discussed the problem of coupling loss by considering the single HE_{11} mode as an example. Small waveguide losses of the hollow-core fibers indicate that they can be good waveguides to confine light beam in the hollow core as well as discharge tube. Theoretical calculations of coupling loss indicate flat mirror close to the end of hollow-core fiber is an efficient feedback configuration for the hollow-core fiber to form a laser cavity. Besides the structure of Fabry-Perot cavity, other types of feedback configurations such as using FBG and ring-form are also investigated. Due to the loss of connection, flat mirror closed to the end of hollow-core fiber seems to be the best choice at present.

References

1. P. W. Smith, “A waveguide gas laser,” *Appl. Phys. Lett.*, vol.19, pp.132-134, 1971.
2. E. A. J. Marcatili and R. A. Schmeltzer, “Hollow metallic and dielectric waveguides for long distance optical transmission and lasers,” *Bell Syst. Tech. J.*, vol. 43, pp. 1783-1809, 1964.

3. J. J. Degnan and D. R. Hall, “Finite-aperture waveguide-laser resonators,” *IEEE J. Quantum Electron.*, vol. 9, pp. 901-910, 1973.

4. S. Wang, “Proposal of periodic layered waveguide structures for distributed lasers,” *J. Appl. Phys*, vol. 44, pp. 767-780, 1973.

5. V. W. H. Seelig, “Verstärkung von He-Ne-Lasern mit sehr dfünnen Entladungsrohren,” *J. Appl. Math. Phys. (ZAMP)*, vol. 25, pp. 728-736, 1974.

6. http://www.polymicro.com.

7. R.F. Cregan, B.J. Mangan, J.C. Knight, T.A. Birks, P.St.J. Russsell, P.J. Roberts, and D.C. Allan, “Single-Mode Photonic Band Gap Guidance of Light in Air,” *Science*, vol.285, pp.1537-1539, 1999.

8. J. C. Knight, T. A. Birks, P. S. J. Russell, and D. M. Atkin, “All-silica single-mode optical fiber with photonic crystal cladding,” *Opt. Lett.*, vol. 21, pp. 1547-1549, 1996.

9. http://www.crystal-fibre.com.

10. B. Temelkuran, S. D. Hart, G. Benoit, J. D. Joannopoulos, and Y. Fink, “Wavelength-scalable hollow optical fibres with large photonic bandgaps for CO_2 laser transmission,” *Nature*, vol. 420, pp. 650-653, 2002.

11. G. Vienne, Y. Xu, C. Jakobsen, et al., “First demonstration of air-silica Bragg fiber,” *Post Deadline Paper PDP25, Optical Fiber Conference 2004*, Los Angeles, 22-27 Feb. 2004.

12. M. Ibanescu, et al., “Analysis of mode structure in hollow dielectric waveguide fibers,” *Physical Review E*, vol. 67, p. 46608, 2003.

13. G. Vienne, et al., “Ultra-large band-width hollow-core guiding in all-silica Bragg

fibers with nano-supports," *Opt. Express*, vol. 12, pp. 3500-3508, 2004.

14. M. Foroni, et al., "Confinement loss spectral behavior in hollow-core Bragg fibers," *Optics letters*, vol. 32, pp. 3164-3166, 2007.
15. I. M. Bassett and A. Argyros, "Elimination of polarization degeneracy in round waveguides," *Opt. Express*, vol. 10, pp. 1342-1346, 2002.
16. M. Miyagi, "Bending losses in hollow and dielectric tube leaky waveguides," *Appl. Opt.*, vol. 20, pp. 1221-1229, 1981.
17. M. E. Marhic and E. Garrnire, "Low-order TE_{0q} operation of a CO_2 laser for transmission through circular metallic waveguides," *Appl. Phys. Lett.*, vol. 38, pp. 743-745, 1981.
18. M. Miyagi, K. Harada, and S. Kawakami, "Wave propagation and attenuation in the general class of circular hollow waveguides with uniform curvature," *IEEE Trans. on Microwave Theory and Techniques*, vol. 32, pp. 513-521, 1984.
19. T. Sorensen, J. Broeng, A. Bjarklev, E. Knudsen, and S.E.B. Libori, "Macro-bending loss properties of photonic crystal fibre," *Electronics Letters*, vol. 37, pp. 287-289, 2001.
20. J. C. Baggett, T. M. Monro, K. Furusawa, V. Finazzi, and D. J. Richardson, "Understanding bending losses in holey optical fibers," *Opt. Commun.*, vol. 227, pp. 317-335, 2003.
21. M. D. Nielsen, N.A. Mortensen, M. Albertsen, J.R. Folkenberg, A. Bjarklev, and D. Bonacinni, "Predicting macrobending loss for large-mode area photonic crystal fibers," *Optics Express*, vol. 12, pp. 1775-1779, 2004.
22. Y. Tsuchida, K. Saitoh, and M. Koshiba, "Design of single-moded holey fibers

with large-mode-area and low bending losses: The significance of the ring-core region," *Optics Express*, vol. 15, pp. 1794-1803, 2007.

23. J. Olszewski, M. Szpulak, T. Martynkien, W. Urbanczyk, F. Berghmans, T. Nasilowski, H. Thienpont, "Analytical evaluation of bending loss oscillations in photonic crystal fibers," *Opt. Commun.*, vol. 269, pp. 261-270, 2007.
24. T. Martynkien, J. Olszewski, M. Szpulak, G. Golojuch, W. Urbanczyk, T. Nasilowski, F. Berghmans, and H. Thienpont, "Experimental investigations of bending loss oscillations in large mode area photonic crystal fibers," *Optics Express*, vol. 15, pp. 13547-13556, 2007.
25. T. P. Hansen, J. Broeng, C. Jakobsen, G. Vienne, H. R. Simonsen, M. D. Nielsen, P. M. W. Skovgaard, J.R. Folkenberg, and A. Bjarklev, "Air-guiding photonic bandgap fibers: Spectral properties, macrobending loss and practical handling," *J. Lightwave Technol.*, vol. 22, pp. 11-15, 2004.
26. B. Temelkuran, S. D. Hart, G. Benoit, J. D. Joannopoulos, and Y. Fink, "Wavelength-scalable hollow optical fibres with large photonic bandgaps for CO_2 laser transmission," *Nature*, Supplementary information, vol. 420, pp. 650-653, 2002.
27. M. Skorobogatiy, K. Saitoh, and M. Koshiba, "Full-vectorial coupled mode theory for the evaluation of macro-bending loss in multimode fibers. application to the hollow-core photonic bandgap fibers," *Opt. Express*, vol. 16, pp. 14945-14953, 2008.
28. R. L. Abiams, "Coupling losses in hollow waveguide laser resonators," *IEEE J. Quantum Electron.*, vol. 8, pp. 838-843, 1972.

29. S. Wang, “Proposal of periodic layered waveguide structures for distributed lasers,” *J. Appl. Phys*, vol. 44, 767-780, 1973.

30. R. L. Abiams, “Coupling losses in hollow waveguide laser resonators,” *IEEE J. Quantum Electron.*, vol. 8, pp. 838-843, 1972.

31. J. J. Degnan, “The waveguide laser: A review,” *Appl. Phys.*, vol. 11, pp. 1-33, 1976.

32. H. Kogelnik, T. Li, “Laser beams and resonators,” *Applied Optics.*, vol. 5, pp. 1550-1567, 1966.

33. H. Steffen and F. K. Kneubühl, “Dielectric tube resonators for infrared and submillimeterwave lasers,” *Phys. Lett. A.*, vol. 27, pp. 612-615, 1968.

34. P. Belland, D. Veron and L. B. Whitbourn, “Mode study, beam characteristics and output power of a CW 377μm HCN waveguide laser,” *J. Phys. D: Appl. Phys.*, vol. 8, pp. 2113-2122, 1975.

35. D. Véron, P. Belland, and M. J. Beccaria, “Continuous 250mW gas discharge DCN laser at 195μm,” *J. Infrared. Phys.*, vol. 18, pp. 465-468, 1978.

36. P. Belland, “Waveguide CW 118. 6-mu-m H_2O Laser,” *Appl. Phys. B*, vol. 27, pp. 123-128, 1982.

37. V. V. Kubarev, E. A. Kurenskii, “Very-low-noise H_2O laser with rf pumping,” *Quantum Electron*, vol. 25, pp. 1141-1145, 1995.

38. V. V. Kubarev, “Xenon as an effective buffer gas in submillimetre lasers based on vibrational—rotational transitions,” *Quantum Electron*, vol. 26, pp. 191-192, 1996.

39. V. V. Kubarev, “Ultralow-noise high-power DCN laser with rf pumping,”

Quantum Electron, vol. 26, pp. 303-306, 1996.

40. P. W. Smith, "A waveguide gas laser," *Appl. Phys. Lett.*, vol. 19, pp. 132-134, 1971.
41. T. J. Bridges, E. G. Burkhardt, and P. W. Smith, "CO_2 Waveguide Lasers," *Appl. Phys. Lett.*, vol. 20, pp. 403-405, 1972.
42. I. M. Beterov, V. P. Chebotayev, A. S. Provorov, "CW high-pressure tunable CO_2 laser with a mixture of CO_2 isotopes," *IEEE J. Quantum Electron.*, vol. 10, pp. 245-247, 1974.
43. S. A. Gonchukov, S. T. Kornilov, V. N. Petrovskii, E. D. Protsenko, Yu. G. Rubezhnyi, "Helium-neon waveguide laser," *Sov. J. Quantum Electron*, vol. 5, pp. 232-233, 1975.
44. K. O. Hill, G. Meltz, "Fiber Bragg grating technology fundamentals and overview," *J. Lightwave Technol.*, vol. 15, pp. 1263-1276, 1997.
45. T. Szkopek, V. pasupathy, J. E. Sipe and P. W. E. Smith, "Novel multimode fiber for narrow-band Bragg gratings," *IEEE J. on Selected Topics in Quantum Electron.*, vol. 7, pp. 425-433, 2001.
46. F. Benabid, F. Couny, J. C. Knight, T. A. Birks, and P. St. J.Russell, "Compact, stable and efficient gas cells using hollow-core photonic crystal fibres," *Nature*, vol. 434, pp. 488-491, 2005.
47. T. Ritari, J. Tuominen, H. Ludvigsen, J. C. Petersen, T. S rensen, T. P. Hansen, and H. R. Simonsen, "Gas sensing using air-guiding photonic bandgap fibers," *Opt. Express*, vol. 12, pp. 4080-4087, 2006.
48. R. Thapa, K. Knabe, K. L. Corwin, and B. R. Washburn, "Arc fusion splicing of

hollow-core photonic bandgap fibers for gas-filled fiber cells," *Opt. Express*, vol. 14, 9576-9583, 2006.

49. L. M. Xiao, M. S. Demokan, W. Jin, Y. Wang, and C. L. Zhao, "Fusion splicing photonic crystal fibers and conventional single-mode fibers: microhole collapse effect," *J. Lightwave Technol.*, vol. 25, pp. 3563-3574, 2007.
50. F. Couny, F. Benabid, and P. S. Light, "Reduction of Fresnel back-reflections at splice interface between hollow-core PCF and single-mode fiber," *IEEE Photon. Technol. Lett.*, vol. 19, pp. 1020-1022, 2007.
51. X. Yu, X. Zheng, and H. Zhang, "PMD measurement of hollow-core photonic bandgap fiber by investigating power penalty of optically generated microwave signals," *IEEE Photon. Technol. Lett.*, vol. 19, pp. 279-281, 2007.
52. Y. Wang, W. Jin, J. Ju, H. Xuan, H. L. Ho, L. Xiao, and D. Wang, "Long period gratings in air-core photonic bandgap fibers," *Opt. Express*, vol. 16, pp. 2784-2790, 2008.

CHAPTER 4

THEORIES OF WAVEGUIDE HE-NE LASER WITH SMALL BORE SIZE

The positive column theory of conventional helium-neon (He-Ne) lasers with ordinary dimensions (>2 mm diameter tubing) matches well with experimental results. When the bore diameter reduces to a very small value, new phenomena would appear and have not been studied previously to our knowledge. In this chapter we will discuss the previous theories of the waveguide He-Ne laser and present the calculation results of our own about small bore diameter (<200 μm), which have not been discussed in the previous works.

4.1 Modeling of transverse RF excited waveguide He-Ne laser

The gas discharge in a small tube is a very complicated process that is hard to describe by using an analytical mathematical model. From the macroscopic view, it is related to the excitation method: longitudinal DC excitation or transverse RF excitation, the value of current, the voltage and the frequency of the RF. From the microcosmic view, it is related to the electron impaction with other particles, the transitions of atoms in different energy levels [1] as shown in Fig. 4.1. It is always needed to simplify the model and neglect some trivial physical process. Finally the model needs to match with experimental results.

Although the first waveguide He-Ne gas laser had been reported by Smith [2] in 1971, less theoretical research was carried out on the calculations of the electron

energy distribution, population inversions, and the output power. Most attentions are on waveguide CO_2 lasers and the coupling loss of the cavity.

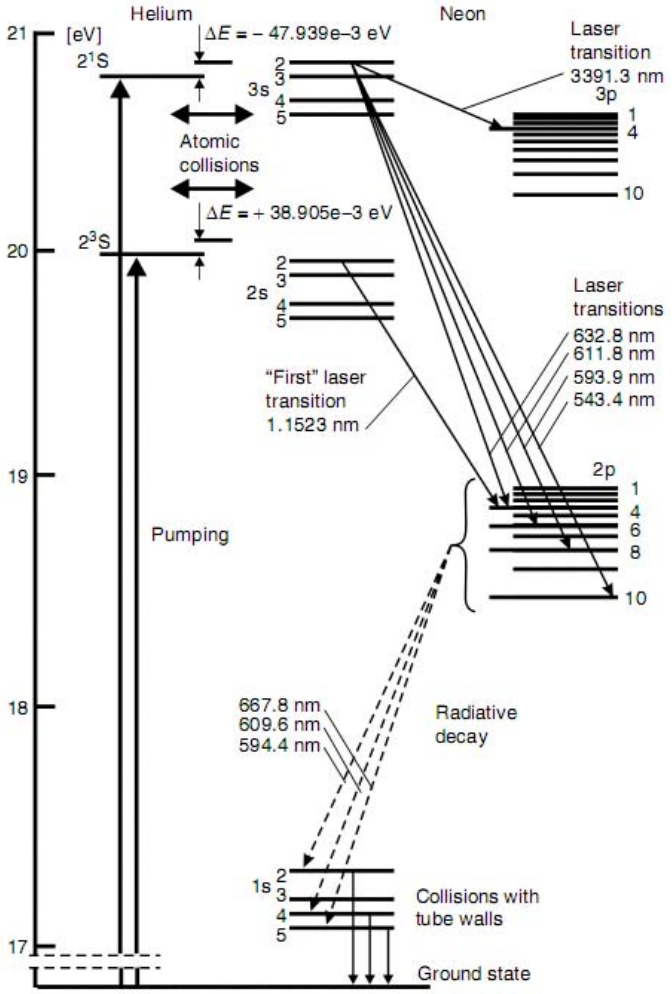

Figure 4.1 Energy level diagram of a helium-neon atomic system [1].

Sun et al. [3] carried out theoretical modeling of a waveguide He-Ne laser with transverse RF excitation. By solving the Boltzmann equation and the coupled rate equations, the electron energy distribution functions (EEDFs) and population inversion were obtained. By using the calculated EEDF with the known collision-sections and other atomic data, the specific atomic process coefficients under different conditions were determined. They investigated population inversion of different laser levels for various gas pressures and input power densities and the results are shown in Fig. 4.2.

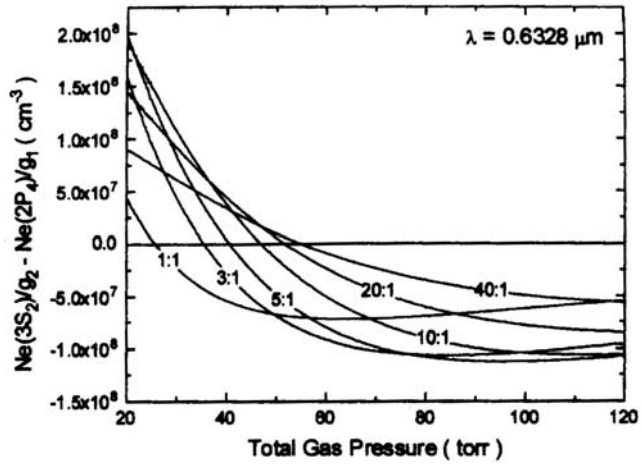

(a)

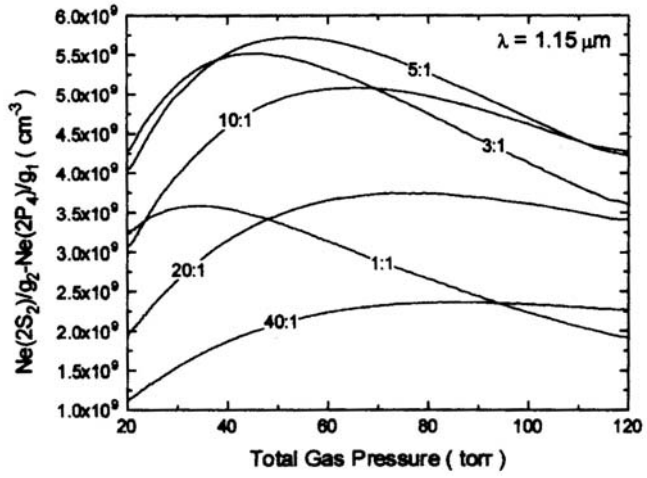

(b)

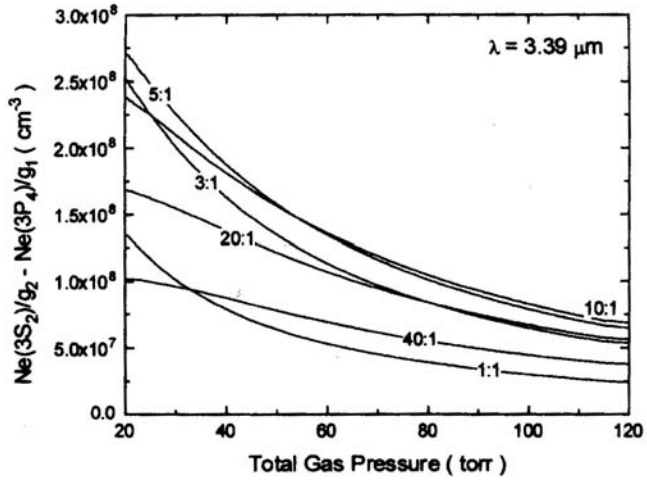

(c)

Figure 4.2 Population inversions at 632.8nm (a), 1.15μm (b), and 3.39μm (c) wavelength under different pressures [3].

The calculation results indicated that for a RF transverse excited He-Ne laser working above 60 Torr gas pressure conditions, there is no population inversion between Ne ($3S_2$) and Ne ($2P_4$) for the 632.8 nm laser as shown in Fig. 4.2a. With the increase of gas pressure the population inversion has a downward trend and there would no population inversion happen beyond about 60 Torr. This theory includes three types of transition: between Ne ($3S_2$) and Ne ($2P_4$) for the 632.8 nm; between Ne ($3S_2$) and Ne ($3P_4$) for the 3.39 μm laser; between Ne ($2S_2$) and Ne ($2P_4$) for the 1.15 μm laser.

They took the values of 2×2 mm^2 (cross section) for the calculations. This dimension is larger than a normal size (several hundred microns) of the waveguide He-Ne resonator. Their theoretical calculations pointed to large size cavities (almost equal to the size of conventional He-Ne laser), and they didn't consider the influence of small bore diameter on the discharge process. When the bore dimension reduces to small values, there must be some physical phenomenon different to conventional He-Ne lasers to be considered. Therefore, the theory of Sun et al. [3] is still in the category of the conventional theory, which can only provide limited references to our project.

4.2 Modeling of longitudinal DC excited waveguide He-Ne laser with tube diameter ≥ 200 μm

The maximum output power of the He-Ne lasers depends on the electron temperature and the spatial distribution of the electrons that excite the laser levels. In the case of narrow tubes as used in miniaturized waveguide lasers, the electron temperature

depends on the current, and a strongly falling characteristic is obtained. The pure diffusion theory is not sufficient to calculate electron temperature and electron density distribution.

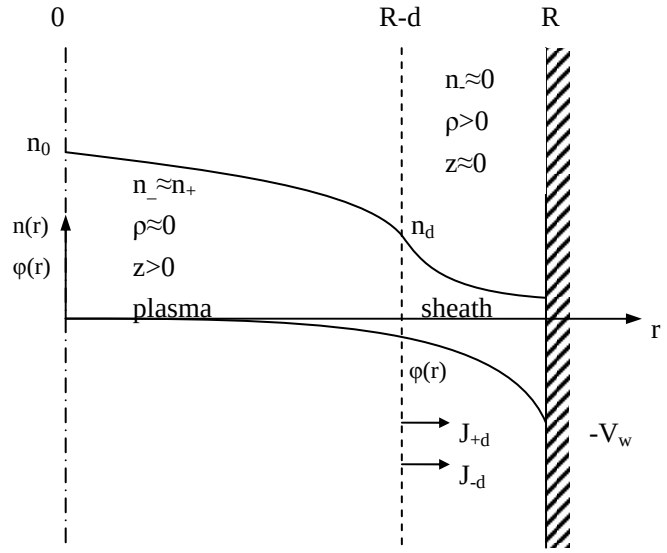

Figure 4.3 Column's half cross section from the middle axis to the wall (radius R).

Based on the positive column theory of He-Ne lasers, Schuöcker et al. [4] assume that there exists the space charge sheath in the narrow tube as shown in Fig. 4.3. Electron density n_(r) and potential φ(r) are plotted as function of radius *r*. The discharge channel has the radius *R-d* and the space charge sheath with the thickness *d*; ρ is the space charge density; J_{+d}, J_{-d} are the ion and electron current densities at *r=R-d* directed to the wall.

The width of that sheath rises with decreasing current and constricts the plasma column, thus causing the electron temperature and the column voltage to rise. This theory has been proved in the case of pure helium and yields voltage-current characteristics that fit experimental results remarkably well [4]. Subsequently Schuöcker et al. [5] use this model and numerical methods to obtain a series of parameters such as electron density distribution, population inversions, gain, maximum

output intensity, and their dependence on the geometry, gas data, and current.

As shown in Fig 4.3 they make several assumptions to simplify the model [5]. It is assumed that all quantities are constant in axial direction and that the column is in a nearly stationary state. Because of the wall sheath which compensates the negative wall charges only fast electrons can reach the wall. In the sheath the electron density decreases exponentially with radius according to Maxwell-Boltzmann statistics, and impact ionization is considerably reduced. For simplicity, it is assumed that impact ionization can be neglected entirely in the wall sheath. In the remaining part of the discharge tube of cross section the electron and positive ion densities are nearly equal except for a small transition region that is neglected for simplicity. In the space charge free plasma region, electrons ionize the gas by impact. Stepwise ionization is neglected according to the experiment results [6]. Charge carriers are lost by ambipolar diffusion in radial direction to the walls. Volume recombination loss is neglected [7].

According to the theory of the diffusion column, the radial carrier density distribution in the plasma region is:

$$n(r) = n_0 J_0(r\sqrt{\frac{z}{D_a}}) \tag{4.1}$$

where z is the impact ionization rate and D_a is the ambipolar diffusion coefficient, n_0 is the axial density of the electrons.

The radial diffusion current density of the electrons in the $r=R-d$ is $+eD_a(\frac{dn}{dr})_{R-d}$. The electron current density in the sheath, according to Maxwell-Bolzmann statistics, is $-(e\bar{v}_- n_{R-d}/4)\bullet\exp(-eV_w/kT_e)$ ($\bar{v}_- = \sqrt{\frac{8}{\pi}\frac{kT_e}{m_-}}$ is the average thermal velocity of the electrons, V_w is the wall potential, T_e is the temperature of the electrons). Both current

densities must be equal at the $r=R-d$ in the stationary state:

$$-D_a(\frac{dn}{dr})_{R-d} = \frac{\bar{v}_- n_{R-d}}{4}\exp(-\frac{eV_w}{kT_e}) \tag{4.2}$$

Using the abbreviation $\alpha = (R-d)\sqrt{(z/D_a)}$, equation (4.1) and (4.2) yield:

$$\frac{J_0(\alpha)}{J_1(\alpha)} = \frac{4\sqrt{zD_a}}{\bar{v}_-}\exp(\frac{eV_w}{kT_e}) \quad (d, T_e \text{ are unknown parameters}) \tag{4.3}$$

$$V_w = \frac{kT_e}{e}\ln(\frac{2}{\sqrt{\pi}}\sqrt{\frac{m_+}{m_-}}) \tag{4.4}$$

where m_+ is the average ion mass, m_- is the electron mass.

The sheath thickness can be obtained as:

$$d = \frac{16}{\sqrt{3}}\sqrt{\frac{3}{2}kT_e\frac{\varepsilon_0}{e^2}\frac{1}{n_{R-d}}} \quad (d, T_e, \text{ and } n_0 \text{ are unknown parameters}) \tag{4.5}$$

where ε_0 is the free-space permittivity.

In a stationary state, the electron temperature is related to the gradient by the energy balance of the electrons which gain energy in the electric field and lose energy by impacts. This can be expressed as the following equation:

$$E = \sqrt{\frac{m_-\bar{v}_-}{e^2}}\sqrt{\frac{w}{\lambda_-}} \quad (E, T_e \text{ are unknown parameters}) \tag{4.6}$$

where w denotes the inelastic energy loss of an electron, and λ_- is electron mean free path.

In order to calculate the discharge current, only the electronic part of the current must be considered. The discharge current follows from integrating over the cross section of the plasma region:

$$I = 2\pi\frac{e^2\lambda_-}{m_-\bar{v}_-}En_0\sqrt{\frac{D_a}{z}}(R-d)J_1(\alpha) \quad (d, T_e, n_0, E \text{ and } I \text{ are unknown parameters}) \tag{4.7}$$

From the Eqs. (4.3), (4.5), (4.6) and (4.7), we can decide d, T_e, n_0, E for every

giving value of I on the premise that: bore radius R, the ratio f of the He:Ne mixture and the whole pressure p as shown in Fig. 4.4.

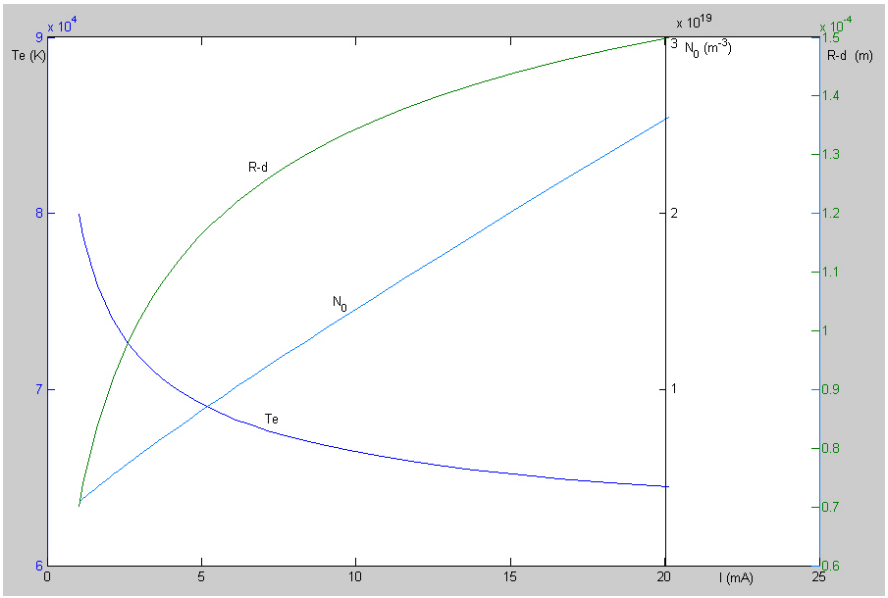

Figure 4.4 The relations between I, T_e, N_0, and R-d when R=200μm, p=10Torr, He:Ne=8:1.

Fig. 4.4 shows dependence of electron temperature T_e, plasma region radius R-d, and electron density N_0 at the axis as functions of current I of a positive column in 8:1 He:Ne mixture. From this figure, we can see that the electron temperature and the width of the sheath decrease with the rise of the current. The electron density at the central axis N_0 has approximately linear relationship with the current.

Since the visible laser transition is 632.8 nm wavelength, the density of helium atoms in the metastable 2^1s state and the densities of neon in the $3s_2$ upper laser level and the $2p_4$ lower laser level have to be studied. The helium density in the ground state is denominated M_0 and in the 2^1s state M_1, the neon density in the ground state N_0, in the $1s_2$ state N_1, in the $2p_4$ state N_2, and in the $3s_2$ state N_3. To calculate these densities, the balance equations are used [8].

$$\frac{\partial M_1}{\partial t} = \frac{M_0}{\Theta_M} + \frac{N_3}{t_{NeHe}} - (D_M \Delta + \beta n_- + \gamma + \frac{1}{t_{HeNe}}) M_1 \qquad (4.8)$$

$$\frac{\partial N_3}{\partial t} = \frac{M_1}{t_{HeNe}} - N_3\left(\frac{1}{t_{NeHe}} + \frac{1}{\tau_3}\right) \tag{4.9}$$

$$\frac{\partial N_2}{\partial t} = \frac{N_0}{\Theta_{02}} + \frac{N_3}{\tau_{32}} - \frac{N_2}{\tau_{21}} \tag{4.10}$$

where $1/\Theta_M$ is the electron impact excitation frequency that characterizes the transition from the helium ground level to the helium 2^1s level; t_{NeHe} is the time constant that characterizes resonance transitions from the neon $3s_2$ level to the helium 2^1s level; t_{HeNe} is the time constant that characterizes resonance transitions from the helium 2^1s level to the neon $3s_2$ level; β is the destruction rate of metastables by electron impact; γ is the destruction rate of metastables by impacts with neutrals; D_M is the diffusion coefficient; τ_3 is the coefficient which characterizes the spontaneous emission of the $3s_2$ level; $1/\Theta_{02}$ is the electron impact excitation frequency that characterizes the transition from the neon ground level to the neon $2p_4$ level ; τ_{32} is the coefficient characterizes the optical transition from the $3s_2$ upper level; τ_{21} is the coefficient characterizes the optical transition from the neon $2p_4$ level to 1s level.

Using the Eqs. (4.8), (4.9), (4.10), and the values of T_e, N_0, d, I that have been calculated before and a series of other parameters that can be obtained from previous literatures [3, 4], we can calculate the average population inversion for different R, mixture ratio f, p, I values:

$$\overline{\Delta N} = \frac{1}{R^2\pi}\int_0^R \Delta N(r) 2\pi r dr \qquad \left(\Delta N(r) = N_3 - \frac{g_3}{g_2} N_2\right) \tag{4.11}$$

where g_3 and g_2 are the statistical weights of $3s_2$ level and of $2p_4$ level respectively.

4.3 Modeling results for longitudinal DC excited waveguide He-Ne laser with tube diameter <200μm

For ordinary tubing with diameters >1 mm, there always exist population inversions for some pressures and mixture ratios, which have been proved by experiments for many years. Schuöcker et al. [5] have calculated the tubing diameter larger than 100 μm, there also exist population inversions and they presented that the tube radius $R \approx 100$ μm is an optimal tube radius which can lead to maximum output intensity. However, for our concern, the core radius in the range 2.5~125 μm, most of tube size in this range are much smaller than the ones that they have calculated. Whether population inversions will occur or not, it still need to be studied. By using the model of Schuöcker et al. [5], we calculate the radius of the tube in the range from 1μm to 20μm for six pressures 10, 100, 200, 300, 400, 500 Torr and fixed mixture He:Ne ratio 19:1 (f=0.95). We choose the ratio f=0.95 because that from the empirical equation the optimal ratios f varies inversely with the capillary diameter. He-Ne waveguide lasers that have ever been constructed have ratios bigger than 90%.

For every given p, R, we calculate the population inversion for a series of I values and find the maximum population inversion ΔN and the corresponding values of I, T_e. The maximum population ΔN for the tube radius range 1~20μm with different filling pressures are shown in Fig. 4.5. We define the cut-off radius R_c as the critical value bellow which no population inversions will occur (ΔN<0) regardless of the value of the current I. The cut-off radii for p=10, 100, 200, 300, 400, 500Torr are respectively 12.5, 5.9, 5.4, 5.3, 5.4, 5.5 μm. It turns out that an optimal tube radius in the range of R=10~12 μm exists at which population inversion could reach its maximum

(ΔN=0.5~0.8×$10^{17}$$m^{-3}$) in the range of 1~20 μm if the sufficient gas filling pressure is used.

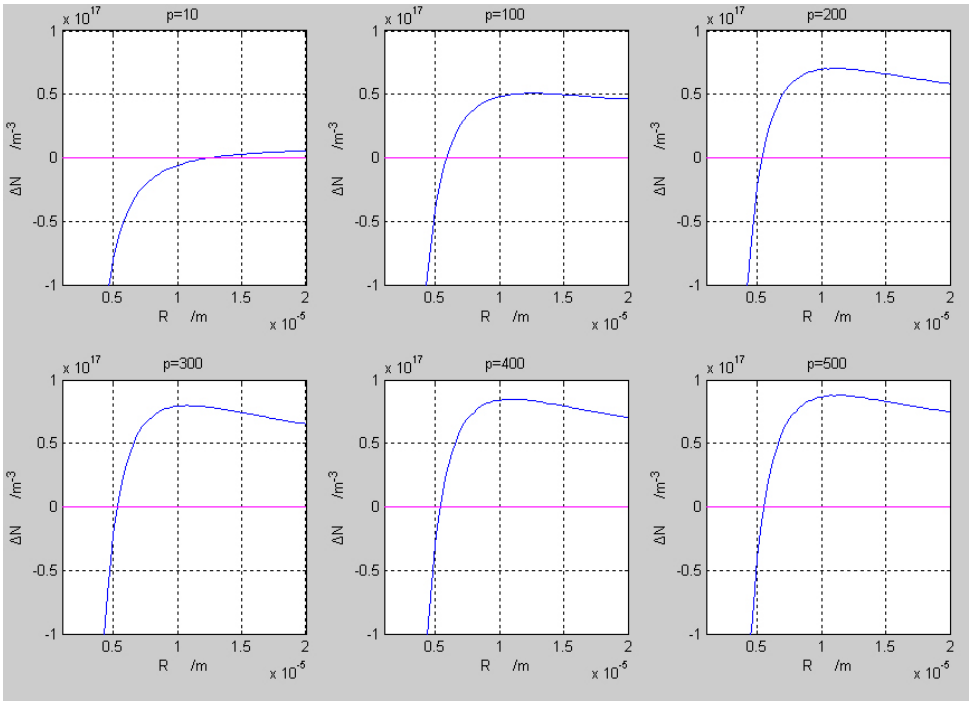

Figure 4.5 Maximum population inversions Vs tube radius for various pressures.

The conventional He-Ne lasers always use filling pressures p<10 Torr. The waveguide He-Ne lasers that have been constructed previously have filling pressures around 7 Torr. From empirical data the optimal pressures p and the bore diameters D satisfy the equation [9, 10]:

$$p \times D = (4 \sim 6.6) \times 10^2 \, Pa \cdot mm \quad \text{(Accurate when } D \text{ is in the range 1~15 mm)} \quad (4.12)$$

When D=450 μm, p= (6.68~11.03) Torr from Eq. (4.12), this is still reasonable because it matches the experiment value 7 Torr. When D=5.1 μm, p= (589.71~973.02) Torr from Eq. (4.12). This value may be deviate from the practical value, but it tells us that considerable working pressure is necessary for very small radius tubes. From the Fig. 4.5 we also find that ΔN increase with the rise of the total pressure p.

Although the model of Schuöcker et al. [5] has been used to simulate the real

environment of the plasma discharge and coupled transition between different energy levels by using some accurate parameters published in previous works, the whole system may be different from the true fact. The parameters that have ever been used in the modeling are obtained from the ordinary environment (R>500 μm, p<10 Torr), so they are possibly not accurate when the R reduces to very small values and the pressure increases to high level. From their model our calculated results show that there exists a cut-off radius R≈5.3 μm. It seems that there exists no population inversion when the tubing radius at R=2.55μm (the value of HC-633-1 [11]), but this still needs to be proven by the experiment because of the possible deviation in the model of Schuöcker et al. [5]. The commercial hollow-core PCF working at 633 nm that can be found in the market is only the HC-633-1; however there were large-core-area hollow PCF have been reported with a diameter of ~50 μm [12, 13]. We expect that hollow-core PCF with a large bore, which has low attenuation loss, would be available in the market in future. We will also perform experiments with such new hollow-core PCFs to identify which size is optimal for fiber gas lasers.

$$g_{\max} = f_1(S, \overline{\Delta N}) \tag{4.13}$$

$$(1-A)(1-T)\exp\left[(g_{\max}-\alpha)L\right]=1 \tag{4.14}$$

$$P = S \cdot T \tag{4.15}$$

where S is the radiation intensity; A is the mirror loss; T is the transmission of the output window; L is the length of the laser tube; α is the waveguide loss; P is the output of laser power.

If A=0.001 and α is known, based on the calculated population inversions $\overline{\Delta N}$, the optimal reflectivity and laser power for 50-cm length hollow-core fibers with different

core radii can be determined by Eqs (4.13), (4.14) and (4.15). Since Eq. (4.13) in [5] is possibly not accurate when the pressures are larger than 40 Torr, we only give the optimal output reflectivity and laser power when the gas pressure is smaller than 40 Torr as indicated in Table 4.1.

Table 4.1 The optimized values of *I*, *Te*, $\overline{\Delta N}$, the output reflectivity and laser power

R (μm)	*p* (Torr)	*I* (mA)	*Te* (10^4K)	$\overline{\Delta N}$ (10^{15}m^{-3})	Output reflectivity (%)	Power (mW)
10	150	0.03	33.78	77.9		
25	60	0.034	29.55	46.47		
25	30	0.079	102.6	23.35	86.18	0.06
75	20	0.034	29.55	17.43	92.7	0.628
125	10	0.052	27.146	9.05	97.41	0.897

There are no other works that have ever considered the waveguide He-Ne laser with RF excitation. The theory of Sun [3] is not a useful model that is suitable to small bore diameter tubes. Exciting in small bore size hollow-core fibers may bring deviation from the predictions of past models, and further experiments are needed to validate the past models and build more accurate new models.

4.4 Summary

We reviewed the past theories of population inversions about the waveguide He-Ne laser in this chapter. By using the model of Schuöcker et al., we calculate laser tubes with inner radius from 1 to 20 μm which will be used in our experiments. The calculation results indicate that considerable working pressure is necessary for very small radius tubes. Since the parameters that have ever been used in the modeling are obtained from the ordinary environment (R>500 μm, p<10 Torr), so they are possibly

not accurate when the *R* reduces to very small values and the pressure increases to high level. The modeling results in this chapter can only provide limit reference for us at present. A series of experiments are needed to be performed to build a more accurate model for fiber gas lasers which have small bore sizes.

References

1. M. Endo and R. F. Walter, *Gas lasers*, CRC press, 2006.
2. P. W. Smith, "A waveguide gas laser," *Appl. Phys. Lett.*, vol.19, pp.132-134, 1971.
3. X. Sun, J. G. Xin and W. Zhang, "Electron energy distribution functions and population inversion in a radio-frequency transverse discharge excited waveguide helium-neon laser," *International journal of Optoelectronics*, vol. 12, pp. 59-65, 1998.
4. D. Schuocker, W. Reif, R. Erlacher, and G. Schiffner, "Properties and current-voltage characteristics of discharges in waveguide gas lasers," *Appl. Phys.*, vol. 14, pp. 277-282, 1977.
5. D. Schuöcker and W. Reif, "Theoretical description of discharge plasma and calculation of maximum output intensity of He-Ne waveguide lasers as a function of discharge tube radius," *IEEE J. QE*, vol. 15, pp. 232-239, 1979.
6. E. Spenke, "Die diffusionstheorie der positiven saule mit berucksichtigung der stufenweisen ionisierung," *Z. physik*, vol. 127, pp. 221-242, 1950.
7. R. Seeliger, "Untersuchungen aus dem gebiet der gasentladungsphysik," *Z.*

Naturforschung, vol. 8, pp. 74-79, 1953.

8. G. Herziger, W. Holzapfel, and W. Seelig, “Berechnung und experimenteller vergleich des verstarkungsfaktors fur den laserubergang 6328Å in einer he-ne-gasentladung,” *Z. f. Phys.*, vol. 200, pp. 103-116, 1967.
9. P. W. Smith, “On the optimum geometry of a 6328Å laser oscillator,” *IEEE J. Quant. Electron*, vol. 2, pp. 77-79, 1966.
10. E. I. Gordon, A. D. White, “Similarity laws for the effects of pressure and discharge diameter on gain of He-Ne lasers,” *Applied Physics Letters*, vol. 3, pp. 199-201, 1963.
11. http://www.crystal-fibre.com/products/.
12. S. O. Konorov, A. B. Fedotov, L. A. Mel'nikov, et al., “Large-core-area hollow photonic-crystal fibers,” *Laser Physics Letters*, vol. 1, pp. 548-550, 2004.
13. S. O. Konorov, A. B. Fedotov, A. M. Zheltikov, et al., “Phase-matched four-wave mixing and sensing of water molecules by coherent anti-Stokes Raman scattering in large-core-area hollow photonic-crystal fibers,” *JOSA B: Optical Physics*, vol. 22, pp. 2049-2053, 2005.

CHAPTER 5

VACUUM SYSTEM AND GAS FLOW IN HOLLOW-CORE FIBERS

When constructing He-Ne gas lasers, a vacuum system is needed to pump the laser tube down to 10^{-5} Torr or lower. Our designed vacuum system is described in this chapter. Since hollow-core fibers used to building fiber gas lasers have smaller bore diameters compared with conventional laser tube, gas flow in these hollow-core fibers is studied preliminarily from theory in this chapter.

5.1 Vacuum system

The vacuum system is composed of several parts: a pumping station, vacuum gauges, a residual gas analyzer (RGA), a gas mixing chamber, two gas chambers and corresponding connection pipes and controlling valves. The vacuum system can realize two functions: evacuating the hollow core of the fiber and then inflating the gas mixture into the hollow-core fiber. To monitoring the vacuum level in the whole system, two vacuum gauges with different working ranges and a manometer are used. We also add a RGA in the system to analyze the gas species and detecting the leaks. The whole vacuum system is shown in Fig. 5.1.

No single pump can have working range from 1 atm (760 Torr) to 10^{-6} Torr. Pumping station consisted of a forepump and a turbomolecular pump can achieve the range needed. Considering that reducing vapor and oil vapor in the laser tube is a key point of the whole process, we choose diaphragm pump as the forepump to form a dry

pumping station although the use of a rotary vane pump as the forepump could provide a little higher ultimate vacuum than diaphragm pump.

As shown in Fig. 5.1, this vacuum system includes a RGA. This RGA can measure a mass range from 1 to 200 amu (atomic mass unit) and can be used for analyzing gas ingredients in the vacuum system and their differential pressures. It can also be used to detect leaks in the whole vacuum system with some auxiliary methods. Since the RGA needs to work with a pressure lower than 10^{-4} Torr, a variable leak valve is added to allow a small amount of working gases flow from right to left while keeping the working pressure of the right side of the system unchanged (above 1 Torr) and the pressure at the left side lower than 10^{-4} Torr. Vacuum gauge *(a)* has a measuring range from 10^{-8} to 1000 mbar. It can be used to indicate whether the pressure is low enough for turning on the RGA.

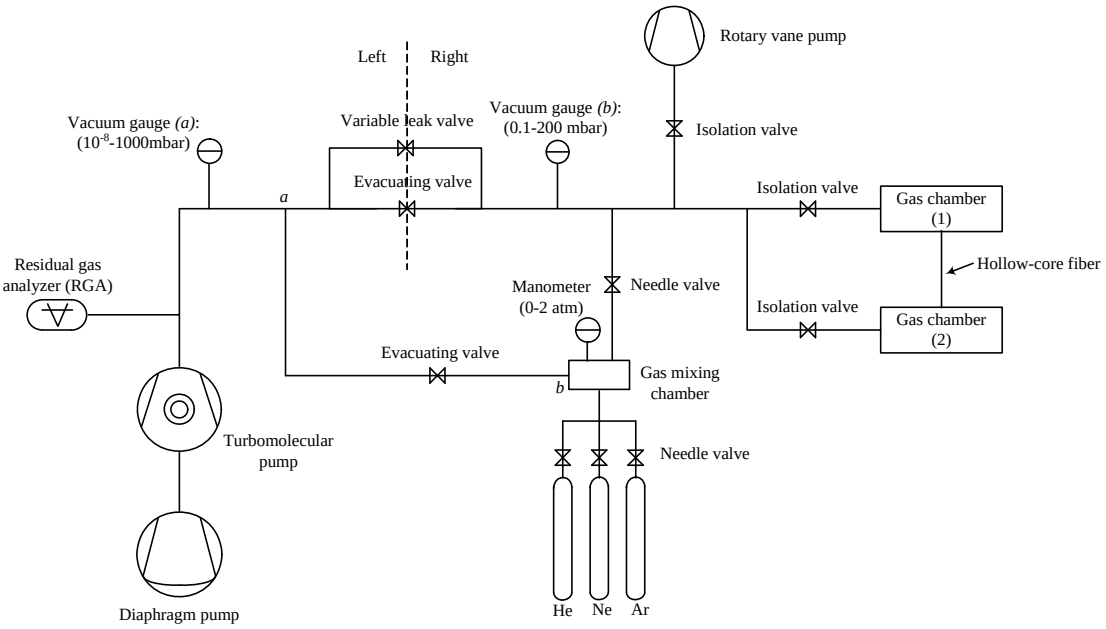

Figure 5.1 Schematic of vacuum system.

The evacuating valve has a big aperture to ensure effective pumping speed. Vacuum gauge *(b)* has a measuring range from 0.1 to 200 mbar. Its measurement is

independent of gas species and it can indicate the pressure value accurately in the gas chambers. A small rotary vane pump is used to regulate the pressure in the gas chambers. When the pressure is higher than what we need in the experiment, we can turn on the pump and open the isolation valve to reduce the pressure to the appropriate value. Although the variable leak valve can perform the same function, it is safe to use another small pump because misoperation such as opening the evacuating valve will damage the turbomolecular pump.

The three needle valves in the vacuum system have small apertures and allow small regulating of flow coefficient. This specificity provides roughly control of gas flowing to the gas mixing chamber. When carrying on experiments, mixing gases at different pressures with the same ratio is needed to find out the optimized working pressure. The gas mixing chamber is set to simplify the procedures. Different gases are mixed in the gas mixing chamber with high pressure. A manometer can indicate the value of pressure from 0 to 2 atm (1 atm=760 Torr). Another needle valve is used to control the amount of gas mixture flowing from the gas mixing chamber to the two gas chambers.

An additional vacuum pipe of the type of NW16 is connected from the point of *a* to *b* of the gas mixing chamber. This pipe has a bigger aperture than other pipes connected to the gas mixing chamber. This pipe is needed because the gas mixing chamber can be evacuated effectively only through a larger aperture pipe.

The smallest standard vacuum pipe is the type of NW10 which has inner diameter of 10 mm. It is much bigger than the size of hollow-core fibers which have inner diameter from 20 to 250 μm and outer diameter from 125 to 343 μm. Therefore it is necessary to make two gas chambers as intermediaries as show in Fig. 5.1. The two gas

chambers are connected to the vacuum system by standard ports, and the evacuation and inflation of the hollow-core fiber are via the two gas chambers.

5.2 Gas flow in hollow-core fibers

The nature of the gas and the relative quantity of gas flowing in a pipe determines the characteristics of gas flow. The nature of the gas is determined by examining Knudsen's number (*Kn*), whereas Reynolds' number (*Re*) describes the relative flow. Gas flow is generally divided into three regions: viscous (*Kn* <0.1), molecular (*Kn* >0.5) and transition (0.01< *Kn* <0.5).

In the viscous gas region (high pressures) the flow is called continuum flow. This flow can be further divided into laminar (*Re* <2300) and turbulent (*Re* >~4000). Turbulent flow is chaotic, like the flow behind a moving vehicle or the rising smoke some distance from a cigarette. Laminar (also called stream) flow occurs when the velocity and surface irregularities are small enough for the gas to flow gently past obstructions in laminar streamlines. In the molecular gas region, the mean free path is so long comparison to the pipe size that the flow is called molecular flow. Between the continuum flow region and the molecular flow region is the transition region. In this region gas molecular collide with each other and with walls.

The boundary between turbulent and laminar flow can be expressed in terms of Reynolds' dimensionless number *Re* for round pipes [1]:

$$Re = \frac{U \rho d}{\eta} \tag{5.1}$$

where ρ is the mass density (kg/m^3), of the gas of viscosity η flowing with stream

velocity *U* in a pipe of diameter *d*. When *Re* >~4000, the flow was always turbulent and when *R* <2300 the flow was always laminar. In the region 2300<*R*<4000 the flow was laminar or turbulent, depending on the geometry of the inlet and outlet and the nature of the piping irregularities.

Knudsen's number *Kn*, is a dimensionless ratio of the mean free path λ to a characteristic dimension *d*—the diameter of a pipe [1]:

$$Kn = \frac{\lambda}{d} \tag{5.2}$$

For air at 22ºC the mean free path can be expressed as [2]:

$$\lambda(\text{cm}) = \frac{5\times10^{-3}}{P(\text{Torr})} \tag{5.3}$$

When the mean free path is equal to or greater than the pipe diameter, say *Kn* >0.5, the flow is called molecular flow. Reynolds' number does not have any meaning for a gas in the free-molecular regime, because classical viscosity cannot be defined.

The inner diameters of hollow-core fibers used in our experiments are in the range from 5 to 250 μm. When the pressure *P* is below 0.1 Torr , the molecular flow is the characteristic of gas flow for these small bore hollow-core fibers. When building conventional He-Ne lasers, it is necessary to evacuate the laser tube to the pressure smaller than 10^{-5} Torr [3]. The whole process of pumping may be divided into two stages. In the first stage, the pressure in the hollow-core fiber reduces from 1 atm to 0.1 Torr. The gas flow in the hollow-core fiber changes from the initial turbulent flow to viscous flow. In the second stage, the pressure in the hollow-core fiber reduces from 0.1 Torr to 10^{-5} Torr. The gas flow in the hollow-core fiber is molecular flow.

A general mathematical treatment of viscous flow results in the Navier-Stokes

equations, which are most complex to solve [4]. Considering viscous flow in a long round tube with a length of *l* and inner diameter of *d*, the conductance can be expressed as [5]:

$$C = \frac{\pi d^4}{128\eta l} \bullet \bar{P} \tag{5.4}$$

For air at 22ºC the conductance of viscous flow can be simplified as [5]:

$$C = 182\frac{D^4}{L} \bullet \bar{P} \qquad C(\text{Liter/s}), D(\text{cm}), L(\text{cm}), \bar{P}(\text{Torr}) \tag{5.5}$$

For air at 22ºC the conductance of molecular flow can be expressed as [5]:

$$C = 12.1\frac{D^3}{L} \qquad C(\text{Liter/s}), D(\text{cm}), L(\text{cm}) \tag{5.6}$$

When evacuating small bore size hollow-core fibers, it is necessary to evaluate the time that is needed to reduce pressure in hollow-core fibers from 1 atm to 10^{-5} Torr or lower. It is too complex to calculate the time of the whole process. The conductance of gas flow in viscous regime has close value as that of gas flow in molecular regime in case of hollow-core fibers in our experiments. To simplify this problem, we only calculate the second stage where gas pressure in hollow-core fiber drops from 0.1 Torr to 10^{-5} Torr.

Considering a simple model as show in Fig. 5.2, the isolation valve is closed and gas chamber is evacuated to a pressure of 10^{-5} Torr. The pumping speed in the gas chamber is 15 Liter/s. The initial pressure in the hollow-core fiber is 0.1 Torr. Open the isolation valve, the gas flow from hollow-core fiber to gas chamber is molecular flow according to previous equations. The pumping speed S_1 inside *x* point of hollow-core fiber can be expressed as $S_1 = \frac{S \times C}{S + C} = \frac{C}{1 + \frac{C}{S}} \approx C \quad (S \gg C)$, where *C* is conductance

of a tube with length of x. When x> 2 mm, S_1 don't depend on S at all, and then $S_1 \approx C$. If l=10 cm, d=250 μm, the conductance of the half long round tube from Eq. (5.6) will be 3.78×10^{-5} L/s which is much smaller than S=15 Liter/s.

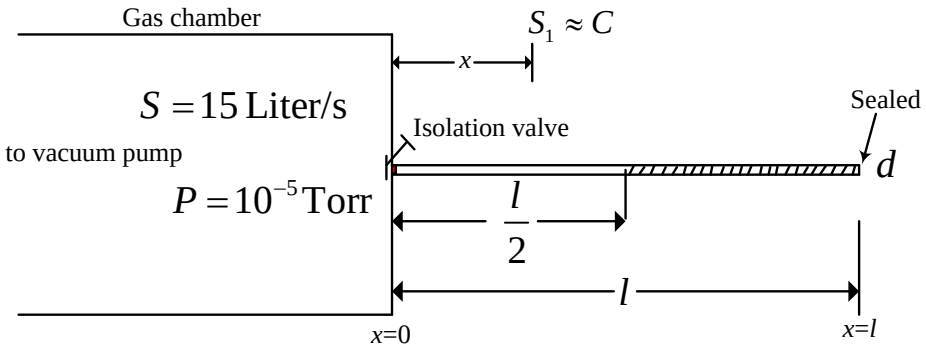

Figure 5.2 Evacuating a hollow-core fiber in molecular regime.

Pumping speed at inlet of a chamber is S_1, and the chamber has a volume of V. Supposed that no outgassing exists in the chamber, the time that gas pressure reduces from P_0 to P_1 can be expressed as [1]:

$$t = 2.3\frac{V}{S_1}\log\frac{P_0}{P_1} \tag{5.7}$$

If x=5 cm, l=10 cm, and reducing the pressure of the right part of the hollow-core fiber ($5 \le x \le 10$) from P_0=0.1 Torr to $P_1=10^{-5}$ Torr, then the calculated times of d=460, 250, 50, 20, 5 μm are listed in Table 5.1.

Table 5.1 Evacuating time

d (μm)	460	250	50	20	5
t (s)	0.3	0.6	3	7.5	29.9

When the bore diameter of tubes becomes small, the evacuating time doesn't increase significantly from the theoretical calculation. Although this calculation only includes the second stage of the whole process, it still can provide some valuable

reference. Evacuating the hollow-core fibers with inner diameters from 250 to 5μm don't bring significant longer pumping time compared with the commercial laser tube with an inner diameter of 460 μm. It seems that evacuating small bore size hollow-core fibers don't bring any problems from the theoretical calculation. However, we ignored outgassing, permeability etc in the simple model. The further investigation by experiments needs to be carried on to prove this point.

Table 5.2 Difference value of pressure between two ends

d (μm)	460	250	50	20	5
ΔP (Torr)	4.5×10^{-5}	1.5×10^{-4}	3.8×10^{-3}	2.4×10^{-2}	0.38

If the pressure at x=0 is P_0, the pressure at $x=l$ is P_l and outgassing in the hollow-core fiber is not ignored, then P_0 and P_l have following relationship [6]:

$$\Delta P = P_l - P_0 = \frac{\pi \cdot d \cdot a \cdot l}{2C} \tag{5.8}$$

where a is outgassing rate per unit area per unit time, C is the conductance of the hollow-core fiber. Due to the existence of outgassing, the balance between evacuating and outgassing forms the difference of pressure between the two ends of the hollow-core fiber which can not be eliminated by increasing the pumping speed at the end of the hollow-core fiber.

The outgassing rate of Pyrex after exposed at vacuum for one hour is $a=98\times10^{-7}$ Pa•m/s, and we take this value for the calculation. Also if l=10 cm, the difference value of pressure between two ends are listed in Table 5.2 for d=460, 250, 50, 20, 5 μm. It is obvious that outgassing of inner face inside hollow-core fibers will bring big troubles in the process of building fiber gas lasers particularly for hollow-core fibers with inner

diameter smaller 50 μm. The impurity of gas mixture inside the hollow-core fiber will results the failure of lasing. The outgassing rate can be reduced by some technical handles such as baking at high temperature and exposing at vacuum for a longer time. To obtain low outgassing rate in small bore size hollow-core fibers is necessary to be studied in the future work.

5.3 Summary

We have described the new vacuum system which will be used for building the novel fiber gas laser. Gas flow in hollow-core fibers is different from conventional laser tube because of their small bore sizes. Evacuating the hollow-core fibers with inner diameter from 250 to 5μm take longer pumping time compared with the commercial laser tube with an inner diameter of 460 μm, however the difference is not significant from the simple model. When considering the outgassing rate of inner face of the hollow-core fibers, the calculations indicate that outgassing will bring big troubles in the process of building a He-Ne fiber gas laser. Effective methods of reducing outgassing rate in hollow-core fibers are necessary to be studied.

References

1. D. J. Hucknall and A. Morris, *Vacuum technology: calculations in chemistry*, Royal Society of Chemistry, UK, 2003.
2. J. F. O'Hanlon, *A user's guide to vacuum technology*, Wiley, 2003, 3rd ed.

3. C. L. Stong, , “The Amateur Scientist: The Helium Neon Laser”, *Scientific American*, Sept. 1964, Dec. 1965.

4. B. B. Dayton, *Trans. 6th Natl. Symp. Vac. Technol*. (1959), Pergamon Press, New York, 1960.

5. C. H. Xu, et al., *Vacuum engineering technology*, Chemical industry Press, 2006.

6. J. Delafosse and G. Mongodin, *Les Calculs de la Technique du Vide*, La Societe Francaise des Ingenieurs et Techniciens du Vide, Paris, 1961.

CHAPTER 6

GAS DISCHARGE IN HOLLOW-CORE FIBERS

We have illustrated that hollow-core fibers can serve as good waveguide to confine laser beam. Theoretical calculation of coupling loss also indicates that there exists an efficient feedback configuration to form a laser cavity by use of such hollow-core fibers. In this chapter, we present the results of gas discharge experiments which are the first key step toward the construction of a fiber gas laser. We carried out a series of experiments to explore the gas discharge in small size hollow-core fibers and succeeded in obtaining gas discharge in 250, 150, and 50 μm inner-diameter (i.d.) hollow-core fibers by using longitudinal direct current (DC) excitation. Stable glow discharges of at least several minutes were observed for these hollow-core fibers. A flash glow was also observed for a hollow-core fiber with an i.d. of ~20 μm. Breakdown of helium and argon gases in a 26.2cm-length 250μm-i.d. hollow-core fiber was achieved with a voltage of less than 30kV.

6.1 Excitation methods for waveguide gas lasers

Waveguide gas lasers can be divided into several types according to excitation methods and laser medium. For example, the laser medium may be static or flowing. In flowing gas planar waveguide lasers, the flow of the active medium may be parallel (longitudinal flow) or perpendicular (transverse flow) to the flow of light radiation in the guide. Electrically excited lasers may utilize longitudinal or transverse discharges and may be operated in either a CW or a pulse mode.

The first operating He-Ne laser consisted of a glass tube filled with He-Ne mixture, which was inductively coupled into RF resonant circuit allowing RF excitation of plasma inside the tube. However, it was quickly replaced by DC excitation technique, which was much more efficient. The use of RF technique for laser plasma excitation became popular in the 1980s, when the idea of diffusion cooled molecular laser appeared in waveguide and slab configurations. The general idea is to form gas discharge between two electrodes formed in planar or annulus configurations. These configurations allow us to decrease an electrode separation to about 2 mm gap and as a result, to increase the pressure up to 100-150 Torr. A new practical parameter, the extraction of output power from unit area, has been introduced. For example, 20 kW/m^2 can be extracted from RF-excited CO_2 slab lasers. The RF excitation was applied mainly to molecular lasers. RF excitation technique enabled the development of novel waveguide lasers, slab lasers, slab-waveguide lasers, and waveguide arrays. These techniques substantially minimize the dimensions of laser constructions at the kilowatt scale.

The natural continuity of the RF excitation (from tens of MHz to a few hundred MHz) seems to use the microwaves as an efficient plasma excitation technique. Attempts have been made to get such excitations for CO_2 and excimer lasers [1, 2]. However, till today no practical ways for effective excitation of plasma have been demonstrated. The formation of laser plasma by use of microwave excitation is quite attractive and prospective, but it requires some sophisticated and clever solutions.

Transverse RF excitation by square or planar metal waveguide is widely used in commercial waveguide CO_2 laser now. The waveguide He-Ne lasers reported in the

literatures mostly used a combination of longitudinal DC and RF excitation [3-5]. Exciting by using RF alone in waveguide He-Ne laser has not been reported in the literature to our knowledge.

A RF transversely excited (TE) waveguide laser has the potential advantage of providing efficient excitation of the laser medium at high gas-filling pressures. Transverse RF excitation requires no electrodes inside the discharge tube, this makes it easy to construct. The contamination due to sputtering and sealing electrodes in the laser tube can be avoided by adopting transverse RF excitation.

Transverse RF exciting for plasma applications has been reported a lot in the literatures. Toader obtained helium discharge plasma column in a capillary with inner diameter of 1.6 mm and in the frequency range from 28.5 to 36.6 MHz by inductive coupling [6]. Yoshiki et al. excited gases in quartz tubes with inner diameters of 2 and 4mm and an outer diameter of 6mm by transverse 13.56 MHz RF with a power bigger than 3W [7]. However, transverse RF exciting in tubes with inner diameter smaller than 400 μm has not been explored so far.

Although capillary discharge to achieve X-ray emission has been popular since the 1990s, the capillaries used in their experiments are usually on the millimeter level [8]. Smaller size capillary discharge has not been performed to our knowledge since Smith constructed the first waveguide He-Ne laser in 1971 [3], the characteristics of gas discharge in tubes with bore-diameter smaller than 400 μm have seldom been concerned in the past. For the attempting to construct novel hollow-core fiber gas laser, we adopt longitudinal DC excitation as the first step.

6.2 DC discharge regimes

The main characteristics of the DC discharge such as the breakdown voltage, the voltage current characteristic, and the structure of the discharge depend on the geometry of the electrodes and the vessel, the gas used, and the electrode material. By adjusting the ballast resistor in the circuit diagram, we can sweep out a voltage current characteristic as shown in Fig. 6.1.

Three general regions can be identified in Fig. 6.1, the dark discharge region, the glow discharge region, and the arc discharge region. Each of these general regions encompasses many interesting phenomena [9].

The regime between A and E on the voltage-current characteristic is termed a dark discharge because, except for corona discharges and the breakdown itself, the discharge remains invisible to the eye. During the background ionization stage of the process (A-B), the charge density is extremely low. The electric field applied along the axis of the discharge tube only sweeps out the ions and electrons created by ionization from background radiation. The background radiation originates from cosmic rays, radioactive minerals, or other sources. It produces a constant and measurable degree of ionization in air at atmospheric pressure. Under the force of the electrical field the ions and electrons migrate to the electrodes producing a weak electric current. When voltage is increased, more charged particles are drawn to the electrodes and the current increases. An avalanche reaction does not occur at this stage.

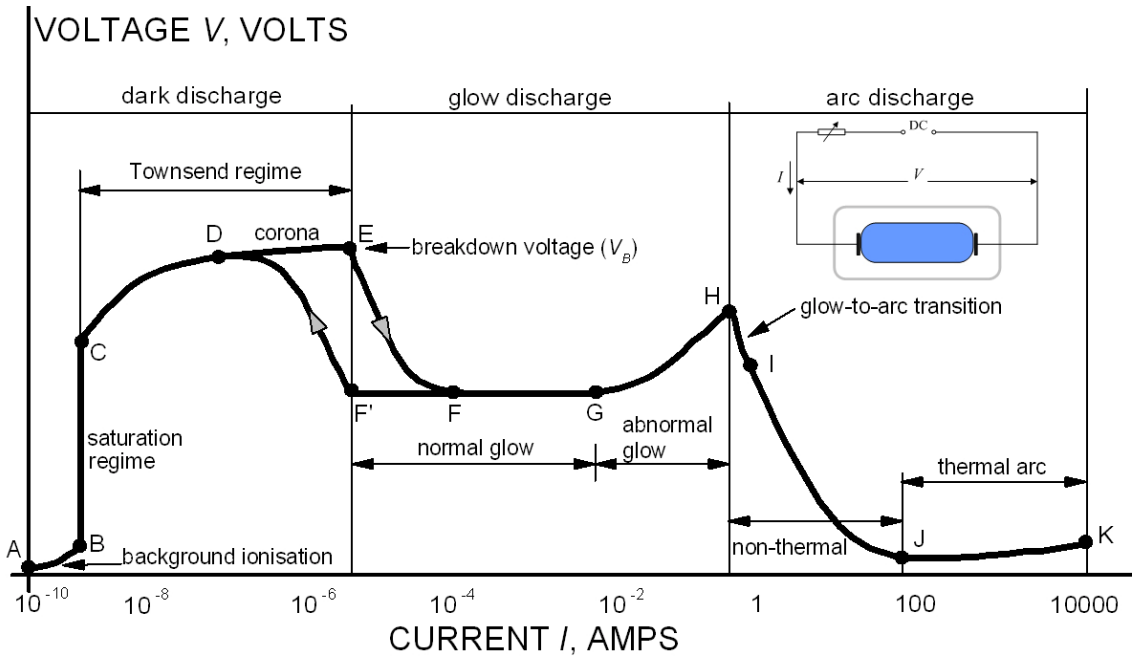

Figure 6.1 Schematic of DC discharge regime [9].

If the voltage between the electrodes is increased to a sufficiently large, eventually all the available electrons and ions are swept away, and the current saturates. In the saturation region (B-C), the current remain constant while the voltage is increased. This current depends linearly on the radiation source strength, a regime useful in some radiation counters.

If the voltage across the low pressure discharge tube is increased beyond point C, the current will rise exponentially. The electric field is now high enough, so the electrons initially present in the gas can acquire enough energy before reaching the anode to ionize a neutral atom. As the electric field becomes even stronger, the secondary electron may also ionize another neutral atom leading to an avalanche of electron and ion production. The region of exponentially increasing current is called the Townsend discharge.

Corona discharges (D-E) occur in Townsend dark discharges in regions of high electric field near sharp corners, edges, or wires in gases prior to electrical breakdown.

If the coronal currents are high enough, corona discharges can be technically “glow discharges”, visible to the eye. For low currents, the entire corona is dark, as appropriate for the dark discharges. Related phenomena include the silent electrical discharge, an inaudible form of filamentary discharge, and the brush discharge, a luminous discharge in a non-uniform electric field where many corona discharges are active at the same time and form streamers through the gas.

Electrical breakdown (E point) occurs in Townsend regime with the addition of secondary electrons emitted from the cathode due to ion or photon impact. At the breakdown, or sparking potential V_B, the current might increase by a factor of 10^4 to 10^8, and is usually limited only by the internal resistance of the power supply connected between the plates. If the internal resistance of the power supply is very high, the discharge tube cannot draw enough current to break down the gas, and the tube will remain in the corona regime with small corona points or brush discharges being evident on the electrodes. If the internal resistance of the power supply is relatively low, then the gas will break down at the voltage V_B, and move into the normal glow discharge regime. The breakdown voltage for a particular gas and electrode material depends on the product of the pressure and the distance between the electrodes, $p \times d$, as expressed in Paschen’s law (1889) [10].

The glow discharge regime owes its name to the fact that the plasma is luminous. The gas glows because the electron energy and number density are high enough to generate visible light by relaxing of excited particles. The applications of glow discharge include gas lasers, fluorescent lights, DC parallel-plate plasma reactors, “magnetron” discharges used for depositing thin films, and electro-bombardment

plasma sources.

After a discontinuous transition from E to F, the gas enters the normal glow region, in which the voltage is almost independent of the current over several orders of magnitude in the discharge current. The electrode current density is independent of the total current in this regime. This means that the plasma is in contact with only a small part of the cathode surface at low currents. As the current is increased from F to G, the fraction of the cathode occupied by the plasma increases, until plasma covers the entire cathode surface at point G. In the abnormal glow regime above point G, the voltage increases significantly with the increasing total current in order to force the cathode current density above its natural value and provide the desired current. Starting at point G and moving to the left, a form of hysteresis is observed in the voltage-current characteristic. The discharge maintains itself at considerably lower currents and current densities than at point F' and only then makes a transition back to Townsend regime.

At point H, the electrodes become sufficiently hot that the cathode emits electrons thermionically. If the DC power supply has a sufficiently low internal resistance, the discharge will undergo a glow-to-arc transition (H-I). The arc regime, from I through K is one where the discharge voltage decreases as the current increases, until large currents are achieved at point J, and after that the voltage increases slowly as the current increases.

It shall be mentioned that our discharge experiments consider two important parts of the whole process. The first is the breakdown voltage (E point). The previous literatures concern more on discharge between the parallel-plate and discharge in tubes with bore diameter much bigger than 400 μm. Whether smaller size tubes can be

breakdown or not is still needed to be investigated. The second we concerned is the normal glow discharge (F-G-F-F'). To design suitable power supply for fiber gas lasers, the current-voltage (I-V) characteristics is also necessary to be studied.

6.3 Gas breakdown in hollow-core fibers

6.3.1 Gas breakdown theories

Assuming that discharge can be self-sustained, the following relation can be obtained from Townsend model [10]

$$Apd\exp(-\frac{Bpd}{V_B})=\ln(1+\frac{1}{\gamma}) \tag{6.1}$$

where p is gas pressure, d is the distance between the two plate electrodes, V_B is the breakdown voltage, γ is the secondary electron emission coefficient due to ion bombardment at the cathode, and A and B are constants dependent on gases.

Townsend's model has been extensively tested by experiments and is suitable for the study of gas discharge between two parallel-plates. However Townsend model didn't consider the wall effect hence it may not be suited for the study of gas discharge in small bore diameter tubes. Wang and Huang modified Townsend's model by introducing an electron-loss coefficient caused by wall-effect, and from the modified model the following relation for gas breakdown is obtained [11]

$$Apd\exp(-\frac{Bpd}{V_B})-C\frac{d^2}{R^2V_B^{1/4}(Pd)^{3/4}}=\ln(1+\frac{1}{\gamma}) \tag{6.2}$$

where C is a constant dependent on gases and R is the inner radius of the tube.

Wang and Huang performed experiments with different bore diameter tubes (1.1, 1.8 and 3.2 mm) and parallel-plates. Their experimental data match well with that predicted

from Eq. (6.2), which verifies the suitability of the modified model for the study of gas discharge in millimeter bore diameter tubes.

6.3.2 Experimental setup and phenomenon

The hollow-core fibers used in our experiments have outer diameter of ~343μm and various i.d. of from 20 to 250μm. They are either pure silica tubes or silica tubes with a higher index Ge-doped-silica inner layer. The experiment setup is shown in Fig. 6.2. Two gas chambers are connected to a vacuum system and the two open-ends of a hollow-core fiber are inserted into the two gas chambers with good seal. The hollow-core fiber serves as a channel to ensure gas flow between the two gas chambers. The two gas chambers and the centre-hole of the hollow-core fiber are pumped to high vacuum before gas to be studied flowing into the chambers. Two electrodes are placed respectively inside the two gas chambers and close to the two ends of the hollow-core fiber.

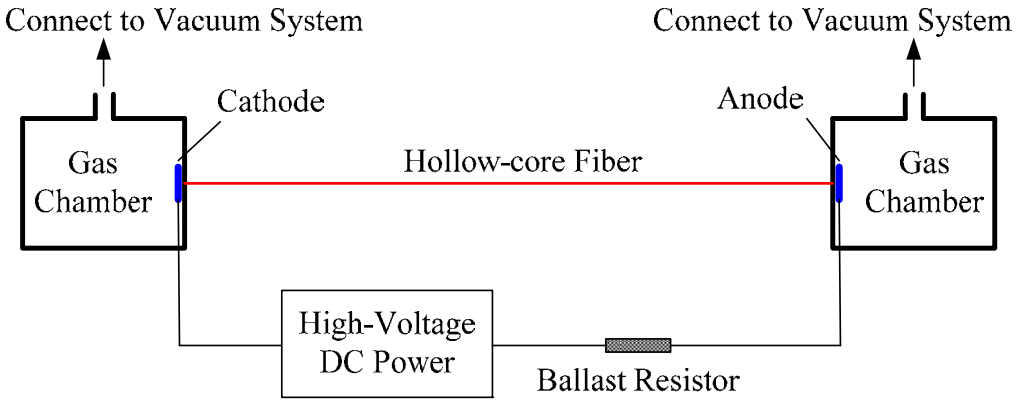

Figure 6.2 Schematic of gas discharge experiment.

Two different types of electrodes are used in our experiments as shown in Fig. 6.3: (1) Brass column electrodes (Φ21mm×8mm) with a hole (Φ0.8mm) in each electrode; the two ends of the hollow-core fibers are placed inside holes in the electrodes, and the distance between the electrode and the center-hole of the hollow-core fiber may be

regarded the same as the thickness of the fiber wall and is from 46 to 162μm, depending on the fiber samples used; (2) Tungsten pin electrodes (Φ1.5mm×40mm rod with one end polished as sharp as possible) with their tips placed close to the ends of the hollow-core fiber with a distance of ~2mm.

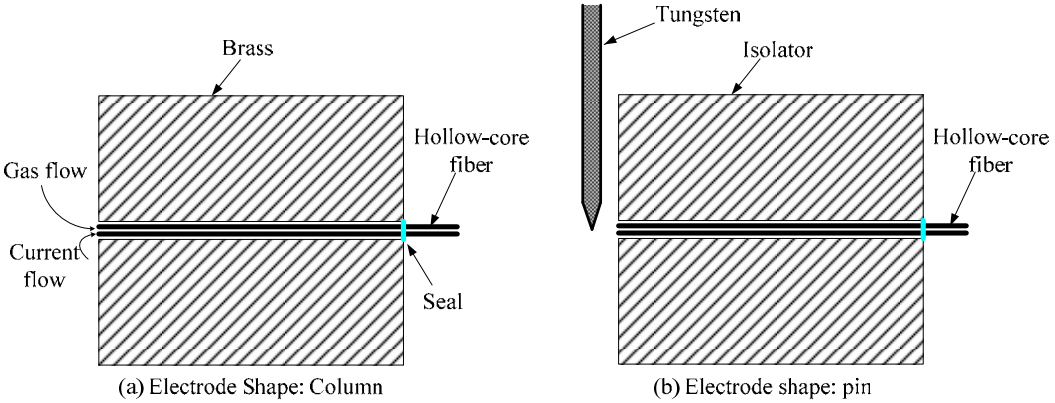

Figure 6.3 Two types of electrodes.

Our first experiment used a thermometer tube with 13cm-length and 344μm-i.d.. We succeeded to discharge gases (Ar, He and CO_2) and observed purple glow light emitting from the central bore as shown in Fig. 6.4.

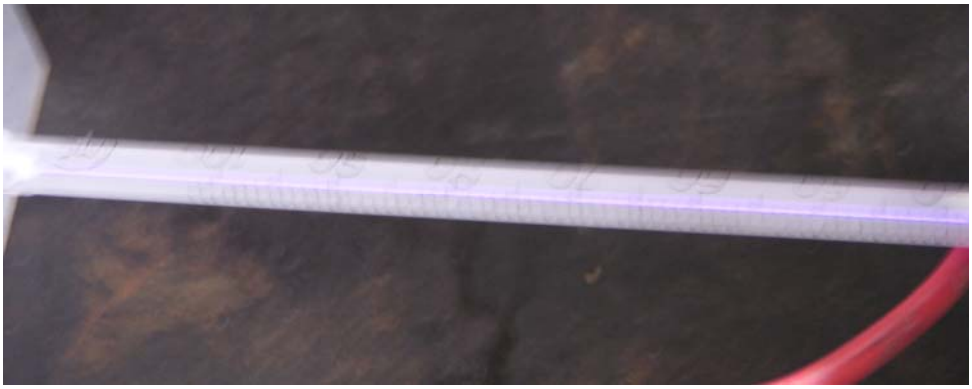

Figure 6.4 Discharging in a thermometer tube.

Fig. 6.5 shows the side view and end view of the glow discharge inside an 8cm-length 250μm-i.d. hollow-core fiber filled with helium gas. We also succeeded in exciting Ar, He, Ne and CO_2 in hollow-core fibers and observed similar glow discharge. Purple glow light is dominant regardless of gas types in the view of human eyes, which

is different from discharge phenomenon in conventional larger size glass tubes. The reason is not clear since that the fiber spectrometer used in the measurement has a range of 450-1150nm and the color of purple corresponds to the wavelength range of 380-440nm. Further investigation on the spectral content of the glow light and the physics behind it is needed.

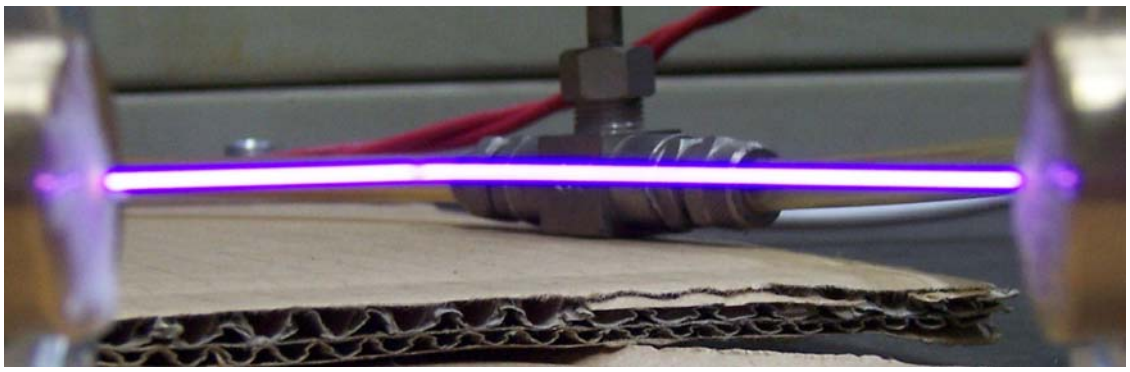

(a)

(b)

Figure 6.5 Side view (a) and End view (b) of glow discharge inside a hollow-core fiber with 250μm-i.d. and 8cm-length filled with helium gas.

6.3.3 Experimental results

To examine the effect of electrode shape on the breakdown voltage, we carried out discharge experiments of helium and argon gases in 250μm-i.d. hollow-core fibers with approximately the same length (8.2cm and 8cm) but with column and pin shaped electrodes. The breakdown voltages as functions of gas pressures are shown in Fig. 6.6. Different types of gases seem have little effect on the breakdown characteristics for both

types of electrodes. The breakdown voltages for pin electrodes are lower than that for the column electrodes. This is expected because that the pin electrodes can form stronger electric field in its tip and the breakdown voltage in case of pin electrodes hence should be smaller.

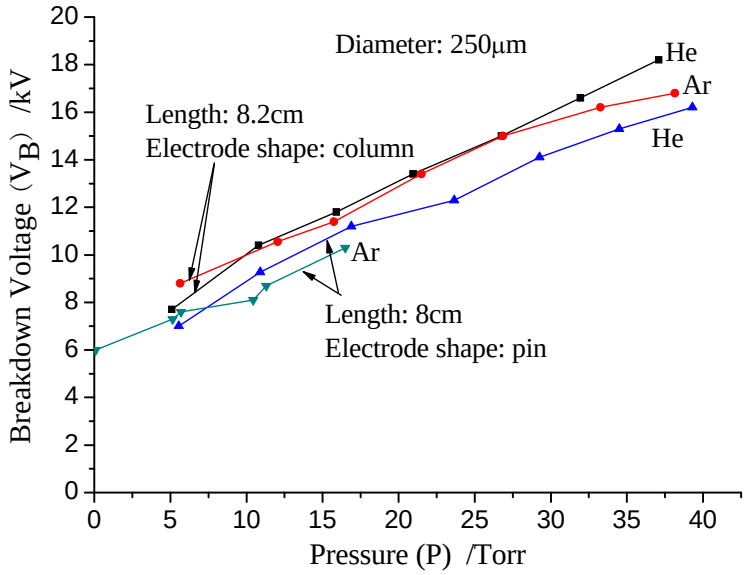

Figure 6.6 Comparison of the breakdown characteristics with column and pin electrodes.

Fig. 6.7 shows the experimental breakdown characteristics of helium and argon gases in a 26.2cm-length, 250μm-i.d. hollow-core fiber. Experimental results indicate that helium gas has a little higher breakdown voltage than argon gas, and this coincides with the fact that ionization energy of argon is smaller than that of helium. However theoretical results based on Eq. (6.2) show quite different results: breakdown curve of argon is above the curve of helium and they have great discrepancy as compared with experimental results. For gas pressure below 15 Torr, discrepancy between theory and experiment is large with the theoretical breakdown voltage increase rapidly with a decrease in gas pressure while the experimental data show a relatively slow decrease. We believe that there should be an uptrend for breakdown voltage when gas pressure is reduced to certain level, because high vacuum has good insulation performance and it is

hard to break down. However we did not observe this uptrend in the range from 1 to 35 Torr.

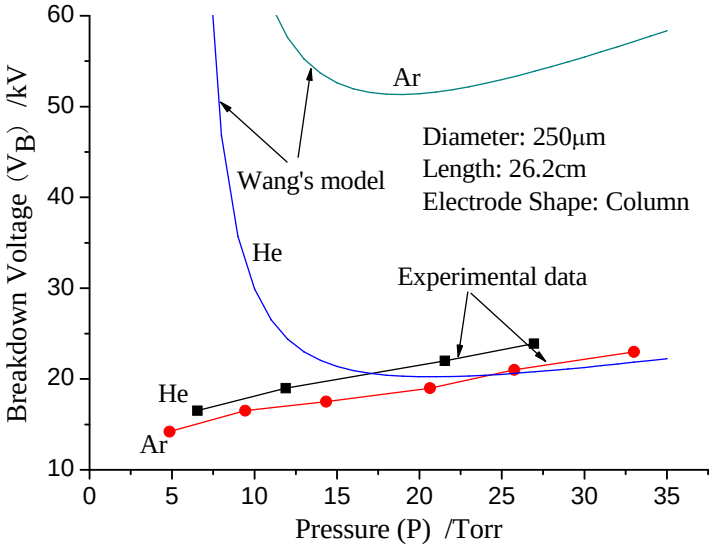

Figure 6.7 Comparison between experimental data and theoretical data for a hollow-core fiber with 250μm-i.d. and 26.2cm length.

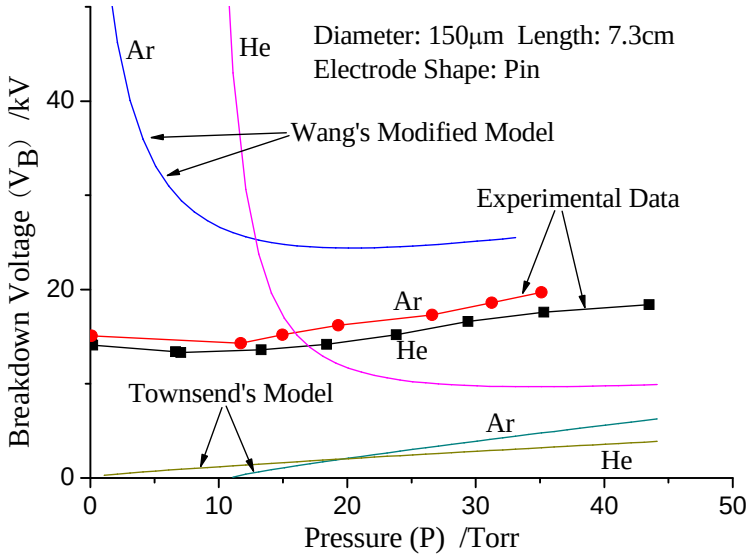

Figure 6.8 Comparison between experimental and theoretical results for a hollow-core fiber with 150μm bore diameter and 7.3cm length.

Fig. 6.8 shows the comparison between breakdown voltages measured experimentally and calculated theoretically by using Eqs. (6.1) and (6.2) for gas

discharge in a 7.3cm-length, 150μm-i.d. hollow-core fiber. Compared with Wang's modified model, Townsend's model is relatively flat and similar in trend with the experimental curves. No crosspoint was observed between the experimental curves of helium gas and argon gas; however both theoretical models indicate a crosspoint. The curve predicted from Towsend's model is much lower than experimental results, indicating that the wall effect should be considered when interpreting discharge phenomenon in small bore diameter tubes. On the other hand, the wall effect in Wang's model may be over emphasized. This viewpoint is also supported by our experimental results for gas discharge in smaller i.d. hollow-core fibers as for the case shown in Fig. 6.9.

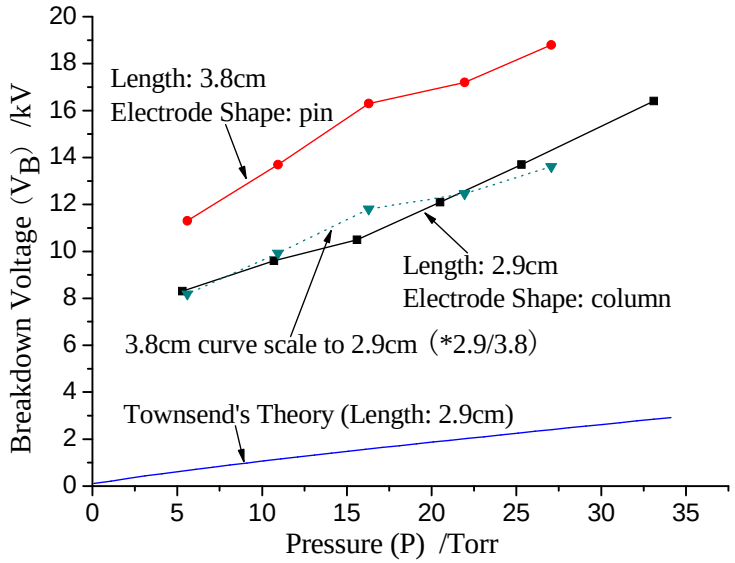

Figure 6.9 Experimental results of discharge in a hollow-core fiber with 50μm bore diameter filled with argon gas.

We succeeded in obtaining gas discharge in 50μm-i.d hollow-core fiber with 3.8cm length (pin electrode) and 2.9cm length (column electrode) respectively and the results for argon gas are shown in Fig. 6.9. The theoretical results obtained from Townsend's model are also shown in Fig. 6.9. The theoretical results from Wang's modified model

are not shown because they are much larger than 100kV. This tremendous deviation from measured values indicates that Wang's modified model is no longer suitable for studying discharge in such small bore-diameter tubes. The measured V_B–P curve is similar in trend as, but significantly larger than that calculated from Townsend's model. This suggests that further theoretical investigation is needed to understand the unique characteristics of gas discharge in hollow-core fibers with i.d. smaller than 250μm. We also scaled the V_B–P curve for the 3.8cm hollow-core fiber with the pin electrode down to 2.9cm length and the results are shown as a dashed curve in Fig. 6.9. The dashed curve is very close to the results from the 2.9cm hollow-core fiber with column electrodes, suggesting that effect of electrodes shapes have little effect on the breakdown characteristics for such small bore diameters.

Due to the limitation of our discharge system, we can not measure the breakdown voltage when the filling pressure is very low, because other channels of the vacuum system have much bigger bore diameter than the hollow-core fiber and the breakdown between these other channels will occur earlier and hence extinguish the breakdown in the center-core of the hollow-core fiber. In our measurement range from below 1 to 50 Torr, the uptrend of the breakdown voltage with a decrease in gas pressure was not observed. Another conclusion can be drawn from our experimental investigation is that the increasing the length of hollow-core fiber requires larger voltage for gas breakdown and the slope of the V_B–P curve also becomes bigger for longer length. For the same length of hollow-core fiber, the voltage required to break down increases when the bore-diameter reduces. It becomes hard to obtain sustained discharge by using longitudinal direct current (DC) excitation, when the bore diameter is below 30μm.

6.4 *I-V* characteristics of gas discharge in hollow-core fibers

After the gas in the hollow-core fiber is broken down by a strong electrical field, the voltage between the two ends of the hollow-core fiber will drop to a lower value, and steady glow discharge is obtained within the hollow core of the fiber. We will discuss the current-voltage (*I-V*) characteristic of steady glow discharge in this section. The voltage *V* was measured from across the two electrodes, and the the current *I* was calculated from the measured voltage across the ballast resistor.

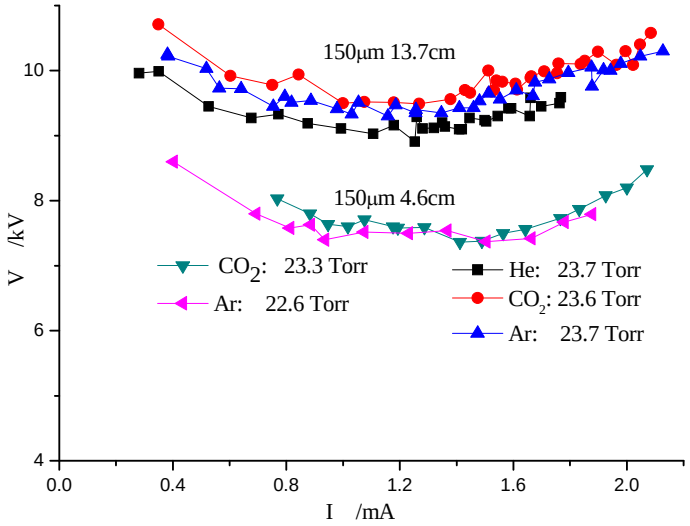

Figure 6.10 *I-V* characteristics of 150μm-i.d. tubes of different lengths and filled with different gases at the same pressure.

We studied three types of gases: He, Ar and CO_2 (actually it is a mixture of gases used in CO_2 lasers and includes five ingredients) in our discharge experiments. We measured the current-voltage (*I-V*) characteristics when hollow-core fibers with various size and lengths are filled with gases at different pressures. The results are shown in Fig. 6.10. In a 13.7cm-length 150μm-i.d. hollow-core fiber, the *I-V* characteristics have little difference when the hollow-core is filled with different types of gases at the same pressure. The results obtained from a 4.6cm-length 150μm-i.d.

hollow-core fiber also indicate this point. Due to the small size of the hollow-core, composition of filling gas in the core-area does not bring much deviation to the *I-V* characteristics. When the length of the discharge tube increases, *I-V* curve shifts upward as shown in Fig. 6.10. The voltage for a 13.7cm-length tube is about 2kV higher than that for a 4.6cm-length tube.

The effect of varying bore diameters on the *I-V* characteristics at comparable pressure can be seen from Fig. 6.11. Although the 50μm-i.d. tube has a shorter length and a slightly lower gas pressure, the voltage is still larger than that for those tubes with larger bore diameters. When the diameter of the hollow-core is further reduced to below 50 μm, the voltage required for sustained glow discharge will be considerably larger and the discharge becomes difficult.

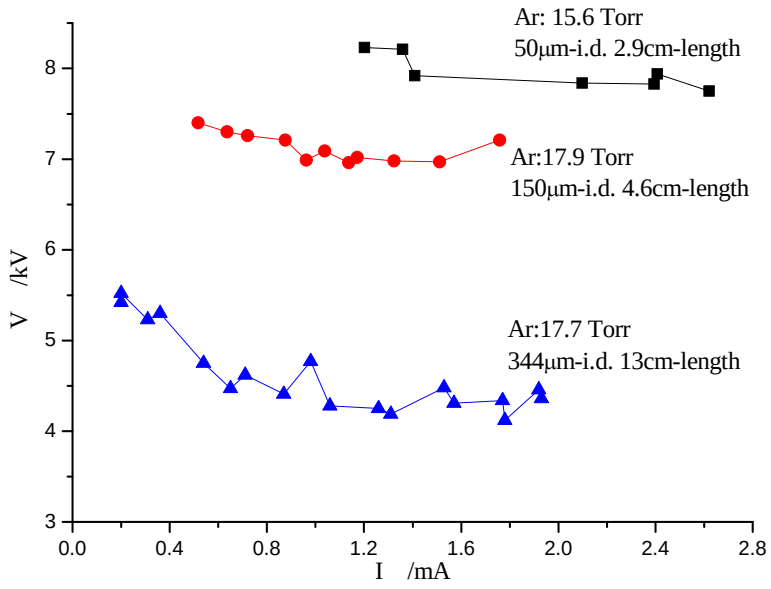

Figure 6.11 Comparison of *I-V* characteristics for different bore diameters.

Little theoretical research on the discharge characteristics of small bore tubes has been reported. Using the model of Schuöcker et al. [12], we calculate the *I-V* characteristics of a 150μm-i.d., 13.7-cm length and a 250μm-i.d., 8-cm length

hollow-core fibers filled with helium gas. The calculated results together with the experimentally measured ones are shown respectively in Figs.6.12a and 6.12b.

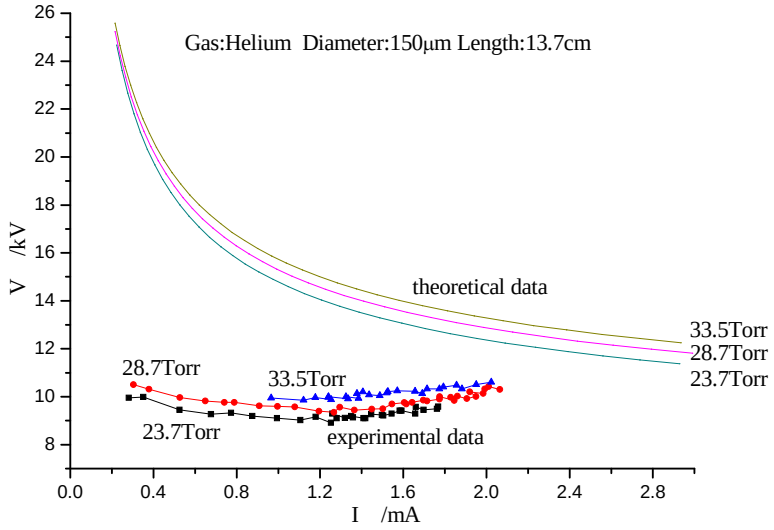

(a)

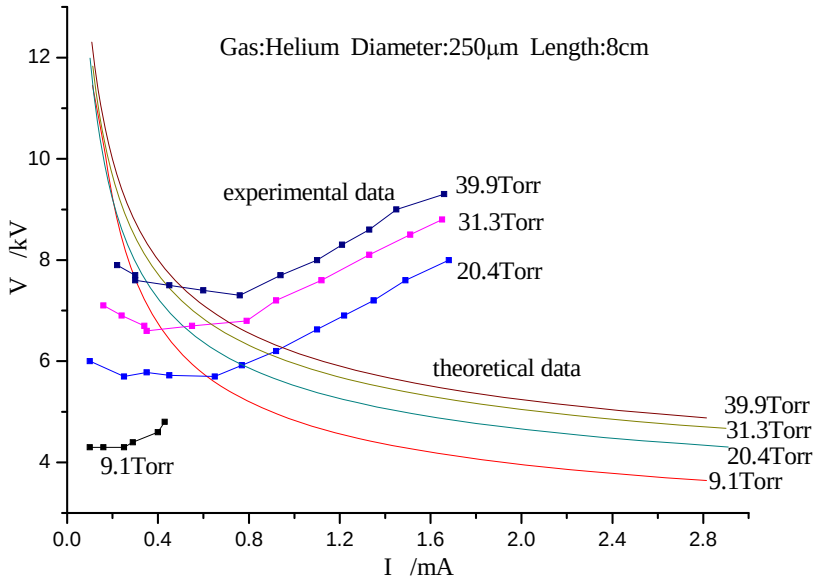

(b)

Figure 6.12 Comparison between experimental data and theoretical data for hollow-core fibers filled with helium gas: (a) 150μm-i.d. and 13.7cm-length; (b) 250μm-i.d. and 8cm-length.

The *I-V* curve shift upward when the filling pressure is increased and this agrees with the modeling results. However, there are large deviations between the

experimental and the theoretical data. Theoretical calculation indicates a decrease of voltage as current increases; however, the experimental voltage curves are either flat (Fig. 6.12a) or even increases with current (Fig. 6.12b), which is in contrary to the trend of the theoretical curves. This indicated that the previous theory may not be fully suited to predict the *I-V* characteristics in such small bore-hole tubes and further investigation is needed to find out the reasons.

In Figs. 6.10-6.12, the smallest currents are above ~0.1mA. Actually, after the gas is broken down, the initial current is bigger than these values. The smallest currents are measured by reducing the voltage after the breakdown. When the current was smaller than the smallest values indicated in these figures, the discharge was extinguished.

6.5 The effect of fiber bend on gas discharge

All the results of gas discharge presented in previous sections are for straight hollow-core fibers. To best utilize the advantage of hollow-core fiber, i.e., bending down to small diameter with minimize loss, we will investigate, in this section, the bending effect on gas discharge in hollow-core fibers.

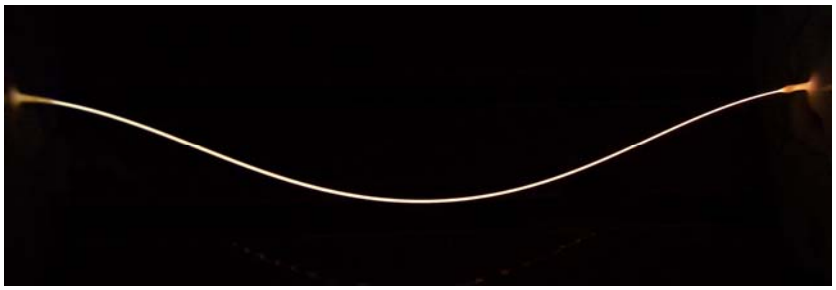

Figure 6.13 A 250μm-i.d. hollow-core fiber with a bending radius of ~11cm.

Fig. 6.13 shows the side view of gas discharge in a 250μm-i.d. hollow-core fiber when it was bent to a radius of ~11cm. The breakdown voltage and *I-V* characteristics

were found to have no measurable difference from that for the straight fiber. Fig. 6.14 shows the glow discharge obtained in a 150-μm-i.d., 13.5-cm-length hollow-core fiber when it was bent to a 3-cm-diameter circle; the breakdown and *I-V* characteristics are also similar to that for a straight fiber.

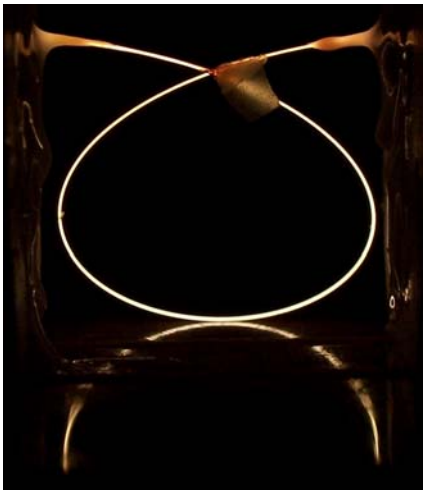

Figure 6.14 A 150μm-i.d., 13.5-cm-length hollow-core fiber bent to a 3-cm-diameter circle.

Bending to smaller radius will exceed the mechanical tolerance of this kind of hollow-core fiber that we used and will be easy to break. Therefore, hollow-core fibers bending to a several centimeter circle will not cause any effect on gas discharge.

6.6 Spectrums of glow discharge

Fig. 6.15 shows the glow discharge spectrums obtained from a 150μm-i.d. and 8cm-length hollow-core fiber filled with helium gas. We used a fiber optic spectrometer to measure the spectrum. Solid line was measured from the end (cathode) of the hollow-core fiber and dashed line was measured from the side of the hollow-core fiber. The peaks at 587.6, 501.5 and 667.8nm are characteristic spectral lines of helium. The intensities of the spectrum lines observed from the end are stronger and sharper than that from the side. Further detailed investigation on the glow

discharge in hollow-core fiber from the view of spectroscopy will be carried out in due course.

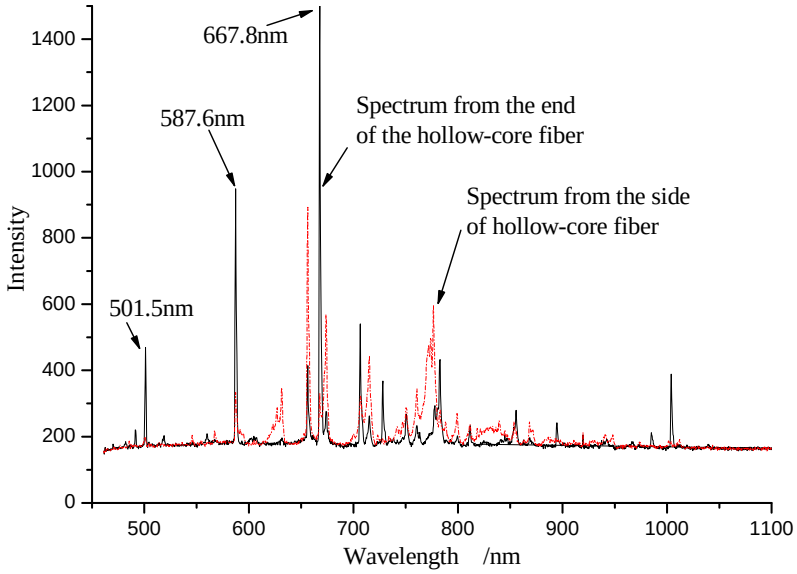

Figure 6.15 Glow discharge spectrums obtained from a 150μm-i.d. and 8cm-length hollow-core fiber filled with helium gas.

6.7 Summary

We succeeded in obtaining gas discharge in 250, 150, and 50 μm inner-diameter (i.d.) hollow-core fibers by using longitudinal direct current (DC) excitation. The reducing of bore diameter, the increasing of the length of the discharge tube, and the increasing of the filling pressure all will make gas discharge becoming difficult. The gas discharge in hollow-core fibers with inner diameter smaller than 20 μm is not stable under the maximum voltage of 30kV. The longest length of hollow-core fiber succeeded in obtaining gas discharge is about 26.2cm for a bore-size of 250μm-i.d., and a longer length is believe to be possible if the higher voltage is applied. Consider the facts that the waveguide gas laser with 430μm-i.d and 20cm-length [3] has been constructed and smaller bore-size and longer length of gain tube would provide larger gain, it should

then be possible to construct hollow-core fiber gas lasers with an i.d. of 250μm or less. Bending experiments indicate that bending the hollow-core fiber down to a few centimeter circle would have negligible effect on the characteristics of gas discharge.

References

1. M. Marz, W. Oestreicher, “Microwave excitation of a diffusion-cooled CO_2 laser,” *J. Phys. D: Appl. Phys.*, vol. 27, pp. 470-474, 1994.
2. V. A. Vaulin, V. N. Slinko and S. S. Sulakshin, “Excimer XeCl laser excited by microsecond megawatt microwave pulses from a commercial 3.07-GHz microwave oscillator,” *Sov. J. Quantum Electron.*, vol. 20, pp. 1449-1450, 1990.
3. P. W. Smith, “A waveguide gas laser,” *Appl. Phys. Lett.*, vol.19, pp.132-134, 1971.
4. S. A. Gonchukov, S. T. Kornilov, and E. D. Protsenko, “Oscillation modes of a gas laser with waveguide resonator,” *Sov. J. Quantum Electron.*, vol. 6, pp. 996-997, 1976.
5. S. A. Gonchukov, S. T. Kornilov, V. N. Petrovskii and E. D. Protsenko, “Helium-Neon waveguide laser,” *Sov. J. Quantum Electron.*, vol. 5, pp. 232-233, 1975.
6. E. I. Toader, “Measurements of electron temperature in radio frequency capillary helium glow discharges,” *J. phys. D: Appl. Phys.*, vol. 29, pp. 2668-2671, 1996.
7. H. Yoshiki, A. Oki, H. Ogawa, and Y. Horiike, “Generation of a capacitively coupled microplasma and its application to the inner-wall modification of a

poly(ethylene terephthalate) capillary," *J. Vac. Sci. Technol. A*, vol. 20, pp. 24-29, 2002.

8. C. D. Macchietto, B. R. Benware and J. J. Rocca, "Generation of millijoule-level soft-X-ray laser pulses at a 4-Hz repetition rate in a highly saturated tabletop capillary discharge amplifier," *Opt. Lett.*, vol. 24, pp. 1115-1117, 1999.
9. Y. P. Raizer, J. E. Allen and V. I. kisin, *Gas Discharge Physics*, Springer, 2001
10. A. von Engel, *Ionized Gases*, second edition, Oxford University Press, 1965.
11. Y. Z. Wang and Z. L. Huang, "Study on low-ignition-voltage helium neon laser (I)-Breakdown characteristics of capillary discharges," *Laser Resonators IV*, V. K. Alexis, H. P. Alan, vol. 4270, pp. 236-244, San Jose, 2001.
12. D. Schuocker, W. Reif, R. Erlacher, and G. Schiffner, "Properties and current-voltage characteristics of discharges in waveguide gas lasers," *Appl. Phys.*, vol. 14, pp. 277, 1977.

CHAPTER 7

PROBLEMS IN DESIGNING FIBER GAS LASERS

In this chapter I will discuss the technical problems associated with the construction of fiber gas lasers. Solving these problems is the key for successful demonstration of such fiber gas lasers.

7.1 The problems due to the requirement of high vacuum

7.1.1 The high vacuum system

As mentioned previously, the construction of He-Ne gas lasers request a vacuum of 10^{-5} Torr or lower. Therefore the vacuum system and connected gas chambers all should have good vacuum performance.

Good performance of vacuum requests vacuum system using metallic (aluminum or stainless steel) pipes as connections. However our previous vacuum system partially used PVC tubes as connections and has small leakage, and hence can not all guarantee the high vacuum level required. We used PVC tubes to connect the two gas chambers to the vacuum system as shown in Fig. 7.1a. This connection is benefit in gas discharge of DC longitudinal excitation because all metallic connections will lead to the conduction between the two gas chambers. There are also other problems due to the connection of PVC tubes that somewhere will discharge early before the discharge in hollow-core fibers, for example, the anode, the valve *a* and the vacuum system can form a loop and discharge earlier and extinguish the discharge in the hollow-core fiber as shown in Fig. 7.1a. When the gas filling pressure is below 1 Torr, it will fail to

discharge in hollow-core fibers. One alternative method is to connect only one gas chamber to the vacuum system, or evacuate the two gas chambers in the beginning and then disconnect one gas chamber from the vacuum system as shown in Fig. 7.1b. We have tried this method but it is harder to achieve discharge in the hollow-core fibers than for keeping the two connections. Further investigation on this phenomenon is needed to understand the reason behind it. If higher vacuum is needed, the metallic connection is necessary; then we should disconnect one connection to allow DC discharge between the two gas chambers as indicated in Fig. 7.1b.

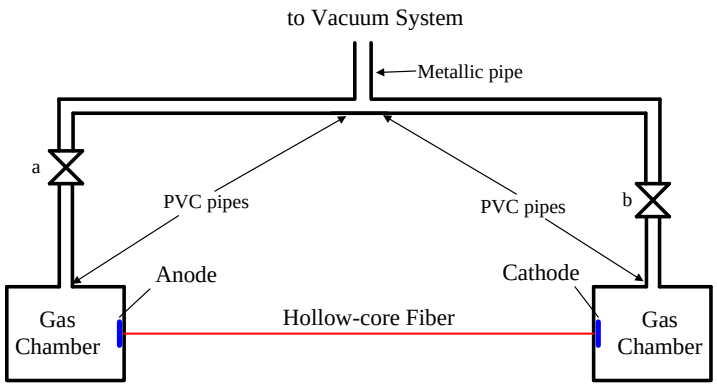

(a)

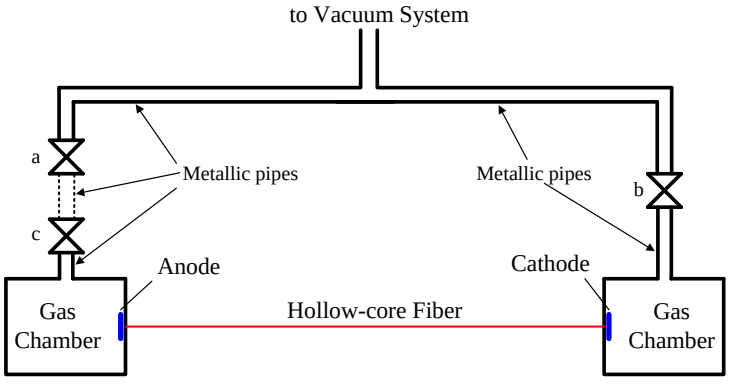

(b)

Figure 7.1 Schematic of vacuum connections: (a) previous connections, (b) new connections.

Although glass tube could also be a choice, the connection between the glass tube and gas chamber would be a problem. The requirement of changing the length of the

fiber during experiments makes the use of glass tube for connection inconvenient.

We have measured the spectrums of glow discharges when the hollow-core fiber was filled with pure He, Ar and O_2. The glow discharge spectrums obtained from a 150μm-i.d. and 8cm-length hollow-core fiber filled with helium gas has been presented in previous chapter. It shall be mentioned that we observed additional spectra-lines that didn't belong to the pure gas we filled in. For example, the spectra-lines of 631.33nm, 656.36nm and 673.83nm were always existed independent of the type of gas filling the hollow core. We believed that the line of 656.36nm is belonged to hydrogen atom which might be originated from the decomposition of oil molecules in the vacuum system. The origin of other spectral lines has not been determined. All these indicate that the vacuum system we used previously was not sufficiently clean for constructing He-Ne gas lasers. Since the vacuum system has been used for CO_2 lasers for many years and we conjecture that the other two spectra-lines belong to gradients of CO_2 laser gas mixture. The vacuum system described in Chapter 5 is a new system that we are building, and we hope to achieve better discharge performance with such a system.

7.1.2 The gas chambers

There are requirements for good performance of vacuum in gas chambers. It is needed to establish a good seal between a hollow-core fiber and the gas chamber. It is also necessary to seal electrodes near the end of hollow-core fiber. We have tried two types of electrodes: column and tip electrodes in our previous experiments. The two types of electrodes have similar performance in gas discharge as discussed previously. We prefer column electrodes since it is more convenient. Our experiments used aluminum as the material of gas chambers. We also tried to use PTFE gas chambers to avoid

strong electrical field outside the hollow-core fiber between two electrodes. No significant advantages were observed for the PTFE chambers. Therefore, using metallic material as gas chamber will be our preferable selections. This will help to solve the problem of embeding electrode into the gas chambers.

Another arising problem is how to seal between hollow-core fiber and gas chambers. Conventional effective sealing method in the field of vacuum is to use O rings. However the hollow-core fibers we used have outer diameters of 343μm or 125μm, there are no O rings that have such a small size. One solution may be to insert the hollow-core fiber into a sleeve with a larger diameter and to use O rings to seal between the sleeve and gas chamber. However, sealing between the sleeve and hollow-core fiber is also required. Welding between the hollow-core fiber and sleeve is not a good idea. The only suitable method may be to use sealant. We used silicone in our initial experiments. The thermal effect at the contact between discharge tube and silicone would bring new problems, e.g. contaminations or vapor produced during this process, that need to be investigated. Vacuum epoxy may be a suitable choice in the final stage but is not economical for repeated experiments because it is hard to clear and not convenient to strip and reuse.

As reported out by Light et al. [1], helium gas can permeate from inside a hollow-core PBG fiber to outside. The permeation will change the He:Ne ratio and total pressure and affect the performance of lasing, therefore this is needed to be investigated by experiments. We have no corresponding vacuum instruments to measure them in our previous used vacuum system. Our newly designed vacuum system has these capabilities and we will study them later.

7.2 The problems due to the alignment of mirrors

7.2.1 Mirrors close to the ends of hollow-core fiber

As discussed in previous chapter, flat mirror close to the end of hollow-core fiber is the best choice for gas lasers with hollow-core fibers of inner diameter smaller than 250 μm (i.e., case I in Table 3.2). According to calculations in Chapter 3, the maximum distance allowed between the flat mirror and the end of the waveguide decreases with the reduction of the tube diameter provided that the coupling loss smaller than 1.3% is required. For hollow-core fibers with D<250 μm, the small gaps between the flat mirror and the end of tube will left no rooms for inserting electrodes in-between the gaps by use of conventional DC excitation or combination of DC and RF excitation. The electrodes near the reflection mirrors would cause damage to the surface of the mirror due to thermal effect. Evacuation of gases in the hollow tube will also become difficult because of the small spacing between mirror and the open-end of hollow-core fiber.

An alternative method is to drill a hole on the side of the hollow-core fiber some distance away from the end and use this hole as the gas flow and discharge channel. Two micromachining techniques may be used to fabricate such holes on silica fibers. There exists two ways about micromachining on silica fibers. One is to use a 157 nm F_2-laser [2-5], and the other is to use a femtosecond laser [6-10].

Since Silica is not transparent for light with wavelength smaller than 180nm [11]. 157nm F_2-lasers can be used for machining on silica effectively. Fig. 7.2 shows the side-holes drilled by using the 157nm laser in Fiber Optic Sensing Technology Research Center of Wuhan University of Technology.

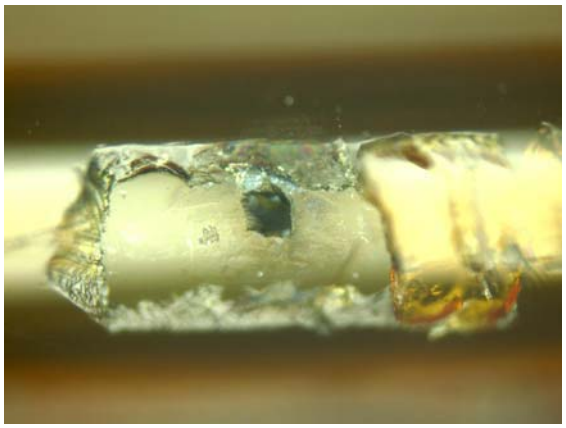

(a)

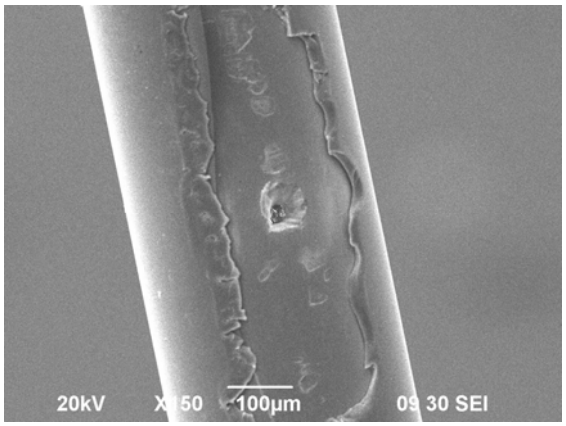

(b)

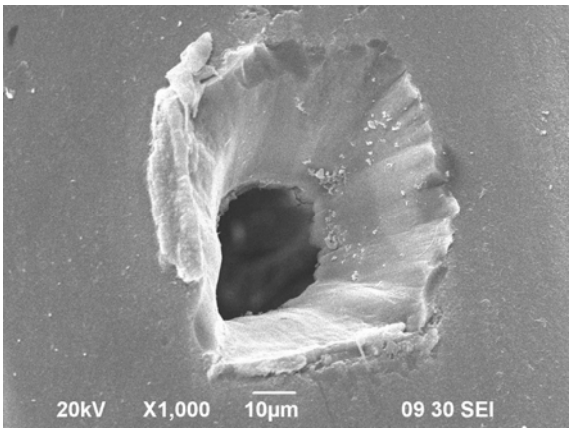

(c)

Figure 7.2 Drilling holes on a 250μm-i.d. hollow-core fiber: (a) photo taken by high-resolution optical microscope; (b) photo taken by SEM at ×150 magnification; (c) photo taken by SEM at ×1000 magnification.

A small part of coating was striped and then a hole was drilled from one side of the

hollow-core fiber. The photos taken by high-resolution optical microscope and SEM are showed in Fig. 7.2. The shape of the hole has an approximated square cone-shape. The size of the hole is ~55μm at the out surface of the fiber, and ~25μm at the interface. In the Fig. 7.2c we can clearly see that the hole is deep into the hollow-core of the fiber.

We have explored the discharge through the drilled hole. One side of the hollow-core fiber is same to what described in Chapter 6.3.2. The other side has a hole drilled 1cm from the end, and the end was sealed by silicone. We observed same discharge phenomenon as described in Chapter 6. This demonstrates that gas discharge can be generated from the electrodes near a side-hole of the fiber. The effect of hole size on the gas discharge and transmission loss are to be investigated to find optimal hole size for constructing fiber gas lasers.

The micromaching by using a F_2 laser need to be done in gas chambers since atmosphere has stronger absorption for ultraviolet light. Therefore it is not convenient to perform in situ measurement of the loss due to the holes.

Comparing to micromaching by using F_2 laser, femtosecond lasers at near infrared wavelength (e.g. 710-920nm) have the advantages [12-16] of without needing to work inside a gas chamber, and hence it is easier to measure the transmission loss due to the introduction of side holes. Hensley et al. [17] reported the drilling a side hole with a diameter of 1.5 μm to the central hollow-core of a hollow-core PBG fiber by using a femtosecond laser as shown in Fig. 7.3. To measure the loss caused by drilling through the side of the fiber, a cutback method was employed. Six evenly spaced holes were drilled over a 2-mm section of a 33-cm length of HC-PBGF (Crystal Fibre, HC-1550-02) with a hollow-core diameter of ~10.9μm. Fusion splicing the HC-PBGF to a

fiber-coupled broadband source allows for a consistent measure of throughput without altering the input coupling. Spectral transmission measurements were then taken before and after the laser-drilled region was cutback. The measured loss due to the drilled region of the fiber is found to be approximately 2.1 dB from 1500-1550 nm. Since the intrinsic loss of the fiber at these wavelengths is negligible (0.1 dB/m), this yields an estimated loss of 0.35 dB (~7.7%) for a single drilled microchannel [17].

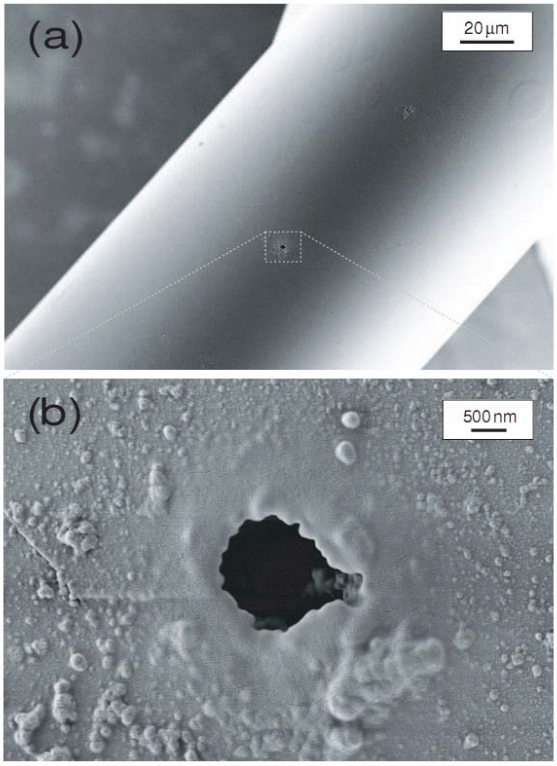

Figure 7.3 (a) SEM image of HC-1550-02 fiber laser drilled with 80-nJ pulses. (b) Closeup image of drilled capillary formed in the side of fiber, the surface diameter of the channel is 1.5 µm [17].

Smith [18] cut a length of 356µm along the axis of a hollow-tube with an inner diameter of 412µm. The measured the loss of such a cut is about 0.5%, with no observable mode conversion. This indicates that the method of drill or cut to form a discharge channel is suitable for tubes with bigger inner diameters. However this might

be not applicable to tubes with very small inner diameter. Since for such small tubes, low transmission loss requires smaller size cuts or holes which may be difficult to perform DC discharge. This conclusion is not absolute because discharge may still pass through the hole even their diameters are small. Further experiments are needed to examine the effect of hole-size on the transmission loss and discharge characteristics.

7.2.2 Alignment of mirrors

In a conventional He-Ne laser, the bore-hole or capillary used to form the cavity is typically straight and the inner diameter of the bore-hole is from 0.5 to 3mm. The alignment of cavity mirrors can be done by using a collimated laser beam.

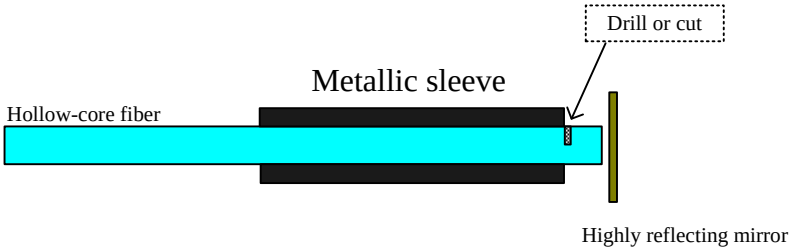

Figure 7.4 Alignment of mirrors.

The hollow-core fibers have inner diameters from 5 to 250μm, and can be bent down to reasonable small diameters. It is then hard to use an external monochromatic light to align the cavity mirrors. However we may solve the alignment problem by proper mechanical design. As shown in Fig. 7.4, a sleeve with an inner diameter slightly larger than the outer diameter of the hollow-core fiber may be used to achieve the required alignment. After the sleeve is aligned with the mirror, the hollow-core fiber is then inserted into the sleeve. Even though there may be small misalignment, we may slightly adjust the relative positions of the mirror and the fiber to achieve accurate alignment. Beside to serve as alignment tube, the metallic sleeve may also be used as

an electrode.

7.3 The problem due to cleaving of hollow-core fibers

As mentioned previously hollow-core fibers with different outer diameters may be used to construct fiber gas lasers. The hollow-core fibers we used have outer diameter of 125 μm and 343 μm. Existing standard fiber cleaver can be used for the former one, which has the same outer diameters as the standard silica fibers. For the fibers with outer diameters of 343 μm, we tried to use a large diameter fiber cleaver to cut them. Fig. 7.5 shows the cleaved ends of three fibers with the same outer-diameter but different inner-diameter of 20, 150, and 250μm.

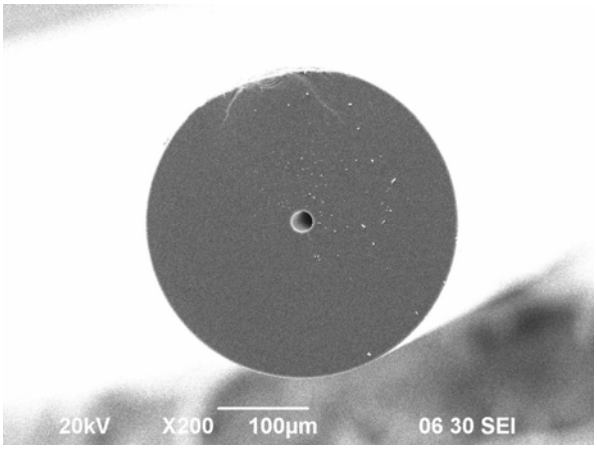

(a)

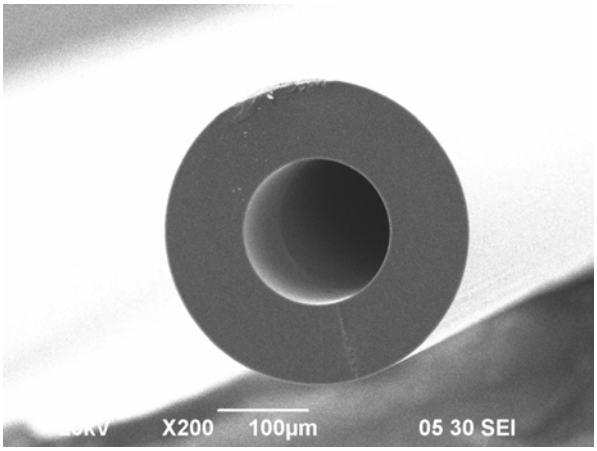

(b)

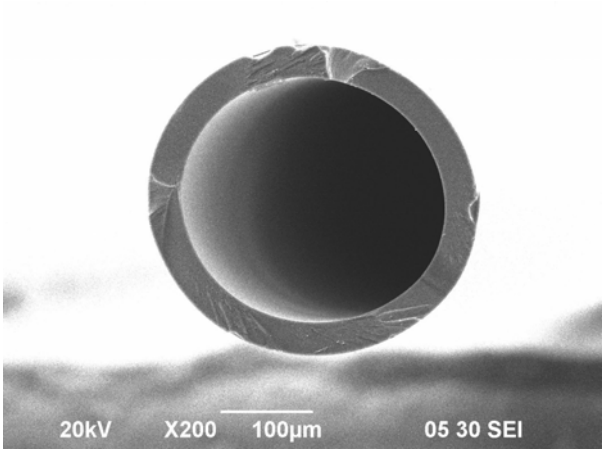

(c)

Figure 7.5 Cutting sections of tubes with i.d. of 20, 150, 250μm respectively.

As shown in Fig. 7.5a, the cleaved end seems all right for the tube with an i.d. of 20 μm, although little debris can still be seen on the surface. From the cross section in Fig. 7.5b, the surface is flat but the shallow white line is actually a crack which coincides with the direction of cleaving. We observed similar phenomenon for several times and the crack is more obvious for tubes with an i.d. of 250 μm. In Fig. 7.5c, the cleaved surface is not flat and it is not a successful cleaving. We tried many times on cutting hollow-core fibers with an i.d. of 250μm and found that they are very easy to be broken. Macomber et al. compared cutting by Standard Cleave, Precision Cleave, Saw Cut, and Laser Cut [19], and concluded that Laser cutting can provide a very smooth, defect free end-face. However they didn't present the figures of cross-section of tubes with 250 or 150 μm inner diameters after cutting.

Further work will be carried out to investigate how to achieve a high quality cleaved ends for these hollow-core fibers by use of the conventional cleaver, CO_2 laser, Femtosecond laser will be studied and contrasted to obtain a perfect cutting surface that will be used in the construction of fiber gas lasers.

7.4 Summary

In this chapter, we have discussed the technical problems encountered in our experimental investigation. To construct a fiber gas laser, the performance of the vacuum system is very important. The theory of laser resonator indicates that the mirrors must be close to the end of the hollow-core fiber, and this may be achieved by drilling side-holes and directly attach the mirrors to the two ends of the hollow-core fiber. The electrodes may be set to close to the side holes to perform discharge. Many other technical problems such mirror alignments and fiber cleaving also need to be solved in the process of constructing a fiber gas laser.

References

1. P. S. Light, F. Couny, F. Benabid, “Low optical insertion-loss and vacuum-pressure all-fiber acetylene cell based on hollow-core photonic crystal fiber,” *Optics Letters*, vol. 31, pp. 2538-2540, 2006.
2. M. L. Ng, P. Herman, A. Nejadmalayeri, J. Li, “F_2-laser Mirofabrication of Efficient Diffractive Optical Phase Elements,” *Proc. SPIE*, vol. 5339, pp. 127-133, 2004.
3. P. R. Herman, K. P. Chen, M. Wei, and J. Zhang, “F_2-lasers: High-Resolution Optical Processing System for Shaping Photonic Components,” *Proc. SPIE*, vol. 4274, pp. 149-157, 2001.
4. K. P. Chen, P. R. Herman, R. Tam, and J. Zhang, “Rapid long-period grating

formation in hydrogen-loaded fibre with 157 nm F_2-laser radiation," *Electronics Letters*, vol. 36, pp. 2000-201, 2000.

5. V. Mezentsev, M. Dubov, A. Martinez, Y. Lai, T. P. Allsop, I. Khrushchev, D. J. Webb, F. Floreani, and I. Bennion, "Micro-fabrication of advanced photonic devices by means of direct point-by-point femtosecond inscription in silica," *Proc. SPIE*, vol. 6107, pp. 6107C1-12, 2006.
6. K. M. Davis, K. Miura, N. Sugimoto, and K. Hirao, "Writing waveguides in glass with a femtosecond laser," *Opt. Lett.*, vol. 21, pp. 1729-1731, 1996.
7. C. B. Schaffer, A. Brodeur, J. F. Garcia, and E. Mazur, "Micromachining bulk glass by use of femtosecond laser pulses with nanojoule energy," *Opt. Lett.*, vol. 26, pp. 93-95, 2001.
8. T. N. Kim, K. Campbell, A. Groisman, D. Kleinfeld, and C. B. Schaffer, "Femtosecond laser-drilled capillary integrated into a microfluidic device," *Appl. Phys. Lett.*, vol. 86, pp. 201106, 2005.
9. D. Ashkenasi, G. Müller, A. Rosenfeld, R. Stoian, I. V. Hertel, N. M. Bulgakova, and E. E. B. Campbell, "Fundamentals and advantages of ultrafast micro-structuring of transparent materials," *Appl. Phys. A*, vol. 77, pp. 223-228, 2003.
10. C. B. Schaffer, A. Brodeur, and E. Mazur, "Laser-induced breakdown and damage in bulk transparent materials induced by tightly focused femtosecond laser pulses," *Meas. Sci. Technol.*, vol. 12, pp. 1784-1794, 2001.
11. H. Endert, M. Kauf, E. E. Mayer, M. J. Scaggs, J. H. Fair, and D. Basting, "Microstructuring with 157-nm laser light," *Proc. SPIE*, vol. 3618, pp. 413-417,

1999.

12. A. Marcinkevicius, S. Juodkazis, M. Watanabe, M. Miwa, S. Matsuo, H. Misawa, and J. Nishii, “Femtosecond laser-assisted three-dimensional microfabrication in silica,” *Opt. Lett.*, vol. 26, pp. 277-279, 2001.
13. X. Liu, D. Du, and G. Mourou, “Laser ablation and micromachining with ultrashort laser pulses,” *IEEE J. Quantum Electron.*, vol. 33, pp. 1706-1716, 1997.
14. Y. Li, K. Itoh, W. Watanabe, K. Yamada, D. Kuroda, J. Nishii, and Y. Jiang, “Three-dimensional hole drilling of silica glass from the rear surface with femtosecond laser pulses,” *Opt. Lett.*, vol. 26, pp. 1912-1914, 2001.
15. Y. Lai, K. Zhou, L. Zhang, and I. Bennion, “Microchannels in conventional single-mode fibers,” *Opt. Lett.*, vol. 31, pp. 2559-2561, 2006.
16. S. Nolte, C. Momma, G. Kamlage, A. Ostendorf, C. Fallnich, F. von Alvensleben, and H. Welling, “Polarization effects in ultrashort-pulse laser drilling,” *Appl. Phys. A*, vol. 68, pp. 563-567, 1999.
17. C. Hensley, D. H. Broaddus, C. B. Schaffer, and A. L. Gaeta, “Photonic band-gap fiber gas cell fabricated using femtosecond micromachining,” *Optics Express*, vol. 15, pp. 6690-6695, 2007.
18. P. W. Smith, “Waveguide gas laser devices,” *US. Patent*, 3772611, 1973.
19. J. Macomber, R. Hintz, T. Ewing, and R. Acuña, “Polyimide Coated Capillary Tubing: A Summary of Cutting Technologies,” As printed in *LCGC, The Application Notebook*, pp. 8, June 2005.

CHAPTER 8

RESEARCH SUMMARY AND FUTURE WORK

8.1 Research summary

We have investigated, theoretically and experimentally, the various issues related to the construction of a fiber gas (e.g. He-Ne) laser. Theoretical investigations include: waveguide losses of different type of hollow-core fibers, various cavity configurations and cavity configuration for achieving optimal couplings, bending losses of hollow-core fibers, population inversions in small bore size hollow-core fibers, gas flow dynamics in hollow-core fibers, and breakdown characteristics. Experimental studies include: design of vacuum system, longitudinal DC discharge experiments, current-voltage characteristic of gas discharge in hollow-core fibers, spectrum measurements, and exploring of optimized design of laser structure.

Conventional simple hollow waveguide theory indicates that waveguide loss will hinder the lasing in smaller bore size tubes although the gain has inverse relation with the tube size. Early researchers suggested that a bore diameter of 200 μm is the optimal value for waveguide He-Ne lasers. This prediction may be right for conventional waveguide He-Ne lasers which are based on capillary waveguide in bulk glass. However no experiments on waveguide He-Ne lasers with a bore diameter smaller than 400 μm have been reported.

Recent advances on microstructured optical fiber allow the demonstration of hollow-core PBG fibers with core diameters ranging from 5μm to 50μm. The

attenuations of these fibers are much smaller than that predicted from the conventional hollow waveguide theory, indicating that special waveguide designs (e.g. hollow PBG fiber and hollow Bragg fiber) can help to obtain small waveguide losses. With these novel hollow-core fibers, compact and flexible fiber gas lasers may be constructed.

Analysis based on the conventional theory of laser resonators indicates that the radius of the mirror and the corresponding distance from the mirror to the waveguide decrease with decreasing bore size of the waveguide. Placing flat mirror near the end of hollow-core fiber may be the only practical choice for hollow-core fibers with bore diameters smaller than 150μm.

The bending losses of various hollow-core fibers have been discussed. Simple waveguide structures (e.g. air-silica or air-silica-doped silica) have large bending losses if the bending radius is smaller than ~20cm. Complicated microstructured waveguide such as hollow-core PBG fibers have excellent bending performance. They can be bent into small coils with diameters of several millimeters with negligible losses. When the bore diameter of hollow-core fiber is reduced, the performance of bending will become better. However our discharge experiments indicate that gas discharge in hollow waveguide with bore diameter smaller than 30μm is difficult and not stable, even though discharge with a short length of such fiber was also achieved. Since the total optical gain is proportional to the discharge length, a short discharge length may not readily lead to lasing. The optimal bore diameter of the hollow-core fiber needs to be investigated to find the balance between the bending performance and output power.

By using previous models, which were developed for large bore-diameter and smaller gas pressure, we calculated the population inversions in hollow-core fibers.

The results indicate that it is hard to achieve population inversions in tubes with diameters smaller than 10 μm. This tentative conclusion still needs to be verified by further experiments. The parameters we used in the modeling are from the previous experiments for R>500 μm, p<10 Torr, and may be not accurate when R reduces to very small values and when p increases to higher levels. Further investigation by experiments is necessary to build a more accurate model.

We carried out our first gas discharge experiment by using a thermometer tube with a bore size of 344 μm and it succeeded! Then we succeeded in obtaining gas discharge in hollow-core fiber with 250, 150, and 50μm inner-diameter (i.d.) hollow-core fibers. Stable glow discharges of at least several minutes were observed for these hollow-core fibers. The smallest hollow-core with which we achieved a stable gas discharge is a grapefruit fiber microstructured with six elliptical holes of ~30μm long axis. A flash glow was also observed for a hollow-core fiber with an i.d. of ~20 μm. The longest hollow-core fiber with which we achieved successful stable gas discharge is a 26.2 cm-length 250 μm-i.d. hollow-core fiber. Comparing our results with the previous conventional waveguide He-Ne laser experiments, we think it is feasible to achieve lasing in hollow-core fiber with bore size of 250μm or lower. The hollow-core fiber with bore diameter smaller than 50μm can achieve discharge in a short length when we use DC excitation in our experiments, which may not provide sufficient gain to obtain lasing. Transverse RF excitation may be used to achieve stable discharge in such smaller hollow-core fiber, which is part of our future research plan.

We compared our experimental I-V and breakdown characteristics with theoretical calculation based on existing models. We found that large discrepancies exist between

theory and experiment. That means that further investigations of theoretical and experimental studies are needed in order to establish new theoretical models.

We designed a new vacuum system, which will be used in our future discharge experiments. Our analysis on the gas flow in hollow-core fibers indicates that evacuating speed only depends on the inner-diameter of the hollow-core fiber and it should not take very long to evacuate a hollow-core fiber with 50μm diameter and having 10 cm of length to 10^{-5} Torr. One potential problem is that outgassing inside the hollow-core fibers may seriously affect the vacuum performance and hence needs to be further examined.

8.2 Future work

Much work needs to be done in order to make a successful fiber gas laser. We are in the process of building a new vacuum system, which is expected to provide better vacuum performance (e.g. $<10^{-6}$Torr).

Further theoretical and experimental investigation of the gas flow in small-bore hollow-core fibers are needed to understand the gas flow dynamics and to determine the degree of vacuum and gas pressure distribution in the hollow-core fibers. The gas flow dynamics in such a small bore size and long tube was seldom encountered in the past, but they become an issue that determines the pumping time required to achieve the targeted vacuum and gas pressure in such hollow-core fibers.

The effect of side-holes on the fiber loss and the discharge characteristics needs to be studied in detail. We now have a femtosecond laser that may allow us to drill micrometer side holes. We will also perform discharge experiments to determine the

optimal sizes of side holes. The losses due to the holes will be measured, and the relationship between the size and losses will be studied. The effect of hole size on the characteristics of gas discharge will also be investigated.

The gain in terms of /m of gas-filled hollow-core fibers for varying gas pressures, discharge currents, and mixing ratios will be experimentally studied to find out the optimal parameters for constructing fiber gas lasers.

As have been shown in the preceding chapters, the discharge voltage increases significantly with a decrease of bore-diameter for discharges in hollow waveguides with inner-diameters smaller than 50μm. The discharge is limited to short lengths of waveguide due to the high DC-voltage required. We plan to use transverse RF excitation (e.g. inductive coupling and capacitive coupling) in our future work. We are also in the process of designing and constructing a laser cavity by placing two mirrors close to the two ends of the hollow-core fiber and a proof of principle demonstration of fiber gas laser will be carried out.

We will also explore the applications of the fiber gas lasers in precision measurement and instrumentation, such as large path-length difference fiber interferometers, fiber ring flow meters and methane gas detectors based on the 3.39μm He-Ne line locked to a methane absorption line, and fiber ring laser gyros.

APPENDIX

PUBLICATIONS

Journals

1. Xin Shi, Xinbing Wang, Wei Jin, and M. Süleyman Demokan, "Characteristics of gas breakdown in hollow-core fiber," *IEEE Photonics Technology Letters*, vol. 20, pp: 650-652, 2008.
2. Xin Shi, Xinbing Wang, Wei Jin, and M. Süleyman Demokan, "Investigation of glow discharge of gas in hollow-core fibers," *Applied Physics B*, vol. 91, pp.377-380, 2008.

Proceedings

1. Xin Shi, Xinbing Wang, Wei Jin, M. Süleyman Demokan and X. L. Zhang, "Progress toward a novel hollow-core fiber gas laser," *Proc. SPIE, Optics East*, vol. 6767, pp. 67670H, Boston, September, 2007.
2. Xin Shi, Xinbing Wang, Wei Jin, and M. Süleyman Demokan, "Characteristics of gas breakdown in hollow-core fibers," *The 8th IEEE Hong Kong LEOS Postgraduate Conference*, December, 2007.
3. Xin Shi, Xinbing Wang, Wei Jin, and M. Süleyman Demokan, "Characteristics of gas breakdown in hollow-core fibers," *19th International Conference on Optical Fibre Sensors, Proc. of SPIE*, vol. 7004, pp. 70042E, Perth, Australia, April, 2008.

Patent

Wei Jin and Xin Shi, “光纤气体激光器和具有该激光器的光纤型环形激光陀螺仪,” *Chinese patent*, CN101165977, and “Fiber gas lasers and fiber ring laser gyroscopes based on these gas lasers,” *US patent*, 20080094636, 2008.

Others

Wei Jin, Xin Shi, Xinbing Wang and M. Süleyman Demokan, “Gas discharge in hollow-core fibers,” *SPIE Newsroom*, http://spie.org/x20202.xml.